

Frederik Weber

Viscose fibres - a model system to
investigate the influence of charges
on the properties of handsheets and
fibre-fibre joints

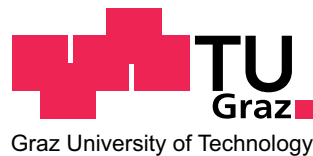
DOCTORAL THESIS

For obtaining the academic degree of

Doktor der technischen Wissenschaften

Doctoral Programm of Technical Sciences

Technical Physics



Graz University of Technology

Supervisor:

Ao.Univ.Prof.Mag.Dr.rer.nat. Robert Schennach
Institute of Solid State Physics

Graz, January 2014

Deutsche Fassung:
Beschluss der Curricula-Kommission für Bachelor-, Master- und Diplomstudien vom 10.11.2008
Genehmigung des Senates am 1.12.2008

EIDESSTÄTTLICHE ERKLÄRUNG

Ich erkläre an Eides statt, dass ich die vorliegende Arbeit selbstständig verfasst, andere als die angegebenen Quellen/Hilfsmittel nicht benutzt, und die den benutzten Quellen wörtlich und inhaltlich entnommenen Stellen als solche kenntlich gemacht habe.

Graz, am

.....
(Unterschrift)

Englische Fassung:

STATUTORY DECLARATION

I declare that I have authored this thesis independently, that I have not used other than the declared sources / resources, and that I have explicitly marked all material which has been quoted either literally or by content from the used sources.

.....
date

.....
(signature)

Abstract

Paper consists of individual fibres, forming a complex network by several interactions. Knowing how and to what degree the individual bonding mechanisms contribute to sheet strength is of major interest to improve paper properties. In order to get a better understanding of the influence of charges on the strength of fibre-fibre joints and sheet tensile strength, several charged and uncharged viscose fibres were investigated. Viscose fibres represent a good model since they are man-made cellulosic fibres, with well known fibre parameters.

The controlled introduction of charges, both cationic and anionic, can be accomplished by the addition of cationic starch and carboxymethylcellulose CMC, respectively. In doing so, the influence of charges on the swelling behaviour of single fibres and on the tensile strength of handsheets was analysed. Thereby, the swelling was investigated by light microscopy and environmental scanning electron microscopy. Tensile strength is increased by both additives. However, while CMC leads to enhanced swelling and tensile strength, cationic starch does not influence the moisture expansion. In addition, the amount of surface charges was analysed by titration, attenuated total reflection infrared spectroscopy and X-ray photoelectron spectroscopy. A significant amount of additives was found on the fibre surfaces by all methods. However, no information about the distribution within the fibre bulk is obtained.

Furthermore, the impact of charges on the relative bonded area of handsheets was investigated by using flat fibres. The relative bonded areas were determined by using the light scattering method and by means of calculations according to the Page equation. For these calculations, the optical bonded area was determined by polarized light microscopy. Finally the joint strength of fibre-fibre joints was determined. It can be clearly seen that no absolute value for the RBA can be obtained with the methods used. Nevertheless, an increase of the RBA due to additives is evident.

Zusammenfassung

Papier ist aus einzelnen Fasern aufgebaut, die miteinander interagieren und durch verschiedene Wechselwirkungen ein Fasernetzwerk bilden. Um Papiereigenschaften, wie zum Beispiel die Papierfestigkeit, zu verbessern, ist es wichtig zu wissen, in welchem Umfang jede einzelne Wechselwirkung Anteil an der Faser-Faser Bindung hat. Um ein besseres Verständnis über den Einfluss von Ladungen auf die Festigkeit von Papieren zu erhalten, wurden mehrere geladene, wie auch ungeladene Viskosefasern untersucht. Viskosefasern sind synthetisch erzeugte Fasern mit wohl definierten Parametern. Somit stellen sie ein ideales Modell für Papierfasern dar. Zusätzlich können sie chemisch modifiziert werden. So können durch Zugabe von Carboxymethylcellulose (CMC) oder kationischer Stärke anionisch oder eben kationisch geladene Fasern erzeugt werden.

Im Rahmen dieser Dissertation wurden verschiedene anionische und kationische Fasern untersucht. Der Einfluss von Ladungen auf das Quellverhalten einzelner Fasern und auf die Festigkeit von Laborblättern wurde bestimmt. Hierfür wurde das Quellen mittels Lichtmikroskopie und Rasterelektronenmikroskopie untersucht. Die Festigkeit der Laborblätter wurde durch beide verwendeten Additive gesteigert. Dabei führte CMC zu erhöhter Quellung und Zugfestigkeit, während kationische Stärke die Quellung nicht beeinflusste. Zusätzlich wurde der Anteil an Oberflächenladungen mittels Titration, abgeschwächter Totalreflexions-infrarotspektroskopie und Röntgen-Photoelektronenspektroskopie analysiert. Ein wesentlicher Anteil von Additiven wurde mit allen verwendeten Messmethoden auf den Faseroberflächen festgestellt. Allerdings konnte keine Ladungsverteilung innerhalb der Faser mit den zur Verfügung stehenden Methoden ermittelt werden.

Weiters ist der Einfluss von Ladungen auf die relativ gebundene Fläche von Laborblättern untersucht worden. Zur Bestimmung der relativ gebundenen Fläche (RBA) wurde die Lichtstremethode sowie die Gleichung von Page verwendet. Die Berechnung mittels der Page-Gleichung konnte nach Bestimmung der optisch gebundenen Fläche von Faser-Faser-Bindungen sowie der Untersuchung der Bindestärke eben jener Bindungen erfolgen. Aus den Ergebnissen wird klar ersichtlich, dass mit den verwendeten Methoden keine absoluten Werte für die RBA ermittelt werden können. Nichtsdestotrotz ist eine Vergrößerung der RBA durch Zugabe von Additiven erkennbar.

Acknowledgement

I would like to thank Prof. Dr. Robert Schennach for his support, helpful advice, the possibility to write this thesis at the Institute of Solid State Physics at TU Graz and for giving me the opportunity to work in the CD-Laboratory for Surface Chemical and Physical Fundamentals of Paper Strength. As I worked at the Institute for Paper, Pulp and Fiber Technology I want to thank Prof. Dr. Wolfgang Bauer for the close integration into the community of the institute. Thanks to Dr. Rene Eckhart as my second supervisor for helping me with problems and for his assistance. I am thankful to Prof. Dr. Herbert Sixta as my second reviewer for his detailed review and many helpful suggestions and hints. I am also grateful to Dr. Steven Keller for reviewing and substantially improving the language of this work. Thanks to Dr. Ingo Bernt, contact person of Kelheim Fibres GmbH, for quick assistance whenever required.

Thanks to Dr. Armin Zankel and Dr. Herbert Reingruber for supporting the investigations via scanning electron microscopy. I am also grateful to Dr. Georg Koller for his commitment and supporting the investigations via X-ray photoelectron spectroscopy. I want to thank Dr. Karin Flöttinger and Astrid Kittla for supporting the BET measurements. Special thanks to Dr. Wolfgang Fischer for his support during the joint strength measurements.

I want to thank Claudia Bäumel, Kerstin Schefzik, Esther Schennach and Elisabeth Stern for their support with administrative tasks. Thanks to Harald Streicher to keep the IT system running. I am also thankful to Barbara Hummer, Adelheid Bakhshi and the whole laboratory staff for preparing the fibre to fibre joints and handsheets. Special thanks to Albrecht Miletzky, Wolfgang Fuchs, Lukas Jagiello, Christian Lorbach, Wolfgang Pacher, Matthias Trimmel, Christian Ganser and Karin Hofer for being great colleagues and friends. Thanks to all members of the CD-Laboratory for the great working relationship.

I want to acknowledge Kelheim Fibres GmbH, Mondi Frantschach GmbH, Lenzing AG and Christian Doppler Research Association for funding this research project.

Finally, a very big thank you to my family and friends. This work is dedicated to them. I would especially like to thank my mother Evelyn Weber and my sister Madelaine Weber for their support and love. You have made all this possible. Hias, Markus, Georg, Kirmi, Michi and Matthias for being the best friends and who have been willing to help with whatever I needed. Last but not least I would like to thank my girlfriend Ann Kathrin for her support and for listening to my problems. You gave me strength in good and bad times.

Frederik Weber
Graz, 07.01.2014

Contents

1	Introduction	1
1.1	CD-Laboratory for Paper Strength	1
1.2	Objective of this thesis	3
1.3	List of Publications	4
2	Background	6
2.1	Wood	6
2.1.1	Tree trunk	6
2.1.2	Anatomy of the cell wall structure of wood fibres	7
2.1.3	Chemical composition of wood fibres	8
2.1.3.1	Cellulose I	8
2.1.3.2	Cellulose II	11
2.1.3.3	Hemicelullose	12
2.1.3.4	Lignin	12
2.2	Paper fibres	13
2.3	Viscose fibres	13
2.3.1	The basic principle of viscose manufacturing	13
2.4	Bonding mechanisms in paper	15
2.4.1	Benefit of investigating viscose fibres	16
3	Analytical Methods	18
3.1	Fibre samples	18
3.2	Swelling	20
3.2.1	Environmental scanning electron microscope	21
3.2.1.1	The Peltier effect	22

3.2.1.2	The cooling unit	23
3.3	Breaking length	24
3.4	Titration	25
3.5	Infrared spectroscopy	26
3.5.1	Attenuated total reflection infrared spectroscopy	27
3.6	X-ray photoelectron spectroscopy	30
3.7	Atomic force microscopy	33
3.7.1	Contact mode	34
3.7.2	Tapping mode	34
3.8	Nitrogen adsorption measurements	35
3.9	Light scattering	35
3.10	Polarized light microscopy	39
3.11	Joint strength measurement	40
4	Investigation of round viscose fibres - determination of the surface chemistry	43
4.1	Swelling	44
4.2	Breaking length	48
4.2.1	Interpretation of the first results	50
4.3	Titration	51
4.4	Attenuated total reflection infrared spectroscopy	52
4.5	X-ray photoelectron spectroscopy	54
4.5.1	Interpretation of the results	57
4.6	Summary	58
5	Investigation of flat viscose fibres – determination of the relative bonded area within a paper sheet	60
5.1	Breaking length	61
5.1.1	Nanointentation	63
5.2	Relative bonded area	64
5.2.1	Nitrogen adsorption measurements	65
5.2.2	Light scattering	67
5.2.3	Polarized light microscopy	70
5.2.4	Joint strength measurements	71
5.2.5	RBA - results	73
5.2.5.1	RBA - Light scattering	73
5.2.5.2	RBA - Page equation	74
5.2.5.3	RBA - Comparison	75
5.3	Summary	78
6	Summary	79
6.1	Round fibres - Surface charge investigations	79
6.1.1	Influence of charge on swelling and breaking length	79
6.1.2	analysing of surface charge	79

6.2	Flat fibres - Relative bonded area of handsheets	80
6.2.1	Breaking length	80
6.2.2	Light scattering method	81
6.2.3	Page equation	81
6.3	Conclusion	82
7	Outlook	83
	Bibliography	92
	List of Figures	94
	List of Tables	95

1 Introduction

1.1 CD-Laboratory for Paper Strength

Paper is one of the oldest media for datastorage. 5,000 years ago the Egyptians used papyrus, a flat uniform sheet made from the papyrus plant, for letters and writing (Junge 2008). Papyrus was made by reaping, peeling and slicing the plant into strips which were laid out in layers, compressed and smoothed to get a sheet (Alén 2008). Another early form of paper, based on a wide variety of materials (e.g., bamboo), was developed in China about 2,000 years ago. The used raw material was treated by potash and beaten to separate each filament (Alén 2008).

In the 15th century, the invention of the movable-type printing press led to a rapid increase in the demand of paper. The paper used in Europe was first made from cotton and linen and later on by wood fibres. Paper has become an everyday item. In the 19th century, the production of paper has therefore become a flourishing industry. Different processes have been used to convert wood fibres into a mass product. A distinction is made between chemically (by means of chemicals), mechanically (by means of refining) or by a combination of both treatments (Alén 2008).

Nowadays, paper is not only used for information storage like in the past but has become a widely distributed high-tech material, modified for several applications. Tissues, hygienic paper and paper bags are just a few examples of paper products. Each paper product has to meet special demands. Hence, specific properties of paper have to be changed, e.g. swelling, tensile strength or opacity. Tensile strength is important for many paper products. Tissues, paper bags or cement bags all must not tear when being used. Cement bags need strong sheets and high porosity to fill them fast in the factory. The production costs of paper must be minimized as well. To

reduce material costs, for example, paper bags are made as thin as possible. To satisfy the demands on paper while reducing the amount of material used, background knowledge of how paper strength originates is necessary.

Paper is a natural product which consists of fibres. These fibres are distinguished between lignin-free (consisting of cellulose and hemicellulose e.g. viscose fibres) and lignin-containing (consisting of lignocellulose e.g. kraft pulp fibres) fibres. The fibres interact with each other, leading to the formation of a complex network. Lindström et al. (2005) identified five mechanisms responsible for fibre-fibre bonds - mechanical interlocking, interdiffusion, hydrogen bonds, induced dipoles, and coulomb interactions (see also chapter 2.4). Due to capillary forces fibres come into close proximity where van der Waals forces and electrostatic forces take effect on the fibres (Wågberg and Annergren 1997). The same was assumed by Erhard et al. (2010) who established a three-stage theory on strength development. At a dry content of about 25% capillary forces and mechanical interlocking of the fibrils lead to an approach of the fibres. In the second stage (dry content of 50%) van der Waals forces begin to act. Furthermore, diffusion of polymer chains occurs. Finally, hydrogen bonds are formed during drying (third stage) (Erhard et al. 2010).

Since several mechanism are acting during sheet formation, it is hard to distinguish, which mechanism contributes to what extend. Knowing how these mechanism contribute to the paper strength would give the opportunity to change certain paper properties by mechanical or chemical treatment. A first estimate of the contribution for hydrogen bonds ($9.1 \times 10^{-23} \text{kJ/mm}^2$), van der Waals interaction ($2.4 \times 10^{-22} \text{kJ/mm}^2$) and Coulomb interaction ($5.3 \times 10^{-9} \text{kJ/bond}$) is given by Schennach et al. (2011). However, it is not possible to measure exclusively surface charge (Schennach et al. 2011). Also the average fibre surface area used for this calculation is just an approximation, since paper fibres exhibit a wide variation of sizes. A first estimate of the contribution of mechanical interlocking is given by Schmied et al. (2013). An increase of the bond strength by about 30-55% was found due to mechanical interlocking. However, the given values are just first approximations without any claim for correctness. Furthermore, the contribution of interdiffusion is still not known.

Fibre properties and therefore, bond strength can be changed by e.g. mechanical stress. Beating of the fibres, for example, is a way to increase the water uptake by the fibres (Sixta 2006b). Thereby, the wet fibres are milled in a so called refiner. By performing such a mechanical treatment, the fibre surface becomes fuzzy. The resulting fibril fluff on the surface will store water (Sixta 2006b) and contributes to the mechanical interlocking. While beating is a mechanical treatment, chemical changes of the fibres can also lead to improved fibre-fibre bonds. Anionic additives for example also lead to improved fibre swelling (Laine et al. 2003a, Lindström 1980). Additionally, these additives lead to induced charges, which improve the bond strength of fibre-fibre bonds as well (Weber et al. (2013)).

To gain a deeper insight into these mechanisms the CD-Laboratory for Surface Chemical and Physical Fundamentals of Paper Strength was founded in 2007. This PhD thesis was carried out at the CD-Laboratory to investigate the influence of charges on the bonding forces of fibre-fibre bonds.

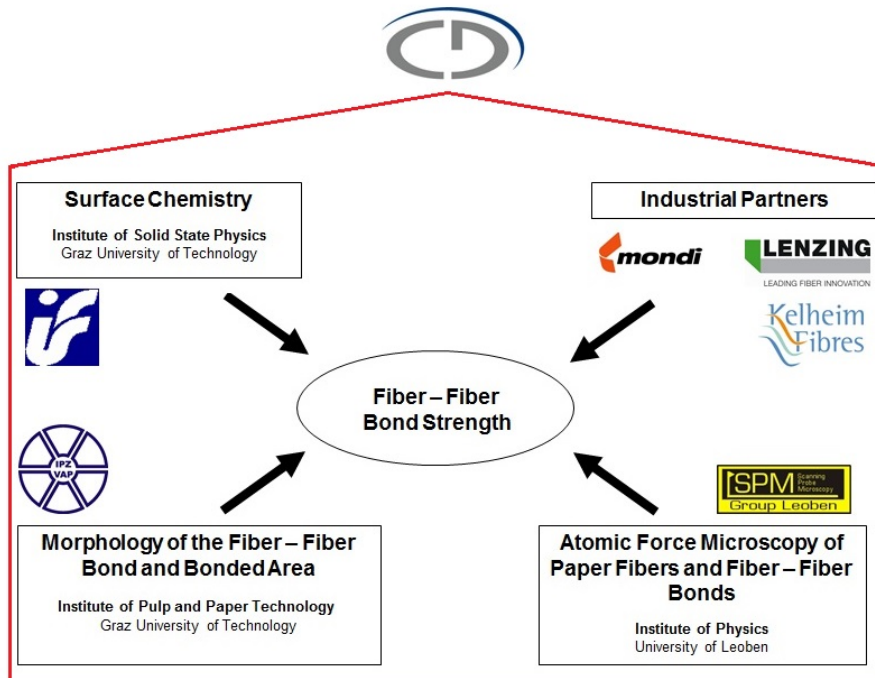


Figure 1.1: Working groups and their object within the CD-Laboratory for Surface Chemical and Physical Fundamentals of Paper Strength.

This CD-Laboratory is composed of four groups. Surface and bulk chemistry is analysed at the Institute of Solid State Physics, while bond strength measurements as well as the investigation of the morphology of bonds are investigated at the Institute for Paper-, Pulp- and Fiber Technology. Both groups are institutes from Graz University of Technology. At the Montanuniversität Leoben (Institute of Physics) atomic force microscopy (AFM) is used for several analyses. Fibre surface, fibre hardness, bonding area and joint strength of single fibre-fibre bonds are investigated by AFM. At last, samples are provided by the industrial partners (Mondi Frantschach GmbH, Kelheim Fibres GmbH and Lenzing AG). Figure 1.1 gives an overview of all groups within the CD-Lab and their contribution to the research project.

1.2 Objective of this thesis

As mentioned before, the complex fibre network is formed because of several fibre-fibre interactions. Until today, there was no clear ranking of the importance of the different interactions (Lindström et al. 2005). In order to clarify the importance of fibre

charges on the bonding strength of single fibre-fibre joints and on the properties of the fibres themselves, types of charged and uncharged viscose fibres were investigated in the present work. Viscose fibres are regenerated fibres which can be physically modified to obtain anionic as well as cationic fibres. Without external fibrillation and uniform dimensions of all fibres, viscose fibres exhibit a good model, in order to get a better understanding of the effect of charges to several fibre and handsheet properties. Furthermore, the fibre surface was investigated in order to verify the existence of surface charges. More details about viscose fibres and the differences to paper fibres are given in chapter 2. The thesis can be divided into two topics:

- Influence of charges on fibre properties and tensile strength of hand sheets made of round viscose fibres as well as analysis of the surface chemistry of the used samples
- Influence of charges on the bonding strength and on the relative bonded area of handsheets made of flat viscose fibres

Both topics examine the effect of charges on the bonding strength and the bonding area.

1.3 List of Publications

Papers

1. Weber, F., Koller, G., Schennach, R., Bernt, I., and Eckhart, R. (2013). The surface charge of regenerated cellulose fibres. *Cellulose*, 20, Nr. 6:2719-2729; DOI: 10.1007/s10570-013-0047-8.
2. Weber, F., Ganser, C., Schennach, R., Teichert, C., Bernt, I., and Eckhart, R. Application of the Page-equation on viscose fibre - hand sheets. In preparation for publication in *Cellulose*.

The thesis is based on these two papers which have been written by Frederik Weber. The XPS measurements done in the first publication were done by Georg Koller at the Institute of Physics at the University of Graz. Titration was done at Kelheim Fibres GmbH represented by Ingo Bernt. The used handsheets were produced and tested by the laboratory staff of the Institute for Paper-, Pulp- and Fibre Technology at TU Graz. Swelling and ATR measurements were done by Frederik Weber. Furthermore, the evaluation and interpretation of all results of breaking length, swelling, titration, XPS and ATR measurements, was done by Frederik Weber in consultation with Robert Schennach and Rene Eckhart.

The used fibre samples, for the second publication, were also provided by Ingo Bernt, representing Kelheim Fibres GmbH. Handsheet were produced by the laboratory

staff of the Institute for Paper-, Pulp- and Fibre Technology at TU Graz. They also performed the tensile strength measurements of these handsheets. Nanointentation measurements were done by Christian Ganser, under the supervision of Christian Teichert, at Montanuniversität Leoben. All further measurements (light scattering, polarized light microscopy and joint strength measurement) were done by Frederik Weber. Calculations of the RBA as well as interpretation of the results was done by Frederik Weber in consultation with Robert Schennach and Rene Eckhart.

Paper contribution

1. Ganser, C.; Weber, F.; Czibula, C.; Bernt, I.; Schennach, R.; Teichert, C. Tuning hardness of swollen viscose fibers. In preparation for publication in *Bioinspired, Biomimetic and Nanobiomaterials*

Contributions to conference proceedings

1. Ganser, C.; Schmied, F.; Weber, F.; Eckhart, R.; Schennach, R.; Teichert, C.: Morphological comparison of native and regenerated cellulose fibers using atomic force microscopy. - in: 61. Jahrestagung der Österreichischen Physikalischen Gesellschaft. EPF Lausanne, Swiss (2011)
2. Weber, F.; Eckhart, R.; Schennach, R.: Viscose fibres - a way to design paper properties? - in: 38th International Annual Symposium DITP. Bled, Slovenia (2011)

Poster contributions

1. Weber, F.; Eckhart, R.; Fischer, W. J.; Bernt, I.; Schennach, R.: Application of the Page Equation on Viscose-Fibre Handsheets. - in: 15th Fundamental Research Symposium. Cambridge, England (2013)
2. Weber, F.; Eckhart, R.; Koller, G.; Bernt, I.; Schennach, R.: Investigation of the surface charge of Viscose Fibres by XPS and ATR. - in: 62. Jahrestagung der Österreichischen Physikalischen Gesellschaft (ÖPG). KFU, Graz, Austria (2012)

2 Background

A short introduction about wood fibres and viscose fibres as well as the differences between paper fibres and viscose fibres will be presented in this chapter. Moreover, a survey of the interactions that determine the specific joint strength in the contact zone between the fibres will be given. At the end of this chapter, the reason why viscose fibres exhibit a good model for paper fibres, will be evident.

2.1 Wood

Wood fibres consists of cellulose, hemicellulose, lignin and extractives. In this chapter an overview of the raw material wood, the anatomy of the fibres and the chemical compounds will be given. Paper as a natural product, produced by pressing together moist fibres, derived from wood. Several mechanism are responsible for interaction between these fibres, leading to the formation of a network.

2.1.1 Tree trunk

As mentioned above, the raw material used for the production of paper and regenerated fibres is wood which is chemically or mechanically treated to extract several unwanted constituent parts. Wood can be divided into two classes, hardwood and softwood. While hardwoods are plants with broad leaves, softwoods are usually cone-bearing plants with needle- or scale-like evergreen leaves (Forest Products Laboratory 2013). Anatomically, softwood exhibits a simpler structure. They are basically composed of tracheids, oriented in longitudinal direction. A special feature of hardwood are vessels, which serve as a conduit for transporting water or sap in the tree. They are responsible for the porosity of hardwood (Sixta 2006a).

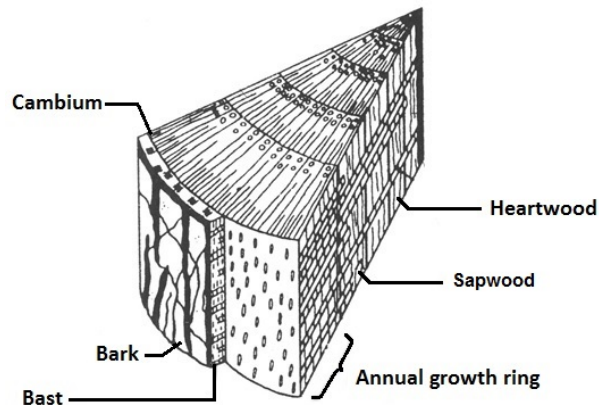


Figure 2.1: Composition of a tree trunk; adapted from Eckhart.

A typical cross section of a tree is given in figure 2.1. The outermost layer is the bark. It consists of dead cells, protecting the tree against drying-out, mechanical damage and microbiological attack. The thickness of the bark is around 2-40 mm and depends on age and tree species.

Next to the bark there is the bast, a small layer of living cells which is used to transport solute nutrients.

The cambium represents the living part of a tree, the growth layer. It only consists of a few cell rows. It is followed by the sapwood which serves as a reservoir for nutrients. Also water is transported through this layer.

Finally the heartwood is found in the center of a tree. Having a high denseness, these dead cells serve as a pillar.

2.1.2 Anatomy of the cell wall structure of wood fibres

Wood is composed of various cell types. Due to the long elongated shape, they are also called, fibres. An illustration of such a fibre is given in figure 2.2.

Each fibre is embedded in the so called middle lamella (ML). The middle lamella mainly consists of lignin and serves as a binder, holding the fibres together. Its thickness is around 0.2-1.0 μm .

The first fibre layer is the primary wall (P) which has a thickness around 0.05-0.1 μm . It consists of a loose matrix of cellulose micro fibrils which are embedded in a matrix of hemicelluloses and pectin. This structure enables the growth of the cell.

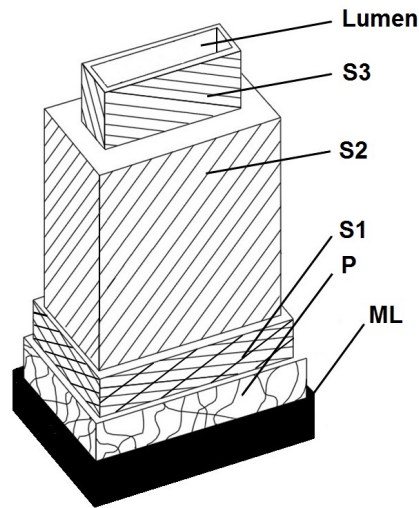


Figure 2.2: Schematic illustration of the cell wall structure of a wood fibre; ML - middle lamella, P - primary wall, S1 - secondary wall 1, S2 - secondary wall 2, S3 - secondary wall 3 and Lumen; adapted from Götze (1951).

The secondary wall consists of three layers. Lignin and hemicelluloses are embedded between each layer. The first formed layer of the secondary wall (S1) shows a crossed fibrillar structure of 0.1-0.3 μm . The microfibrils are helically arranged. The orientation varies between 50° to 70° relative to the cell axis. With a thickness around 1-8 μm , the S2 layer is the thickest layer within a fibre. It is composed of parallel microfibrils which form a laminar structure. Again there is a helix with an angle of 10° to 30° . The last layer of a fibre ($<0.1 \mu\text{m}$) separates the cell wall to the lumen. The fibrils within S3 are helically arranged too. The angle range from 60° to 90° . In some cases there is an additional wart layer on the luminal surface (Götze 1951).

2.1.3 Chemical composition of wood fibres

Wood fibres are basically composed of the three elements carbon, oxygen and hydrogen forming macromolecules, so called polymeres. *Cellulose*, *hemicelluloses* and *lignin* are the three main compounds, formed by these elements.

2.1.3.1 Cellulose I

Cellulose is a linear polymer, built up by glucose monomers (shown in figure 2.3), which are arranged in one plane and linked by β -(1,4)-glycosidic bonds. The molecular structure of cellulose is given in figure 2.4. The length of a chain molecule is known as degree of polymerization (DP). Cellulose in woods has a DP of 7,000-15,000 which may be decreases during pulping. In order to prevent a decrease of the DP-values and therefore large yield losses during chemical pulping or bleaching, chemical reactions must be stopped when the lignin content is low (Sixta 2006a).

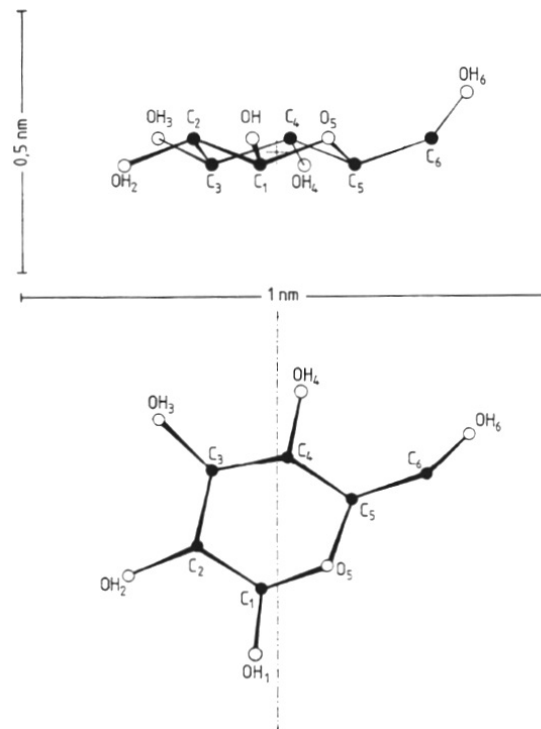


Figure 2.3: Spatial configuration of a glucose molecule; adapted from Fengel and Wegener (2003).

Due to the β -position of the OH-group at C1, the following glucose unit is rotated 180° around the C1-C4 axis. This repeating unit of the cellulose chain is a cellobiose unit. The length of this basic unit is 1.03 nm. There are OH-groups at both ends of the cellulose chain. While the OH-group at the C1-end has reducing properties, the OH-group at the C4-end is non-reducing. That is because the C1-OH is an aldehyde hydrate group, while the C4-OH is an alcoholic hydroxyl (Fengel and Wegener 2003).

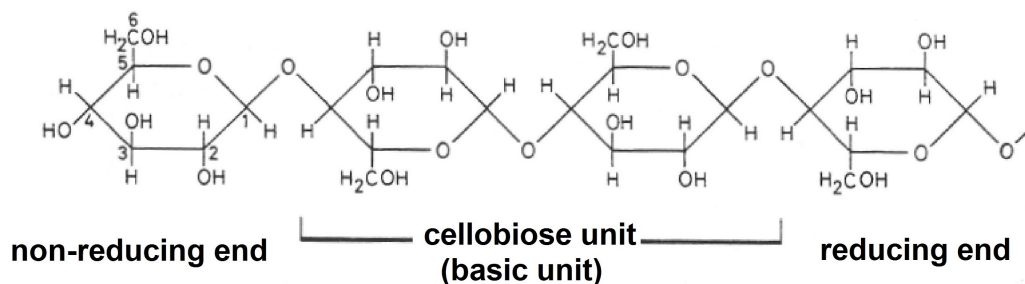


Figure 2.4: The molecular structure of cellulose; adapted from Fengel and Wegener (2003).

The molecular structure of a cellulose chain appears to be rather simple. However, the supramolecular structure is considerably complex because of intramolecular and intermolecular hydrogen bonds. The intramolecular bindings can take place between O2 and O6' within glucose units. Another hydrogen bond is formed between O3 and O5'. Intermolecular bonds can be found between the hydroxyl groups at O6 and O3. While intramolecular hydrogen bonds provide chain stiffness, intermolecular bonds are responsible for crystalline domains and fibrils. In this way, sheets of cellulose chains are built up by hydrogen bonds. According to Gardner and Blackwell (1974a) the C6-O6...O1' bond angle of 77.5° is too acute to form an hydrogen bond between cellulose chains of successive sheets. Therefore, Gardner and Blackwell (1974a) concluded the structure to be composed of hydrogen-bonded sheets extended in the (020) planes which are connected by van der Waals forces. However, from a purely physical point of view, both bonding mechanisms are dipole-dipole interactions, caused by dipoles of different magnitude. The crystalline domains are the basic elements of the supramolecular structure. The crystallites are inaccessible to water and resist acids (Sixta 2006a, Fengel and Wegener 2003). In addition, there are less ordered regions which are called amorphous domains.

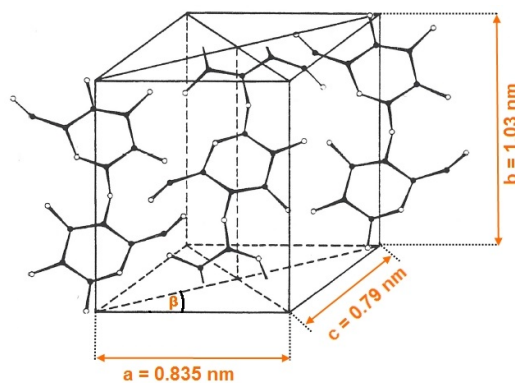


Figure 2.5: Monoclinic unit cell of cellulose I; adopted from Fengel and Wegener (2003).

As already mentioned, the regular system of hydrogen bonds results in a crystalline structure. The lattice was evaluated by Meyer and Misch (1937) to be monoclinic on the basis of X-ray diffraction measurements. An illustration of the unit cell is given in figure 2.5. In this lattice system the three axis are of different lengths (0.835 nm for the a-axis, 1.03 nm for the b-axis and 0.79 nm for the c-axis), forming a rectangular prism with a parallelogram as its base (84° for the β -angel). However, the position of the cellulose molecules within this crystal unit cell is still an unanswered question. While Meyer and Misch (1937) and Viswanathan and Shenouda (1971) assumed an antiparallel arrangement of the cellulose chains, a parallel arrangement was adopted by Gardner and Blackwell (1974b). The theory of a parallel configuration was confirmed by calculations of Sarko (1976).

2.1.3.2 Cellulose II

Cellulose described so far is also known as cellulose I. Regenerated fibres like viscose fibres consist of cellulose II. Cellulose II can be obtained by mercerization or by regeneration from solution (therefore called regenerated fibre). More information about the viscose fibre fabrication is given in chapter 2.3.1. Since cellulose II exhibits a more stable allomorph, the conversion from cellulose I to cellulose II is irreversible (Sixta 2006a). The hydrogen bond network of cellulose II is some way more complex than of cellulose I. Langan et al. (1999) observed intramolecular hydrogen bonds involving O3 as donor and O5 as well as O6 as acceptors. Intermolecular hydrogen bonds were seen between O2 and O6. An additional four center hydrogen bond between two chains was suggested too (Langan et al. 1999). Due to a change in the hydrogen bond network, the lattice is changed as well. According to Andress (1929) the unit cell is still monoclinic but the cell axis dimensions changes ($a=0.841$ nm; $b=1.03$ nm; $c=0.924$ nm) as well as the β -angle (62°). Additionally, an antiparallel arrangement of the cellulose chains is assumed (Langan et al. 2001). Since regenerated fibres are obtained from dissolved cellulose, a change in orientation of the cellulose chains, seems to be imaginable (Fengel and Wegener 2003). These changes in the crystal lattice are also seen in a change of the crystal lattice modulus (elastic modulus of the crystalline regions). Matsuo et al. (1990) investigated the chain modulus for cellulose I and II by X-ray diffraction. Their values for cellulose I and II range from 120-135 GPa and 106-112 GPa, respectively. Nearly the same was found by Sakurada et al. (1962) (cellulose I: 137 GPa) and Sakurada and Kaji (1970) (cellulose I: 130 GPa, cellulose II: 90 GPa).

The degree of crystallinity varies depending on the fibre origin. Different data is found in literature. Values between 60-70% were found for wood pulp by Thygesen et al. (2005). In contrast to regenerated cellulose which shows a crystallinity of about 45% (Hindeleh and Johnson 1974). Much higher values were found by Scallan (1971) (cellulose I 96-89%, cellulose II 85-65%). All these differences between cellulose I and II are reflected by the elastic modulus and tensile strength of single fibres. Fischer analysed both parameters of viscose fibres and kraft pulp fibres. Viscose fibres exhibit an elastic modulus in the range between 5-8 GPa while values of kraft pulp fibres were found between 11-16 GPa. Tensile strength was also seen to be lower for viscose fibres (270-380 MPa) than for kraft pulp fibres (714-970 MPa) (Fischer). Comparable results for viscose fibres are given by Adusumali et al. (2006) (E-modulus: 12 GPa, tensile strength: 400 MPa).

As mentioned in chapter 2.1.2 the wood cell wall is made up of cellulose fibrils. The fibrils are composed of cellulose molecules and contain ordered, and disordered regions. The smallest units of this fibrils, called *elementary fibrils*, have an average diameter of 3.5 nm. The elementary fibrils form higher systems (*microfibrils*) with diameters of about 10-30 nm. The microfibrils again are incorporated into a matrix of hemicelluloses and lignin (Fengel and Wegener 2003).

2.1.3.3 Hemicellulose

The second most common native biopolymers are hemicelluloses. Compared to cellulose, hemicelluloses are heteropolysaccharides and consist of several sugar units which are forming the supramolecular structure. The sugar units can be classified into pentoses, hexoses, hexuronic acids and deoxy hexoses. Hemicelluloses are further divided into softwood and hardwood hemicelluloses. While softwood exhibits a higher proportion of mannose and galactose units, hardwoods show a higher proportion of xylose units and acetyl groups. The molecular masses are much lower compared to cellulose, with a DP of 50-200. Since the content of hemicellulose within the used viscose fibres is only around 1% [w/w] (Bernt b) further information about hemicelluloses see Sixta (2006a) and Fengel and Wegener (2003)

2.1.3.4 Lignin

The third component of wood fibres is lignin. Next to cellulose, it is the most common and important polymer in plants. It occurs in the vascular tissue, where it is responsible for liquid transport and mechanical strength. The lignin content in different plants is quite variable and ranges from 20-40% for wood species. Even for the same plant, the content of lignin is not uniform. It is an amorphous substance which is found in the middle lamella and in the secondary walls of wood fibres. There is more lignin in softwood than in hardwood. Furthermore, there are structural differences between softwood and hardwood lignins (Fengel and Wegener 2003).

Lignin is an integrated part of wood and acts as a glue between the fibers. During pulping and bleaching, lignin is more or less released and used as an energy source.

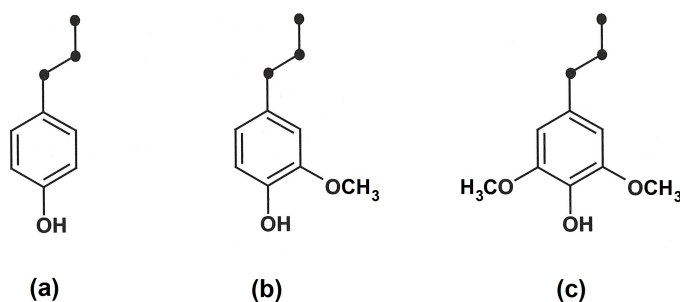


Figure 2.6: Molecular structure of the building units of lignin. (a) p-coumaryl alcohol, (b) coniferyl alcohol, (c) sinapyl alcohol; adapted from Fengel and Wegener (2003).

The complex structure of lignin is formed by radical coupling reactions of three hydroxycinnamyl alcohols which are shown in figure 2.6. Complicated biochemical and chemical reactions lead to a random recombination of these three monolignols. In contrast to cellulose, lignin exhibits a distinctive heterogeneity. Depending on the proportions of the free monolignols, different chemical reactivities are seen (Sixta

2006a). Further details about lignin can be found e.g. in Sixta (2006a) and Fengel and Wegener (2003).

2.2 Paper fibres

During the paper making process, the wood is chopped and then reduced to a fibrous mass, denoted as pulp. The defibration can be done chemically, mechanically, or by a combination of both. During these pulping processes lignin and accessory compounds are dissolved. In the end, paper fibres are obtained. Depending on the raw material and the pulping process, paper fibres consist of cellulose, hemicellulose and lignin to some extent. A typical paper fibre will be shown in figure 2.10 in chapter 2.4.1. Detailed informations about the different pulping processes are given e.g. in Sixta (2006a).

2.3 Viscose fibres

Viscose fibres are pure cellulose fibres. Lignin and hemicelluloses are removed as far as possible. Before some examples of viscose fibres are shown, an overview of the viscose production will be given.

2.3.1 The basic principle of viscose manufacturing

Viscose manufacturing will be explained according to Götze (1951). For a better understanding, all important process steps are shown in figure 2.7. The process steps are indicated by boxes. The raw material for viscose fibres is cellulose which is delivered to the factory. This is shown in the upper left-hand corner of figure 2.7. The cellulose, is first treated with caustic soda to gain alkali cellulose. Thereby the cellulose is steeped into the soda before it is frayed. This step is also called steeping (first box of figure 2.7). The alkali cellulose is then pressed to squeeze out the caustic soda and the mat is shredded (second box of figure 2.7).

Next step is ageing (orange box in figure 2.7). This degradation process consists of highly complex degradation reactions which require the presence of oxygen and traces of transition metal ions. Therefore, in the presence of air, alkali cellulose is left to itself at low temperature or treated at high temperature for a short time period (Sixta). The aim of this step is to reduce the cellulose molecular chain to obtain viscose of sufficiently low viscosity.

After that, carbon disulfide and diluted aqueous NaOH are added to the matured alkali cellulose to form a solution of sodium cellulose xanthate. At last, the xanthate is dissolved by caustic soda in water to gain viscose. This step is called dissolving (light blue box in figure 2.7). After that, the viscose is filtered and vented. Thereby

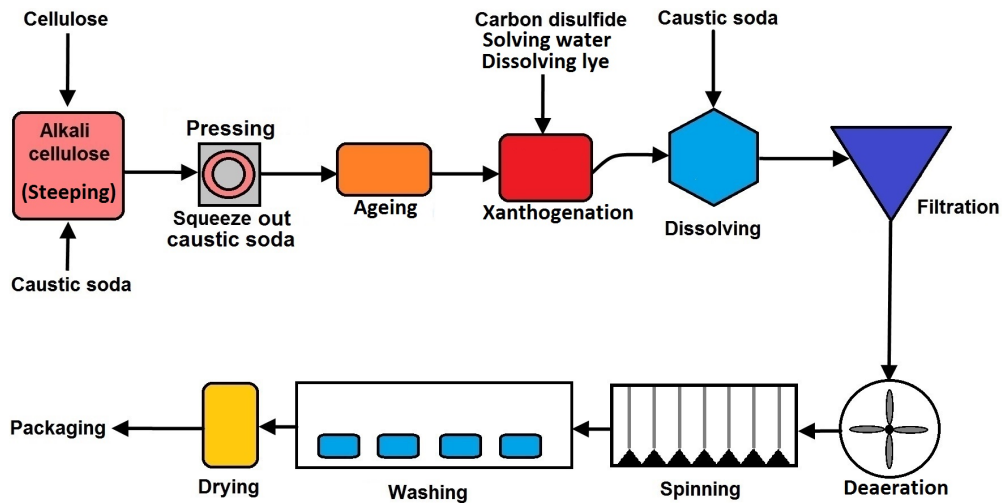


Figure 2.7: Workflow of the viscose manufacture.

the viscose receives spinnability.

At the spinning mill, the viscose is pressed through small holes of a spinning nozzle (symbolized by gray lines in the spinning-box of figure 2.7) into a spinning bath. The spinning bath consists of ammonium or sodium sulfate and acid sulfur in an excess. Zinc sulfate can be used as well as a modifier. Its presence retards the regeneration of cellulose. Thus, the fibres retain in a gel form. Consequently, the draw ratio can be increased which in turn increases the degree of orientation and thus the fiber tenacity (Sixta). The detailed composition of the spinning bath depends on the manufacturer (examples are found in Götze (1951)). In this bath the viscose stream solidifies to thin filaments. Depending on the chemical composition of both, viscose and spinning bath, the xanthate is more or less decomposed to hydrate cellulose.

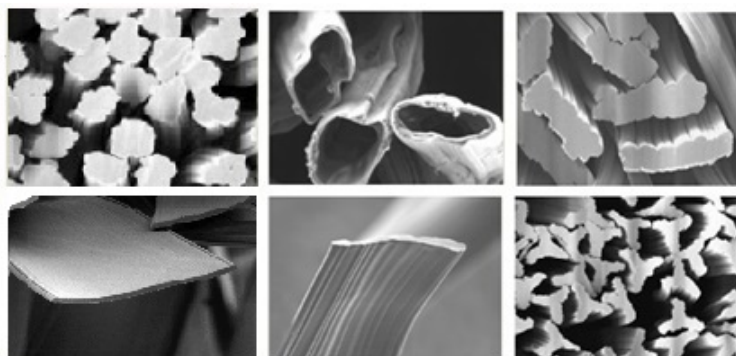


Figure 2.8: Overview of some viscose fibres with different cross sections. Images are adapted from Bernt 2010a.

The filaments contain several impurities like, salts, elemental sulfur and residual acid from the spinning bath. This dirt has to be removed by several washing steps (symbolized by four blue boxes in the washing square in figure 2.7). Finally the fibres are dried and packaged depending on the requirements of the customers.

Viscose fibres are so called regenerated fibres because they are regenerated from a viscose liquid. Hence, they are synthetic fibres. Depending on the spinneret, several cross sections are possible. Figure 2.8 shows some example of possible cross sections.

2.4 Bonding mechanisms in paper

In chapter 2.1 it was mentioned that the single fibres (paper fibres as well as viscose fibres) interact with each other. Joints between individual fibres occur. In doing so, a complex network is formed, a paper sheet. The strength of such a paper sheet depends on the strength of a single fibre and the strength and number of fibre to fibre joints (Page 1969, Torgnydottir and Wagberg 2003). According to Lindström et al. (2005) there are five mechanisms responsible for the formation of joints (visualized in figure 2.9).

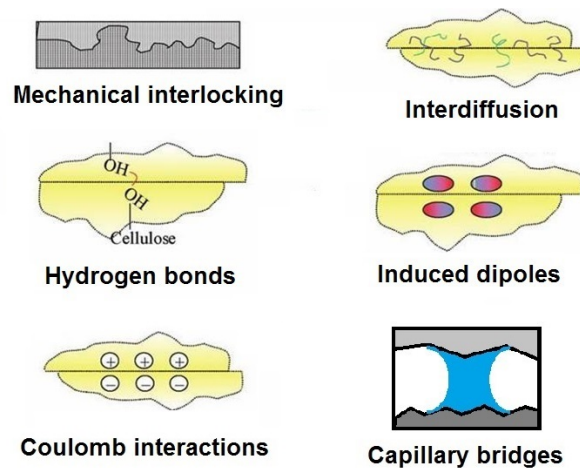


Figure 2.9: Illustration of the bonding mechanisms in paper; adapted from Lindström et al. (2005).

The surface of paper fibres is rough and rather deformable. They adjust towards each other during drying at the paper making process. Thereby an interlocking mechanism occurs. Furthermore, paper fibres show an entanglement of fibrils on their surface. These fibrils lead to mechanical entanglement. **Mechanical interlocking** implies both effects. Molecules may migrate from one fibre surface into another to create linkages between the surfaces. This bonding mechanism is called **interdiffusion**. **Hydrogen bonds** between the hydroxyl groups of cellulose and hemicellulose contribute

to the bonding force as well. Another bonding mechanism is given by **coulomb interaction** between the negatively charged fibre surface and positively charged components on another fibre. Finally, **van der Waals forces** are always present between the surfaces (Lindström et al. 2005).

Additionally to these bonding mechanism, it emerged that **capillary forces** also play an important role. Since water is needed to form a paper sheet, capillary forces can not be ignored (Persson et al. 2013).

2.4.1 Benefit of investigating viscose fibres

Figure 2.10 shows the used viscose fibres ((a) - round fibres, (b) flat fibres) and a bunch of unbleached kraft pulp fibres (c). Pictures were made by using an Environmental Scanning Electron Microscope (ESEM). Differences of the surfaces are seen.

As already mentioned, wood pulp fibres show an entanglement of fibrils on their surface. This can be seen in figure 2.10(c). The surface appears rough and flaked. In contrast to the surface of the viscose fibre which is shown in figure 2.10(a) and (b). The surface appears to be smooth and plain. No entanglement of fibrils is seen. Of course, viscose fibres also have fibrils but they are arranged in such a way, that no fibrillation occurs (Götze 1951). As mentioned in chapter 1.1 beating is used to roughen the fibre surface. Thereby the fibre is squeezed by mechanical shear which leads to external fibrillation. Even this mechanical treatment has no effect on the surface roughness of viscose fibres. It can therefore be considered that mechanical interlocking does not contribute to the joint strength of viscose fibre-fibre bonds. Hence, the influence of the remaining bonding mechanisms can be investigated by using viscose fibres.

In addition to the smooth surface, viscose fibres can be physical modified. By adding carboxymethylcellulose (CMC) to the viscose dope, fibres with improved charge density can be obtained (Duker and Lindström 2008). This also improves the bonding strength between single fibre-fibre joints which was found for paper fibres (Laine et al. 2002b) as well as for viscose fibres (Weber et al. 2013). Another way to improve the bonding strength is by adding cationic starch (CS), a polyelectrolyte, to the fibres (Kontturi et al. 2008, Weber et al. 2013). In this case positively charged fibres are obtained.

Viscose fibres are man-made cellulosic fibres made of a natural polymer. Hence, they can be produced under controlled conditions. All fibres show the same cross section, fibre width and length. Because of a smooth surface, no mechanical interlocking occurs. Therefore viscose fibres represent a simplified model of paper fibres. The influence of fibre length or width on paper sheet properties can easily be analysed by changing one of these parameters. Furthermore, anionic as well as cationic fibres can be produced by adding CMC or CS to the viscose dope. This gives the possi-

bility to investigate the influence of coulomb interaction on tensile strength of hand sheets and on bond strength of fibre-fibre joints without the influence of mechanical interlocking.

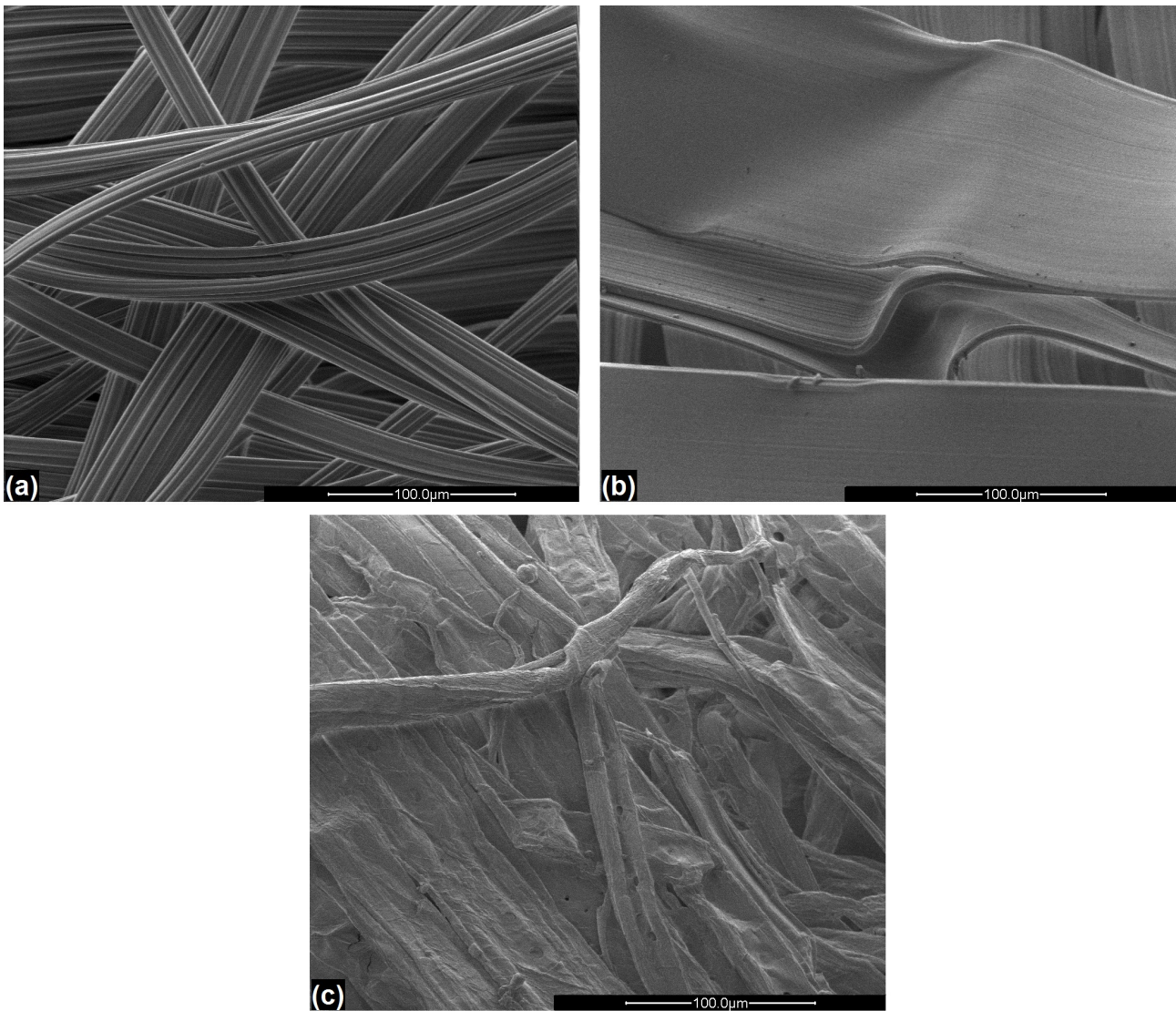


Figure 2.10: Comparison of a paper fibre and the used viscose fibres (ESEM); (a) round viscose fibres, (b) flat viscose fibres, (c) unbleached kraft pulp fibres. Images were made at FELMI Graz.

3 Analytical Methods

3.1 Fibre samples

Fibres of two different cross sections were investigated. Both cross sections are shown in figure 3.1. The fibres used in the first half of this thesis are shown on the left side of figure 3.1. The cross section of these fibres exhibits an irregular, cylindrical, almost kidney-shape, approximating a circular cross section. However, in a first approximation the cross section of these fibres is almost round. To simplify matters, these fibres will be called *round fibres* in this thesis although they are not totally round. In the second half, *very flat fibres* were analysed (right hand side of figure 3.1). Fibres with different charges of both fibre cross sections were investigated. The influence of anionic and cationic charges to the paper properties were analysed.

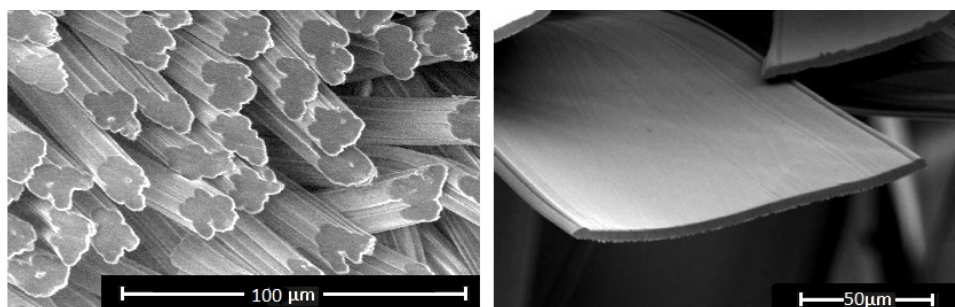


Figure 3.1: SEM images of the investigated fibres. The cross sections are seen. Left image was made at FLEMI Graz, right image is given by Bernt (a).

Round fibres Five different fibre samples were used for the measurements: a reference fibre without any additives (RF1), two anionic fibres (AF1, AF2) blended with

different amounts of CMC and two cationic fibres mixed with cationic starch (CF1, CF2). Additionally, pure CMC was used as a second reference for infrared measurements. The cross section of these fibres is shown on the left hand side of figure 3.1. The fibres had an approximate diameter of 20 μm and a length of 6 mm. Specific parameters of the used samples are given in table 3.1.

Table 3.1: Fibre parameters of the round viscose samples. Data was provided by Kelheim Fibres GmbH; adapted from Weber et al. (2013)

Fibre	Titer [dtex]	fibre strength [cN/tex]	COOH [%w/w]
RF1	2.34	22.85	0.767
AF1	2.55	21.58	2.603
AF2	2.56	20.20	3.777
CMC	-	-	16
			N [%w/w]
CF1	1.62	21.50	0.26
CF2	1.70	20.90	0.13

Titer and fibre strength were measured at Kelheim Fibres GmbH by using a Textechno H. Stein GmbH & Co. KG - FAVIMAT+. The titer (linear density) is determined by using the so called vibration method. Thereby, the resonance frequency of the sample is measured. Using a constant gauge length and a known pre-tension, the linear density can be calculated. Further information is given on the homepage of Textechno H. Stein GmbH & Co. KG. The amounts of COOH and N were also measured by Kelheim Fibres GmbH by titration (see chapter 3.4). A COOH amount of 0.77% for RF seems to be rather high (typical values are 0.3 - 0.5%). According to Sixta et al. (2004) viscose fibres exhibit a maximum amount of 50 mmol COOH/kg or 0.23%, respectively. However, the given values were delivered by the industrial partner. Even if this value seems to be remarkable high, it was used with confidence in accuracy. Nevertheless, further investigations of the COOH content of the used samples appears to be appropriate (see chapter 7). Since pure CMC cannot be titrated (Bernt c), this value was calculated. Based on a degree of substitution of DS=0.77 a COOH amount of 16% is obtained.

Flat fibres Flat fibres (cross section shown in figure 3.1) with 4 dtex (F4), 9 dtex (F9), 12 dtex (F12) and 22 dtex (F22) were investigated. Additional fibres of 9 dtex modified by the introduction of CMC (F9A), cationic starch (F9C) and both additives (F9AC) were studied. Therefore, seven different fibres of this cross section were used. All used fibres had a length of 6 mm, except for F12 and F22 which had a length of 12 mm. The specific parameters of these fibres are shown in table 3.2.

Again, titer, fibre strength and the amounts of COOH and N were measured at Kelheim Fibres GmbH by using a FAVIMAT+ and by titration, respectively (information

Table 3.2: Fibre parameters of the flat viscose samples. COOH/N values of F4, F12 and F22 were not analysed.

Fibre	Titer [dtex]	fibre strength [cN/tex]	COOH [%w/w]	N [%w/w]
F4	4.31	19.85	-	-
F12	11.53	17.80	-	-
F22	25.07	17.82	-	-
F9	9.56	19.25	0.52	-
F9A	9.17	14.80	2.54	-
F9C	9.66	16.44	-	0.25
F9AC	9.34	11.22	1.42	0.31

about the titration method are given in chapter 3.4). Incorporation of CMC was done according to Bernt (2010b) and Smith (1980). Thus, using a conventional rayon spinning equipment, an aqueous alkaline solution of sodium carboxymethylcellulose is injected by a metering pump into the viscose stream. The blend of viscose and sodium CMC is then extruded through a spinneret into the spinning bath (see chapter 2.3.1). More details about the incorporation of CMC to the viscose dope are given in Smith (1980) and Smith (1981). The qualitative and quantitative composition of the used CMC is proprietary information of Kelheim Fibres GmbH. Specification of the chemical structure of the used cationic starch, as well as the incorporation into the used fibres is also proprietary information of Kelheim Fibres GmbH. The determination and the amount of the additives is presented in chapter 3.4.

3.2 Swelling

The influence of charges on the swelling behaviour on single fibres was investigated like shown in figure 3.2. First the microscope (Leica Microsystem, Type 301-371.010) that was used had to be calibrated by using a stage micrometer according to Weber et al. (2013):

„A picture of the micrometer at a given magnification was made. After that, the number of pixels within 1 μm was counted. By this means, the length of 1 μm within a picture made at this magnification is obtained. The fibre width was determined by counting the pixels and converting the number to μm .“

After calibration, the fibre width could be measured. The test assembly is given in figure 3.2. One end of a single fibre was fixed by super glue on a glass slide. Images of the dry fibre were taken near the glue point and near the free end by using a digital microscope camera (Leica DFC 290) mounted on the microscope. The average width of both measurement points was taken and used as fibre width. Since viscose fibres do not show cone-shaped ends like paper fibres, these measurement points are usable. Next, the fibre was moisturised by deionized water and the fibre width was investigated again. Since swelling occurs almost instantly, the wet fibres were anal-

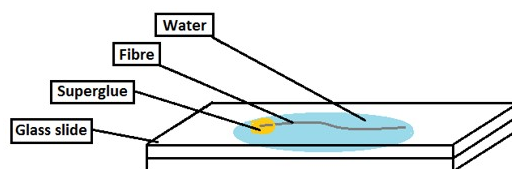


Figure 3.2: Schematic arrangement of swelling determination.

used immediately after wetting. The difference between the fibre in dry and wet state was taken as the amount of swelling.

3.2.1 Environmental scanning electron microscope

Additionally, the swelling was investigated using an Environmental Scanning Electron Microscope (ESEM). The ESEM allows to investigate wet and uncoated samples within a gaseous environment in the specimen chamber. Because of a low-pressure water vapour atmosphere, in situ hydration experiments are possible (Jenkins and Donald 1997).

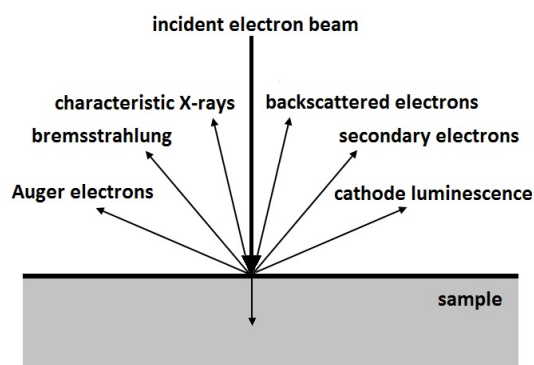


Figure 3.3: Schematic diagram of the signals generated and used in a SEM, adapted from Grogger (2008).

The sample surface is scanned by a high energy electron beam with a diameter of only a few nanometers. The beam interacts with the sample producing several signals containing information about the investigated sample surface. Figure 3.3 illustrates the generated signals which are used for analysis. Information is obtained from backscattered electrons, secondary electrons, characteristic and bremsstrahlung X-rays, as well as Auger electrons and cathodoluminescence. A detailed description of the SEM is given in Reuter (2010) and Grogger (2008). Using an ESEM, no sample preparation is used, and insulating samples can be analysed without any coating. Since the environmental gas is ionized by the electron beam, charge compensation occurs. Consequently, swelling can be investigated by this measurement method.

ESEM measurements were done at the Institute for Electron Microscopy and Nanoanalysis (FELMI) of Graz University of Technology using a FEI ESEM Quanta 600 FEG. The samples (single viscose fibres) were placed on a peltier cooled specimen stage to sustain water on it inside the specimen chamber. This thermoelectric cooling device is shown in figure 3.5 and figure 3.6. By cooling the sample in conjunction with specimen chamber pressure condensation on the sample takes place. A detailed description of the cold stage assembly is found in the corresponding manual (Dufek and Hayles). A brief specification will be given below.

3.2.1.1 The Peltier effect

The cooling device is based on the so called Peltier effect. If current, I , is applied to an electric circuit made of two different metals, A and B, heating and accordingly cooling occurs at the soldering joints (Bergmann et al. 2006). Figure 3.4 illustrates this effect. According to Bergmann et al. (2006), the following applies

$$dW/dt = \Pi_{AB}I \quad (3.1)$$

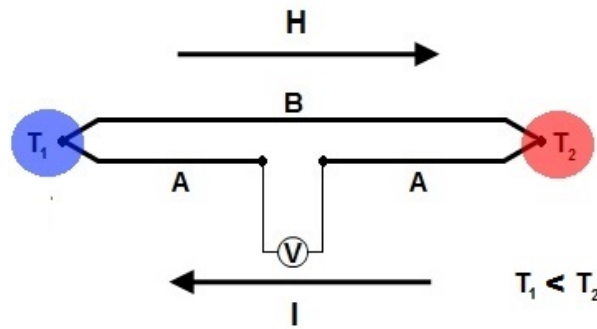


Figure 3.4: Illustration of the Peltier effect; I - current, H - heat, A - metal one, B - metal two, V - voltage source, T_1 - temperature at soldering joint 1, T_2 - temperature at soldering joint 2.

with W , the liberated heat or heat input, and Π_{AB} , the so called Peltier coefficient. The left side of equation 3.1 describes a thermal capacity, the right side an electric capacity. Hence Π_{AB} represents a voltage and is given by the difference of the Peltier coefficients of the metals A and B (see equation 3.2 (Bergmann et al. 2006)).

$$dW/dt = (\Pi_A - \Pi_B)I \quad (3.2)$$

The coefficients Π_A, Π_B are material constants which are depending on the temperature and represent how much heat is carried per unit charge. An approximation is given by equation 3.3. Thus, Π_A is a product of the thermal energy of a conduction electron kT , divided by the electron charge e and multiplied the ratio of the thermal activated conduction electrons T/Θ_F (Θ_F = Fermi-temperature) (Bergmann et al. 2006).

$$\Pi_A = (kT/e)(T/\Theta_{F,A}) \quad (3.3)$$

The Peltier effect originates from a heat flow which is given in a uniform conductor of constant temperature if current is applied. This thermal flow is caused by different flow rates of the conduction electrons which depends on the energy of the electrons. Because of the negative charge of the electrons, the heat flows in the opposite direction of the current. The quantity of this flow is given by $\Pi \cdot I$. Since Π is a material constant, different heat flows are given for metal A and B at the same current flow. This leads to a warming of one joint and cooling of the other (Bergmann et al. 2006).

3.2.1.2 The cooling unit

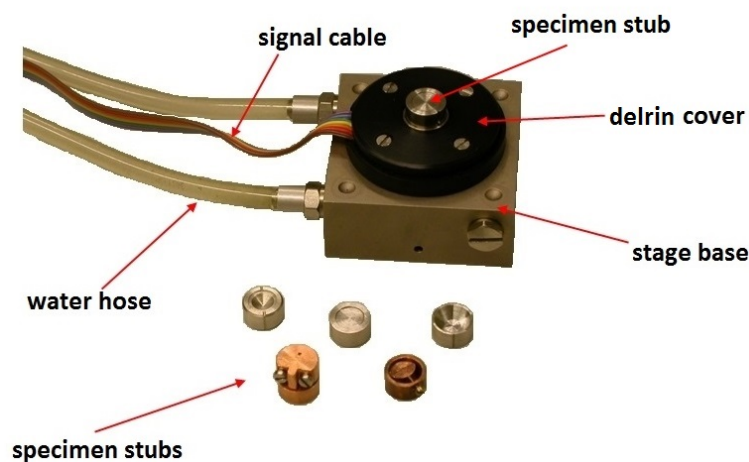


Figure 3.5: Cold stage assembly - the various components of the cooling unit (Zankel).

Figure 3.5 gives an overview of the peltier cooled specimen stage. The temperature is altered by a thermoelectric module. It consists of PN semiconductor elements forming a so called wafer. If current is applied to this wafer, one side will heat and the opposite side will cool. The heat of the hot junction has to be removed. This is done by an external water chiller which allows continuous measurement. The water hose of the chiller are seen in figure 3.5. The temperature is measured by a resistive temperature device (RTD shown in figure 3.6) which is located within the specimen stub holder, in which the specimen stub is applied. The entire assembly is hold in place by a delrin cover. On figure 3.5 also the signal cable is seen, which is permanently attached to the stage base. Several sample holders are available depending on whether flat or powdery samples are investigated (Dufek and Hayles).

The sample is fixed on the specimen stub by double-sided adhesive tape. After that, the stub is mounted on the specimen stub holder. Figure 3.6 shows the cold stage

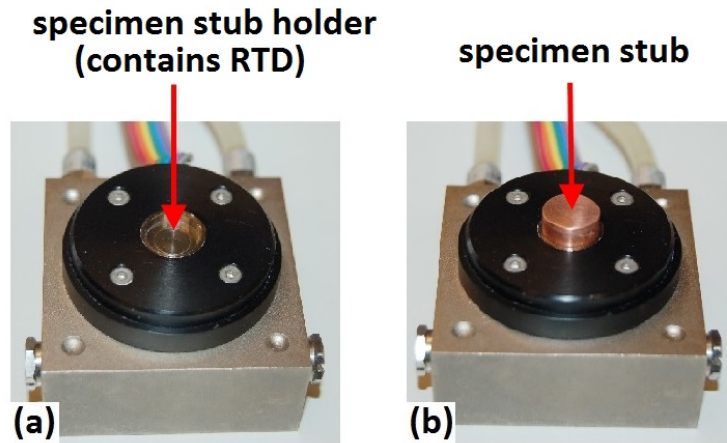


Figure 3.6: Cold stage assembly without and with specimen stub (Zankel).

assembly before (a) and after (b) the stub is mounted. After the cooling device (including the sample) is placed in the specimen chamber, the chamber is evacuated. Condensation is achieved by first cooling down to 3°C. Afterwards, the pressure is raised until water condensation takes place.

3.3 Breaking length

In order to reduce production costs of paper, tensile strength has to be increased while density is decreased at the same time. A connection of both is given by the specific strength in equation 3.4 (Gobecht 2009),

$$\sigma^* = \frac{\sigma}{\rho} \quad (3.4)$$

with, the tensile strength, σ , and the density, ρ , of the tested sample. In material technology this parameter often is divided by the gravitational constant, to obtain the so called breaking length (see equation 3.5) (Gobecht 2009). Breaking length is generally understood as the maximum length of a vertical column of a paper strip (assuming a fixed cross-section) that could suspend its own weight when supported only at the top.

The breaking length is determined by tensile strength measurement. Thereby the force needed to rip a strip of paper is measured. Knowing the paper density, the breaking length can be calculated, according to equation 3.5 (ISO 1924-2) (Gobecht 2009).

$$L_R = \frac{\sigma^*}{9.81} = \frac{\sigma \cdot 102000}{m_A \cdot b} \quad (3.5)$$

The breaking length (L_R [m]) is obtained by the measured tensile strength (F [N])

divided by the grammage (m_A [g/m²]) and sample width (b [mm]). The grammage is given by equation 3.6. Hence, the grammage is obtained by dividing the mass of handsheet [g] by the area of a handsheet [m²].

$$m_A = \frac{m}{A} \quad (3.6)$$

Handsheets were made using a Rapid-Köthen sheet former (DIN EN ISO 5629-2:2004). By using a FRANK Prüfgeräte GmbH Zugprüfmaschine, horizontal, model number 81502, tensile strength of handsheets was measured according to the ISO standard number 1924-2:2008 after sample conditioning (DIN EN 20187:1993).

3.4 Titration

Charge is introduced by incorporation of COOH- and N-groups. Hence, the charge value is given by the amount of these groups. The determination of the total fibre charge occurs by an acid-base titration and was done at Kelheim Fibres GmbH immediately after the fibre production. The measurement method used by Kelheim Fibres GmbH is very similar to the technique described below. However, details about the determination are considered property by Kelheim Fibres GmbH.

The same applies for the determination of cationic charges. The measurement method is based on Kjeldahl (1883) but details are proprietary information of Kelheim Fibres GmbH.

In addition to the measurements done at Kelheim Fibres GmbH, total charge as well as surface charge were analysed at Mondi Frantschach GmbH. The pulp was turned to an acid hydrogenated form and titrated with 0.1 M NaOH. The determination of the surface charge was done by adsorption of a cationic polyelectrolyte, polydiallyldimethylammonium chloride (poly-DADMAC) on pulp in sodium form. Afterwards the filtrate was titrated with a colour indicator and 0.001 N potassium polyvinyl sulfate (KPVS).

Pretreatment of the samples The fibre samples were first washed with an excess of 10⁻² M HCl (pulp consistence around 1%) to remove the metal ions. The pH was set to 2 and kept constant for 30 min. Then the samples were washed with deionized water until the conductivity was below 5 μS/cm. For surface charge determination the samples were then washed with an excess of 10⁻³ M NaHCO₃ (consistence again ~1%). After that, the pH was adjusted to 9 with NaOH and held constant for 30 min. The samples were washed again with deionized water until the conductivity was below 5 μS/cm. The samples were then in the so called sodium form (Horvath et al. 2006).

Total Charge Determination The total charge of the samples was determined accord-

ing to Horvath et al. (2006), Horvath and Lindström (2007) and Katz et al. (1984) by conductometric titration. After pretreatment of the samples 1 g of the pulp was put to a mixture of 10 mL 10^{-2} M NaCl and 5 mL 10^{-2} M HCl. The samples were titrated by 5×10^{-2} M NaOH and the conductivity of the solution was measured.

Surface Charge Determination This measurement is based on the method developed by Katz et al. (1984). Pulp in its sodium form, at a concentration of 5 g/L was used. Polydiallyldimethylammonium chloride (poly-DADMAC) was added to the pulp and the suspension was agitated for 30 min. The fibres were separated from the solution by filtration, dried and the dry weight was measured. Afterwards the filtrate was titrated according to Terayama (1952) in order to determine the amount of poly-DADMAC adsorbed. Since poly-DADMAC is a cationic polyelectrolyte, this measurement was unapplicable for the cationic fibre samples.

3.5 Infrared spectroscopy

A fast and nondestructive approach for surface chemical analysis is given by infrared spectroscopy. The spectrometer used for the determination of the surface chemistry is a Bruker ifs66 v/s Fourier transform infrared (FTIR) spectrometer. A detailed description of the principles of FTIR as well as the measurement equipment is given in Koch (2009) and Gilli (2008). The main part of the FTIR spectrometer is a Michelson interferometer (figure 3.7). It consists of a fixed and a movable mirror (M1 and M2 in figure 3.7) and a beam splitter. Like the entire setup of the spectrometer, the interferometer is inside a vacuum vessel. The movable mirror (M2) is not mechanically connected to the cage but nitrogen gas cushioned. Therefore, the whole optical path is only evacuated down to a pressure of around 2 mbar. Nevertheless, water and carbon dioxide absorption bands as well as air disturbances during the measurement are avoided.

As the beam of light comes from the silicon carbide (SiC) globar (IR-source in figure 3.7), it encounters a germanium-potassium bromide (Ge/KBr) beam splitter. The two partial beams are reflected by the mirrors M1 and M2 in such a manner that the beams are superimposed on to each other, thus causing interference. The superimposed beams are guided to the sample compartment where they interact with the sample. The infrared light is absorbed which leads to vibrational excitations of the molecular bonds. These are characteristic for each bond that is why chemical information of the sample is obtained. In the end, the light is detected by an external mercury-cadmium-telluride detector (MCT-detector). The MCT-detector is a so called quantum detector which is based on the excitation of electrons to a higher energy state by radiation (Connors and Banerjee 1995). Since very low energies have to be sensed in the mid-infrared region, electrons could be excited by thermal agitation in the detector. This effect leads to deterioration of the signal to noise ratio. Therefore, cooling with liquid nitrogen is necessary to gain sufficient sensitivity (Griffiths and de Haseth 1986).

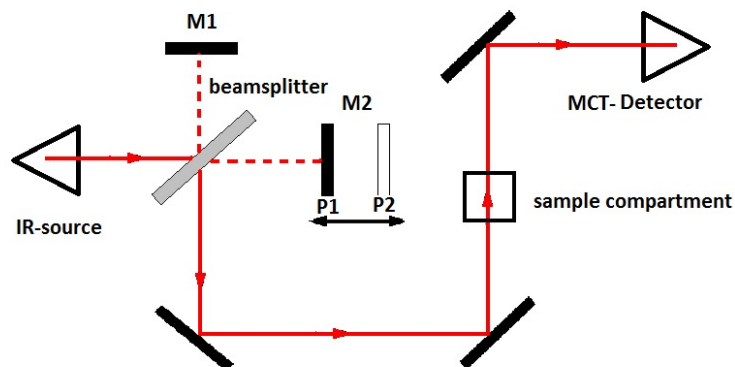


Figure 3.7: Schematic view of a Michelson interferometer; M1 - fixed mirror, M2 - movable mirror, P1 - position one, P2 - position two; adapted from Weber (2010).

A FTIR-spectrum is obtained by first measuring an interferogram of a reference sample. This is then transformed into a single channel signal by Fourier transformation to obtain the so called single channel reference spectrum (R). Next, an interferogram of a sample which has to be investigated is measured. Again, this interferogram is turned into a single channel sample spectrum (S) by Fourier transformation. At last, the transmission spectrum T is received according to equation 3.7 (Herres and Gronholz 1984)

$$T = \frac{S}{R} \quad (3.7)$$

3.5.1 Attenuated total reflection infrared spectroscopy

Since the reflectivity of the samples contribute to the transmission spectrum, problems may occur, if the investigated samples show different reflectivities. This is the case for paper hand sheets because of different flocculation. Peaks may grow or shrink due to different reflectivities. Hence, it is not possible to distinguish if a peak grows due to a change in chemistry or a change in reflectivity of the sample. Attenuated total reflection (ATR) IR spectroscopy is a way to overcome these troubles. First introduced by Harrick (1960) and Fahrenfort (1961) this technique uses an optical near field effect which occurs at total internal reflection.

Figure 3.8(a) shows the reflection of light at an interface. When a ray of light from an optically denser medium 1 enters into an optically less dense medium 2 ($n_1 > n_2$) the following connection exists between the angles and the refraction indices (Demtröder 2013):

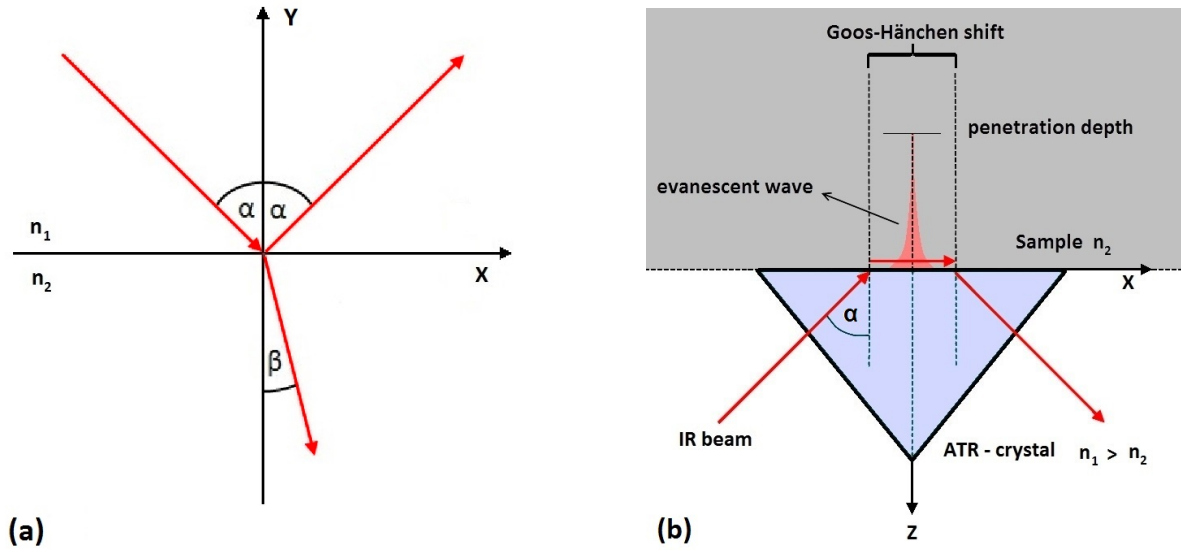


Figure 3.8: Principle of ATR measurement - (a) Reflection at an Interface (x-y-plane); (b) The path taken by the source during internal reflection sampling. The evanescent wave and the Goos-Hänchen shift are pictured as well.

$$\sin\alpha = \frac{n_2}{n_1}\sin\beta \quad (3.8)$$

Equation 3.8 is known as Snell's law. For penetrating into medium 2, $\sin\beta$ cannot become more than 1 from which follows (Demtröder 2013):

$$\sin\alpha \leq \frac{n_2}{n_1} \quad (3.9)$$

On the other hand, if $\sin\alpha > n_2/n_1$ the light is totally reflected at the interface. The angle α_c for which

$$\sin\alpha_c = \frac{n_2}{n_1} \quad (3.10)$$

is the critical angle of total internal reflection (Demtröder 2013). For total internal reflection two conditions must be fulfilled:

1. The light has to move from a material with a higher optical density to one with a lower optical density
2. $\alpha > \alpha_c$

However, even at total reflection the wave penetrates into the rare medium. The intensity of this so called evanescent wave decays exponentially with distance from the surface, leading to a near field effect (Demtröder 2013). The penetration depth d is given by (Griffiths and de Haseth 1986):

$$d = \frac{\lambda}{2\pi \sqrt{n_1^2 \sin^2 \alpha - n_2^2}} \quad (3.11)$$

Knowing the refractive index n_1 of the hemispherical diamond (ATR crystal) and of regenerated cellulose n_2 ; the incidence angle γ of the IR beam and the wavelength λ , d can be calculated.

The evanescent wave, as well as the whole process of total reflection at the sample surface is shown in figure 3.8(b). While exponentially decreasing, the energy of the wave travels parallel to the sample surface until it is reflected. This causes a lateral displacement in x -direction (shown in figure 3.8(b)) of the reflected light which was first detected by Goos and Hänchen (1947). While the light is totally reflected, parts of the evanescent wave are absorbed by the optically rare medium. This absorption is detected in the spectrometer and serves as the basis for ATR-IR spectroscopy.

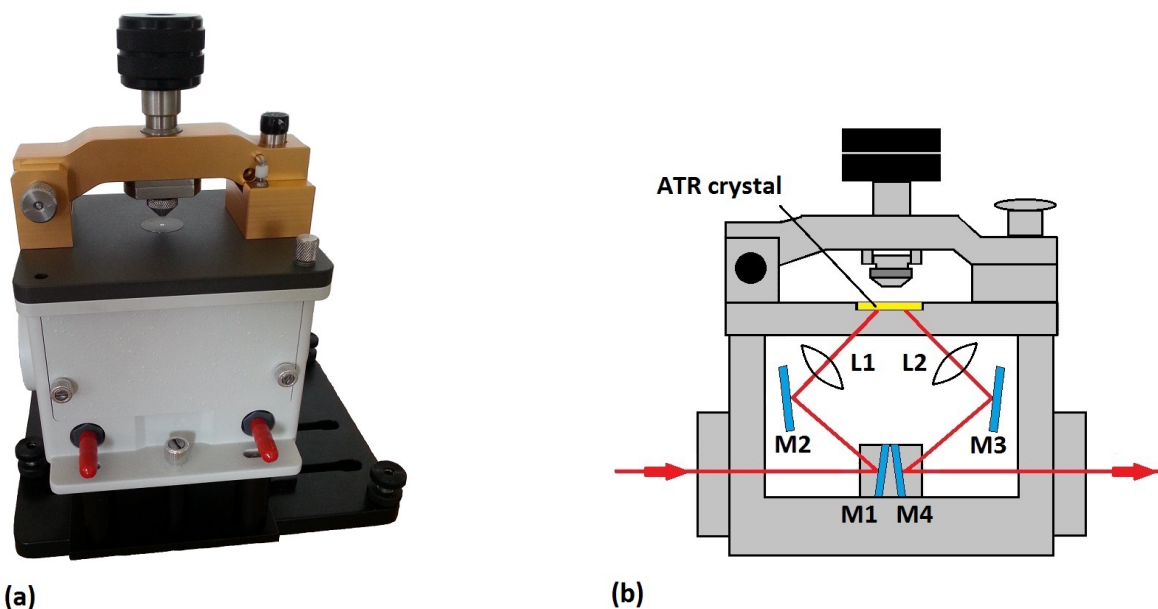


Figure 3.9: The ATR unit and the optical path within - (a) the Specac MKII Golden Gate Single Reflection ATR unit; (b) a schematic view of the ATR unit and the optical path of the IR beam.

ATR measurements were done using a MKII Golden Gate single reflection ATR setup by Specac Inc., shown in figure 4.11(a). A hemispherical diamond is used as ATR crystal. Figure 4.11(b) illustrates the optical path within the ATR unit. The beam enters the ATR unit on the left hand side, being reflected on two mirrors (M1 and M2) before it is focused on the ATR crystal by a lens (L1). After total internal reflection

the beam of light is aligned parallel by L2 and guided to the detector by two more mirrors (M3 and M4). The ATR setup was placed into the sample chamber (figure 3.7) of the Bruker ifs66v/s spectrometer.

3.6 X-ray photoelectron spectroscopy

X-ray photoelectron spectroscopy (XPS), first named "electron spectroscopy for chemical analysis" (ESCA) was developed by Siegbahn et al. (1967). It began to appear as commercial instrumentation in the mid-1970s. Nowadays XPS is one of the most versatile and applicable surface analysis techniques. The essential elements are the light source, the electron energy analyser and a detector system. A schematic view of the experimental configuration is given in figure 3.10. Usually a X-ray tube is used as light source, emitting monochromatic X-ray photons at constant potential and current, superimposed on a bremsstrahlung background. The most common anode materials are aluminium and magnesium, providing characteristic radiation. Often they are combined as a switchable twin-anode which allows to separate photoemitted electrons or Auger electrons, whose energies are fixed. A disadvantage of these X-ray sources is the limited energy resolution as a consequence of the inherent energy width of the lines. Therefore, narrowing of the excitation energy has to be done. One way to do this is by using monochromators. While the line width is narrowed by this way, the intensity is limited as well. To compensate the loss in intensity a multichannel detection system is used (Ertl and Küppers 1974).

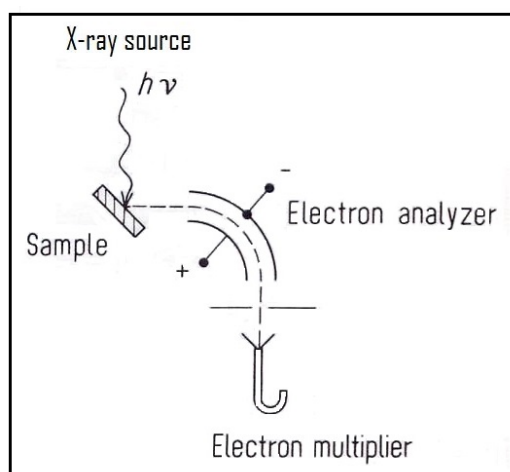


Figure 3.10: Schematic arrangement of a typical XPS system; adapted from Ertl and Küppers (1974).

The principle behind XPS-measurements can be explained with a few sentences: when a sample is exposed to the X-radiation, bound electrons can be knocked out, if the energy of the photons is greater than the binding energy. Thus, the kinetic energy (E_{kin})

of an ejected electron is given by equation 3.12 where $h\nu$ is the energy of the incident X-ray photon and E_b the binding energy of the electron in its orbital (Connors and Banerjee 1995).

$$E_{kin} = h\nu - E_b \quad (3.12)$$

To calculate the binding energy via XPS measurements, the work function of the detector (ϕ_{sp}) also has to be known since the electrons are selected by the analyser with respect to the vacuum level, as illustrated in figure 3.11. The energetic level diagram for X-ray spectroscopy (figure 3.11) visualizes how the binding energy value is obtained. The X-ray photon energy $h\nu$ is absorbed by an electron at an energy level E_b below the Fermi level E_F . Measuring of the kinetic energy E_{kin} will give the binding energy E_b of the ejected electron according to equation 3.13 (Ertl and Küppers 1974). In this way, the chemical composition of a given sample surface can be analysed.

$$E_b = h\nu - E_{kin} - \phi_{sp} \quad (3.13)$$

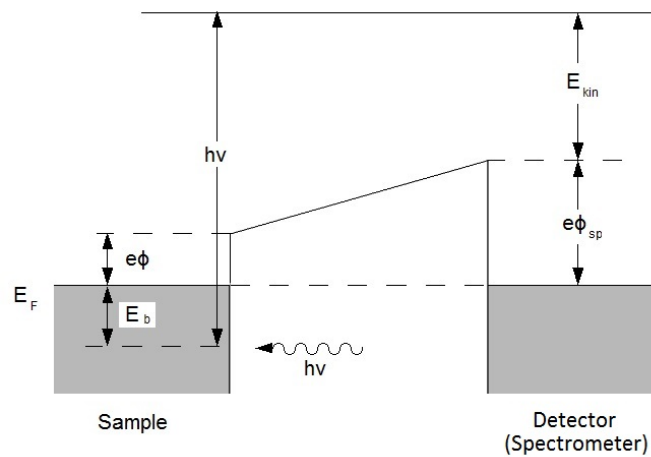


Figure 3.11: Energy level diagram for XPS; adapted from Ertl and Küppers (1974).

Figure 3.11 visualizes the situation for a metal surface, where the sample is electrically connected with the spectrometer. Hence the Fermi energies of both, sample and detector, are at the same level. The Fermi level is given by the onset of the electron emission at the highest kinetic energy. Thus, the Fermi level can be easily determined for metal surfaces. The situation is different for semiconductors, where the emission occurs at the valence band edge but not at the Fermi level. In the case of insulating materials, like paper, the sample becomes charged and fixing the energy scale is more complicated. To overcome these troubles the spectra have to be calibrated. The C 1s peak of ubiquitously present carbon is used for this purpose as a reference.

The analysing depth is given by the mean free path of the emitted electrons. According to Connors and Banerjee (1995) for paper it is in the range of 0.5-10 nm. The

ejected electrons typically have a kinetic energy between 0 to 1500 eV. Because of this low kinetic energy, they cannot travel large distances in matter. Therefore, high vacuum is necessary. Furthermore, a clean vacuum is required to prevent scattering on air molecules. Scattered electrons comprise the background, so only photoelectrons which originate from the sample without any loss in kinetic energy contribute to a XPS peak (Connors and Banerjee 1995).

The analysis of the chemical composition of a surface, by XPS, is based on the fact that the ionization probability of a core level is almost independent of the valence state of the investigated element. Hence, the integrated area below a certain peak is proportional to the number of atoms in the examined area. Before integrating, the background has to be subtracted. This is mostly done by simply drawing a straight line between two proper points (Ertl and Küppers 1974).

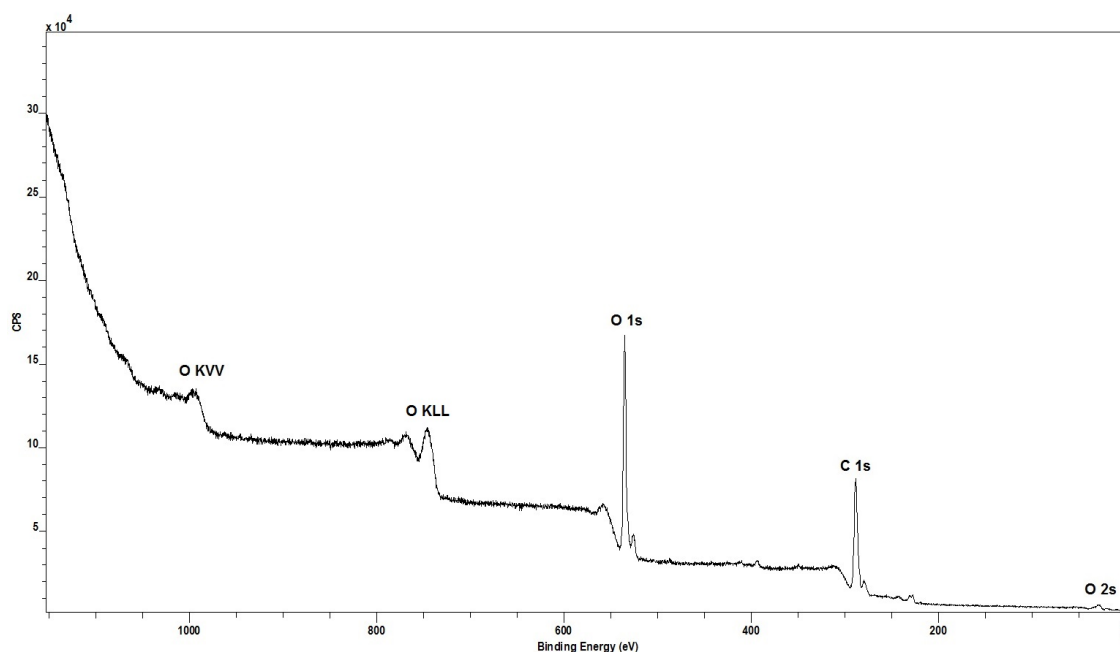


Figure 3.12: X-ray spectrum of cellulose; peaks were identified by using Beamson and Briggs (1992) and the CASA XPS software.

XPS measurements were done at the Institute of Physics at the University of Graz with the help of Georg Koller using a SPECS Phoibus 150 electron energy analyser and a non-monochromated Mg $K\alpha$ (1253.4 eV) X-ray source (Weber et al. 2013). Hence, an overall energy resolution of 0.8 eV was obtained. Samples of 10x10 mm were cut from hand sheets and mounted on a standard SPECS sample plate by conductive carbon tape. To ensure a good vacuum in the measurement chamber, the samples were stored there for 12 hours before measurement. Thus, a pressure better than 3×10^{-9} mbar was given during the measurements. Peak-evaluation was done by

the CasaXPS software (Version 2.3.14dv38). The data set was fit in consideration of physical and chemical correctness. In this way, the number of possible solutions was limited. Finally, the binding energy of all spectra was calibrated according to the literature (Connors and Banerjee 1995). As already described, the C 1s peak was used as reference (Ertl and Küppers 1974).

In figure 3.12 a XPS-spectrum of cellulose is shown. Characteristic peaks are C 1s and O 1s. 1s means that the electron comes from the 1s-Orbital. Additional there are the O KVV peak, which is an Auger-peak and the O 2s peak from the valence band.

3.7 Atomic force microscopy

In order to get information about the surface topography as well as the softness of the investigated fibres, atomic force microscopy (AFM) and AFM nanoindentation (AFM-NI) was used. An overview of the advantages of AFM measurements as well as a description of the possible measurement modes are given by Niemi et al. (2002). The principle of AFM is rather simple (see figure 3.13). An atomically sharp tip is scanned over the sample surface. The distance between tip and sample surface is only a few Ångström. Since the distance is very small, forces start to influence the cantilever to which the tip is attached. A laser beam is directed to the cantilever, so the deflection is proportional to the force according to Hooke's law (Niemi et al. 2002):

$$F = k \cdot \Delta z \quad (3.14)$$

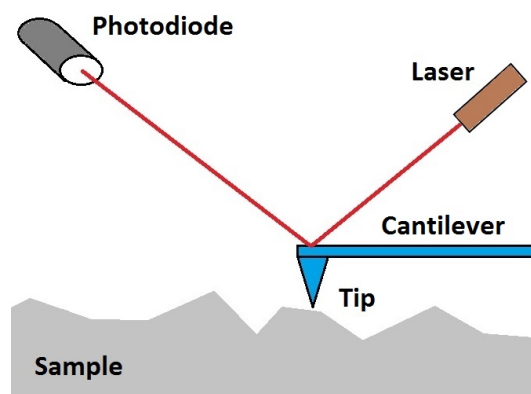


Figure 3.13: Principle of atomic force microscopy.

Hence the force is equal to the spring constant k multiplied by the deflection Δz . The deflection of the cantilever is monitored by using a photodetector (shown in figure 3.13). Thus, a three-dimensional (x, y, z) topographic picture of the sample surface is obtained from the deflection. The AFM can be operated in constant height (height of the tip fixed) or constant force mode (deflection fixed). Nearly no sample preparation

is needed. However, the sample should be relatively flat since the maximum z-height movement is only a few micrometers. Samples are usually fixed on a metal plate with tape or glue. Quite generally, there are two possible modes, contact mode and tapping mode:

3.7.1 Contact mode

In this mode, the tip is in very smooth contact with the sample surface. Hence, the dominant forces are the long-range van der Waals interaction (0.2-100 nm (Niemi et al. 2002)) and capillary forces. The interacting forces can be attractive or repulsive. Since the distance between tip and sample is very small, damages of the tip and of the surface by scratches are possible. Because of that, contact mode is normally used for "hard" surfaces and for high resolution imaging.

3.7.2 Tapping mode

The viscose fibres were investigated in tapping mode, a technique especially for "soft" or fragile samples. In contrast to contact mode, in tapping mode the cantilever is oscillated with high amplitude near its resonance frequency (80 kHz). During the measurement, the tip is touching the surface gently without sticking which is called tapping. Information is obtained by the variation of the amplitude during scanning. The sample surface is not damaged and a three-dimensional topographic image is received.

All AFM and AFM-NI measurements were performed at Montanuniversität Leoben by Christian Ganser using an Asylum Research MFP-3D AFM. A planar closed loop scanner and an Asylum Research closed fluid cell were used for topography measurements as well as for AFM-NI. For AFM-NI the investigated fibres were fixed on the sample holder by a droplet of nail polish. After that, the fibre surface was scanned in tapping mode to find a region with low roughness. Next, the tip was pressed on the sample surface for 10 s to a maximum load of 10 μN . Finally, to compensate thermal drifts and creep effects, the tip was pressed again for 30 s at 0.5 μN . The used loading and unloading rate was 10 μNs^{-1} (Persson et al. 2013 and Ganser et al. 2013).

The surface hardness is calculated according to Ganser et al. (2013):

$$H_{AFM} = \frac{P_{max}}{A_C} \quad (3.15)$$

where P_{max} is the maximum force and A_C the contact area at the contact depth h_C when P_{max} is applied. The contact area is determined by the tip. Hence, the tip shape has to be checked by a TGT1 tip characterization grid (more details about this are found in Ganser et al. (2013)). To investigate the softness of wet fibres, a fluid cell was used. The fluid cell is filled with a mixture of completely dry and humid nitrogen. By

varying the flow rate of both gases, the relative humidity can be controlled. Therefore, dry as well as swollen fibres can be investigated by AFM-NI.

More details about this measurement technique can be found in Niemi et al. (2002), Persson et al. (2013) and Ganser et al. (2013).

3.8 Nitrogen adsorption measurements

Using nitrogen adsorption for surface determination of cellulosic material was used for the first time by Emmett and DeWitt (1941). The method is based on the estimation that nitrogen is not adsorbed on areas involved in bonding. Therefore it should provide an excellent tool for the measurement of unbonded area of cellulosic material.

The surface area is obtained by selecting on an adsorption isotherm the point corresponding to a monolayer. By multiplying the number of molecules required to form a single layer by the average surface area covered by adsorbed molecules the absolute area is received.

Nitrogen adsorption measurements were done by Karin Flöttinger and Astrid Kitla at the institute of materials chemistry at Vienna University of Technology. The specific surface was calculated using a Micromeritics ASAP 2020 instrument. Two samples of each investigated fibre type were analysed, a strip of a handsheet and a bunch of unbonded fibres. The unbonded fibres were obtained after solvent drying according to Haselton (1955). Since the fibres are bonded within the strip, the relative bonded area should be given by the differences of strip and fibre bunch area.

3.9 Light scattering

Light scattering measurements were done to determine the scattering coefficient of viscose hand sheets. This was done to calculate the relative bonded area (RBA) within the paper sheets. More about the determination of the RBA will be found in chapter 5.2.

Mathematical description of the optical properties of cloudy and unclear media is done by the so called Kubelka-Munk theory (Kubelka and Munk 1931, Kubelka 1948). A connection between scattering coefficient S , absorption coefficient K and reflection coefficient R is established by this theory. A short derivation of this correlation will be given below, according to Schmidt (1976).

First of all, some requirements and simplifications have to be done. Based on the assumption that the investigated medium is a homogeneous and ideally scattering matter, S and K are introduced. The incident light has to be diffuse and monochromatic.

Although paper does not fulfill the requirement of being a homogeneous matter, the Kubelka-Munk theory can be applied to compare the optical properties of different samples (Schmidt 1976). Similar to tensile strength measurements, S and K are determined for a certain handsheet made under certain circumstances. Therefore it has to be considered, that no absolute value for S , K or opacity is obtained (Schmidt 1976). Nevertheless, changes of optical properties due to mechanical or chemical treatments of the pulp can be seen.

A given sample of a thickness X is irradiated by a luminous flux i (see figure 3.14). Within a layer dx the light is extenuated by $-(k+s) \cdot i \cdot dx$. The light undergoes this weakening at the whole way to the background, where it will be reflected. The reflected light, marked as j , experiences again a weakening of $-(k+s) \cdot j \cdot dx$. Additionally to this attenuation, scattered light from i contributes to j . The overall change of the luminous flux is therefore (Schmidt 1976):

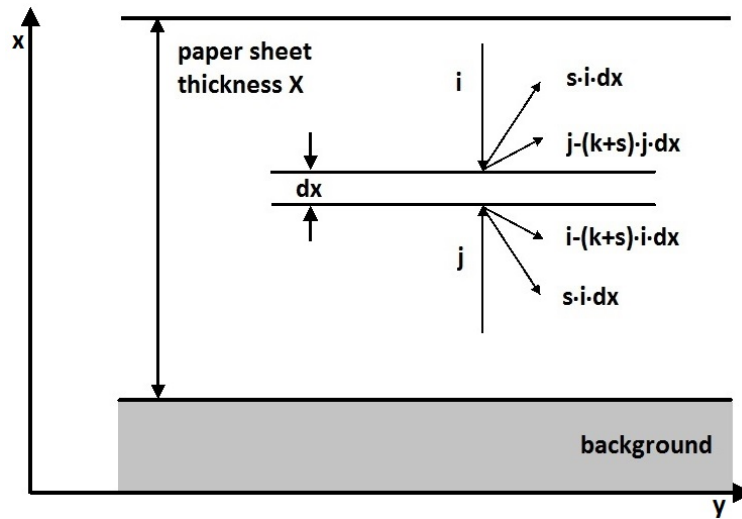


Figure 3.14: Basic considerations for Kubelka-Munk theory, adapted from Schmidt (1976).

$$dj = -(k + s) \cdot j \cdot dx + s \cdot i \cdot dx \quad (3.16)$$

The same applies to i , which is attenuated by a factor proportional to $(k+s)$, i and dx but increased by scattered light from j . The change of the top down light beam is therefore (Schmidt 1976):

$$di = -(k + s) \cdot i \cdot (-dx) + s \cdot j \cdot (-dx) \quad (3.17)$$

These two differential equations (3.16 and 3.17) are the basis for the Kubelka-Munk theory. Reflectivity of dx is given by $\frac{j}{i}$. Dividing of 3.16 by j and 3.17 by i as well as substitute $\frac{j}{i}$ by r gives (Schmidt 1976):

$$\frac{dj}{j} = -(k+s)dx + \frac{1}{r}sdx \quad (3.18)$$

$$-\frac{di}{i} = -(k+s)dx + rsdx \quad (3.19)$$

This yields dr (Schmidt 1976):

$$\begin{aligned} dr &= \frac{1}{i}dj - \frac{j}{i^2}di \\ \frac{dr}{r} &= \frac{dj}{j} - \frac{di}{i} \end{aligned} \quad (3.20)$$

$$\begin{aligned} &= -2(k+s)dx + \left(r + \frac{1}{r}\right) \cdot s \cdot dx \\ &= \left[-2 \cdot \frac{k+s}{s} + r + \frac{1}{r}\right] \cdot s \cdot dx \end{aligned} \quad (3.21)$$

Substitution $\frac{k+s}{s} = a$ yields the differential equation (Schmidt 1976)

$$\frac{1}{r \cdot \left[r + \frac{1}{r} - 2a\right]} \cdot dr = s \cdot dx \quad (3.22)$$

which has to be integrated over the whole sample layer, from $x = 0$ till $x = X$ (see figure 3.14). If the sample lies on a background having a reflectivity of $R(u)$ this has to be considered for $x=0$. For $x=X$ the reflectivity is given by R_u . This gives the integration (Schmidt 1976):

$$\int_{R(u)}^{R_u} \frac{1}{r^2 + 1 - 2ar} \cdot dr = \int_0^X s \cdot dx \quad (3.23)$$

with the result (Schmidt 1976):

$$\ln \frac{(R_u - a - \sqrt{a^2 - 1})(R(u) - a + \sqrt{a^2 - 1})}{(R_u - a + \sqrt{a^2 - 1})(R(u) - a - \sqrt{a^2 - 1})} = 2\sqrt{a^2 - 1} \cdot s \cdot X \quad (3.24)$$

According to equation 3.24 the scattering coefficient S depends on the reflectivities $R(u)$ and R_u . Since the substitution $\frac{k+s}{s} = a$ was done, S depends on the absorption coefficient K too. To overcome this, the sample thickness X is converged to infinity ($X \rightarrow \infty$) whereby $R_u = R(u) = R_\infty$. Equation 3.24 complies with $X \rightarrow \infty$ if the denominator is set to zero (Schmidt 1976). In other words, if

$$R_\infty = a - \sqrt{a^2 - 1} \quad (3.25)$$

According to Schmidt (1976), this can be transformed into

$$\begin{aligned} a &= \frac{1}{2} \left(\frac{1}{R_\infty} + R_\infty \right) \\ \sqrt{a^2 - 1} &= \frac{1}{2} \left(\frac{1}{R_\infty} - R_\infty \right) \end{aligned} \quad (3.26)$$

Using 3.26 equation 3.24 gives

$$\ln \frac{\left(R_u - \frac{1}{R_\infty} \right) \left(R(u) - R_\infty \right)}{\left(R_u - R_\infty \right) \left(R(u) - \frac{1}{R_\infty} \right)} = \left(\frac{1}{R_\infty} - R_\infty \right) \cdot s \cdot X \quad (3.27)$$

Equation 3.27 represents the solution of the initial equations 3.16 and 3.17. According to van den Akker (1949) thickness (X) has to be replaced by grammage. Since the determination and definition of paper sheet thickness is not an easy task, using grammage instead of thickness, helps to overcome this trouble. As a consequence, the dimension of the scattering and adsorption coefficient changes from cm^{-1} to $\text{cm}^2 \cdot \text{g}^{-1}$. Measurements by using a reflection photometer, a totally black underground is used. Hence $R(u) = 0$ and $R_u = R_0$. By doing so, equation 3.27 becomes (Schmidt 1976):

$$\ln \frac{\left(R_0 - \frac{1}{R_\infty} \right) \left(-R_\infty \right)}{\left(R_0 - R_\infty \right) \left(-\frac{1}{R_\infty} \right)} = \left(\frac{1}{R_\infty} - R_\infty \right) \cdot s \cdot X$$

or

$$s \cdot X = \frac{R_\infty}{1 - R_\infty^2} \cdot \ln \frac{1 - R_0 \cdot R_\infty}{1 - R_0/R_\infty} \quad (3.28)$$

Replacing the thickness X by the grammage w leads to (Schmidt 1976)

$$s = \frac{1}{w \left(\frac{1}{R_\infty} - R_\infty \right)} \cdot \ln \frac{1 - R_0 \cdot R_\infty}{1 - R_0/R_\infty} \quad (3.29)$$

The adsorption coefficient is obtained by using $\frac{k+s}{s} = a$ and equation 3.26 (Schmidt 1976):

$$k = \frac{s \cdot (1 - R_\infty)^2}{2 \cdot R_\infty} \quad (3.30)$$

Usually, the investigated material is limited to some extent. Then the measurements can be made over two different backgrounds, a blackbody (R_{bb}) and a background having a special reflectivity (R_{wb}), giving R_b and R_w (Kaarlo 2008). In this way, the following equation is obtained (Kaarlo 2008):

$$a = \frac{1}{2} \cdot \frac{(R_{wb} - R_{bb})(1 + R_w R_b) - (R_w - R_b)(1 + R_{wb} R_{bb})}{R_b R_{wb} - R_w R_{bb}} \quad (3.31)$$

Since the blackbody does not have any reflectivity $R_{bb} = 0$ and $R_b = R_0$. The second background used had a reflectivity of $R_{wb} = 0.79$, giving $R_w = R_{79}$. By substituting the values into equation 3.31, this yields:

$$a = \frac{1}{2} \left[R_{79} \frac{R_0 - R_{79} + 0.79}{0.79R_0} \right] \quad (3.32)$$

Using equation 3.32 and 3.25 gives the theoretically R_∞ value which is needed to calculate S and K.

Additionally, some important facts have to be mentioned. First of all, it has to be noted that in the case of paper, S is no material constant. The scattering coefficient rather depends on the treatment and on the subsequent processing of the pulp. This has some influence on the sheet of paper which has to be made for investigating S. Furthermore w, R_0 and R_∞ have to be measured to calculate S from equation 3.29. Hence, the scattering coefficient depends on the grammage of the paper sheet (Schmidt 1976). These circumstances have to be considered using this theory for paper sheets. Scattering coefficient was measured (ISO 2471 and TIP 0804-03) by using a Technidyne - Color Touch 2 Model ISO.

3.10 Polarized light microscopy

In order to determine the specific bond strength, the bonded area has to be known. To evaluate the optical bonded area of each investigated fibre-fibre bond, polarized light microscopy was used. This technique was already used for paper fibres (Kappel et al. 2009, Gilli et al. 2009, Kappel et al. 2010b, Kappel et al. 2010a). Using polarized light, bonds appear dark, because of the absence of reflection, in contrast to a single fibre, or two unbonded fibres. In this case there is an inner reflection at the back surface of the fibre which is also changed in polarization direction. Therefore, this reflected light can pass the analyser. The fibre appears bright (Kappel et al. 2010b).

According to Page et al. (1962) bonded areas are more clearly dark for ribbon-shaped and fully collapsed fibres. A similar result was found by Kappel et al. (2010b). Thus, polarized light microscopy only yields correct results, if the investigated fibres are parallel. Additionally the fibre wall thickness has to be similar or equal to a certain ratio. Since this is not the common case for paper fibres, incorrect results are obtained. To overcome this trouble, one paper fibre has to be dyed (Kappel et al. 2010a). In the case of unbonded, crossed fibres, an additional reflection from the dyed fibre is seen. If the fibres are bonded, this reflection is absorbed by the black dye. Consequently, bonds appear dark if one fibre is dyed (Kappel et al. 2010a). In the case of viscose fibres, there is no lumen and all fibres nearly have the same thickness. Hence, viscose fibres fulfill the conditions for correct results (according to Page et al. (1962) and Kappel et al. (2010a)) without any dyeing.

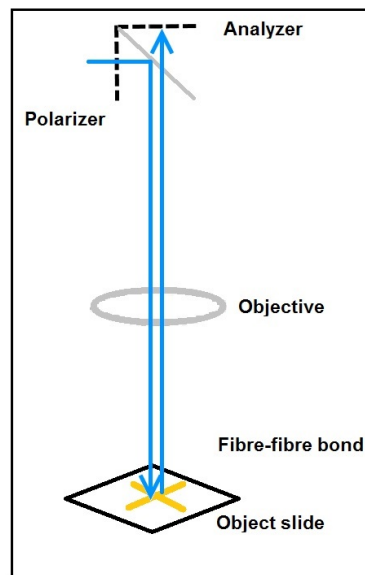


Figure 3.15: Schematic description of polarized light microscopy.

Figure 3.15 shows a schematic description of polarized light microscopy. Light is linearly polarized at the polarizer and hits the sample where it is reflected in the case of a single fibre. Additionally, the polarization direction is changed. Thus, the light can pass the analyser. At the bond, no light is reflected. For bonding area measurement, a picture of the bond is made (see figure 3.16). After that, the optical bonded area is marked and converted into a binary image, as it is shown in figure 3.16. Finally, the area of the binary image is calculated via Matlab.



Figure 3.16: Determination of the optical bonded area.

3.11 Joint strength measurement

To investigate the strength of single fibre-fibre bonds, a testing device designed and built at the Institute for Paper-, Pulp- and Fibre Technology was used. A short overview of the testing device and the testing procedure will be given below. Detailed explanation is found in Fischer et al. (2012).

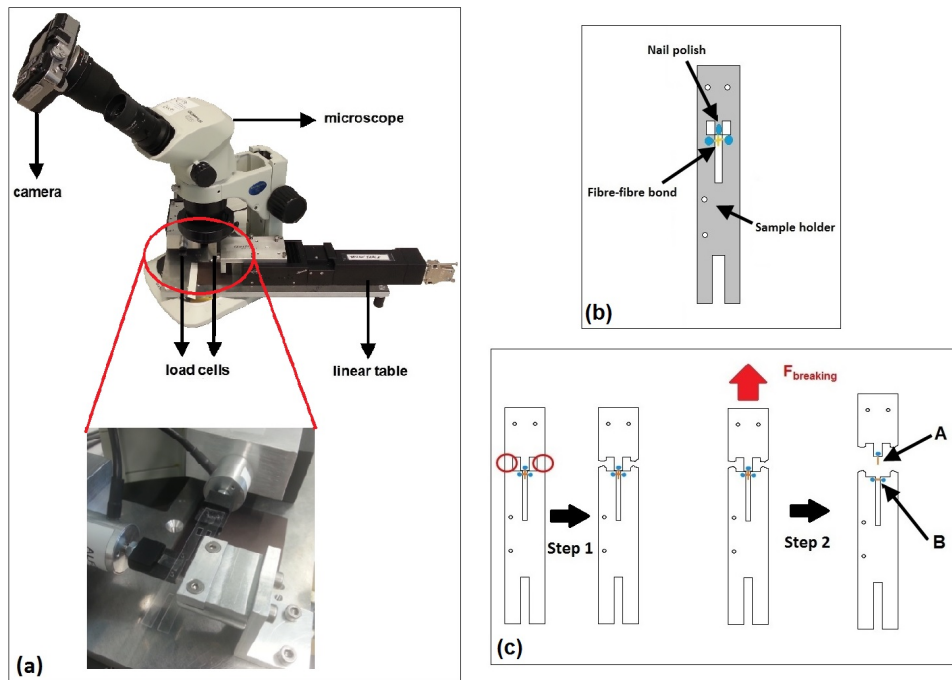


Figure 3.17: Micro bond tester and sample holder for joint strength measurement - (a) Measurement setup; (b) sample holder; (c) testing procedure.

The measuring system is shown in figure 3.17(a). It consists of two load cells (AL-THEN Mess- und Sensortechnik) for force measuring, which are mounted on two linear tables (OWIS GmbH) for force transmission. Having a resolution of 0.5 mN, the maximum force of these load cells is 1.5 N. The displacement range of both linear tables is 20 μm . The displacement speed ranges from 1 to 125 $\mu\text{m/s}$. This setup is placed under a microscope equipped with a camera to make pictures of the fibre-fibre bond and for recording the bond during the measurement. The attached sample holder is enlarged and displayed in figure 3.17(a) as well. The sample holder itself is shown in figure 3.17(b). Using this set up, it is possible to preload the cross-fibre (fibre B in figure 3.17(c)) and to investigate the influence of biaxial load on the fibre-fibre bond. Since, only the bond strength was investigated in this work, no preloading was done. The sample holder (figure 3.17(b)) is cut out of a sheet of acrylic glass (HESAGLAS VOS, Topacryl AG) using an automated laser. The sample holder thickness is about 0.3 mm.

The whole device is controlled via a custom written software in LabVIEW. The data is transmitted via a DAQ-card from National Instruments (Fischer et al. 2012).

Figure 3.17(b) shows the fibre-fibre bond fixed on the sample holder by nail polish ("essence color & go" from cosnova GmbH). Nail polish was used to avoid a film on the fibres, seen by using cyanoacrylate glue (Fischer et al. 2012). The nail polish was

allowed to dry for one day. After that, the sample holder is mounted at the tester. The testing procedure consists of two steps, which are illustrated in figure 3.17(c).

1. In the first step, the bridges are melted (red circles in figure 3.17(c)) by a soldering rod. After this step, the sample holder consists of two parts, which are held only by the fibre-fibre bond.
2. In the second step, the joint is broken. The fibre-fibre bond is broken by pulling away fibre A from fibre B. During the whole measurement, the force versus the distance of the starting position is measured. The result of this, the so called force-distance curve (shown in figure 5.10 at chapter 5.2.4) is obtained which delivers the bond strength.

4 Investigation of round viscose fibres - determination of the surface chemistry

Compared to paper fibres, viscose fibres are stiff and inflexible. Because of this, viscose fibres do not conform to each other very well like paper fibres do. They hardly come into close contact during drying (Young 1972). As a result of this, viscose fibres give a fragile and bulky sheet because of little inter-fibre-bonding. However, bonding strength and paper properties can be improved by using additives (Laine et al. 2002a) as mentioned in chapter 2.4.1.

The first part of this thesis reports about the influence of additives and on the related charges on the tensile strength of hand sheets. Furthermore, the surface of the fibre samples (cross section is seen in figure 4.1) was examined, in order to identify whether charges are primarily located on the fibre surface or in the bulk structure.

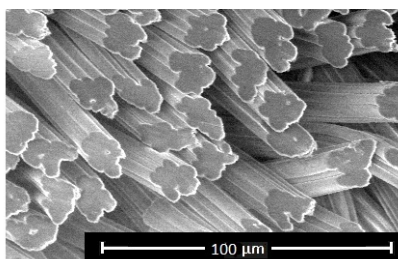


Figure 4.1: Cross section of the investigated fibres. Image was made at FLEMI Graz

4.1 Swelling

The influence of charges on the swelling behaviour of paper fibres was already investigated in the past. According to Lindström (1980) fibre swelling is increased by anionic charges. Especially surface charges contribute to fibre swelling (Laine et al. 2003a). To verify these results for viscose fibres, swelling of RF, AF1 and AF2 were analysed. Additionally, swelling of CF1 was measured, to verify the swelling behaviour of cationic fibres. Measurements were done as described in chapter 3.2. Figure 4.5 shows the measurement points of an investigated AF2-fibre, dry and wet. An increase in fibre width can be seen. Swelling occurs right after wetting as it is displayed in figure 4.2. The swelling of a reference fibre was analysed for one hour. Images of the fibre were made every second to third minute for the first 20 minutes. An increase of fibre width was seen within the first two minutes. Afterwards, nearly no changes in fibre width were seen. Because of this, the last images were made after, 5, 10 and 15 minutes. The differences in the fibre width are due to measurement errors which may occur during pixel counting and focusing of the camera.

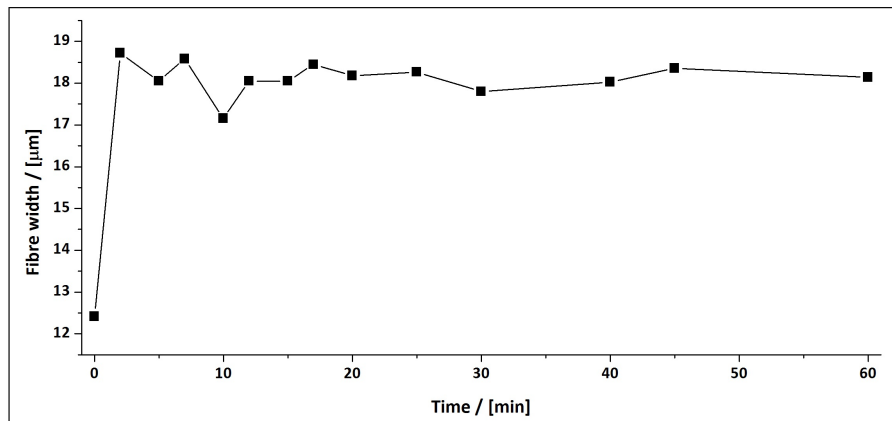


Figure 4.2: Time dependent swelling of the free end of a RF fibre. Fibre width was analysed for 60 min. As it can be seen, swelling occurs within the first minutes.

After verification that swelling occurs right after wetting, the fibre width was determined immediately after fibre wetting. Results of the first measurement series are shown in figure 4.3. An average moisture expansion of 33% was found for the reference fibres. Nearly the same result was observed for CF1. With a value of 34%, there is almost no differences between CF1 and RF. Apparently, cationic charges do not enhance the fibre swelling.

As described in the literature, increased swelling is seen for anionic fibres. Wet fibre width is increased by 45% for AF1 and 55% for AF2. Figure 4.4 displays the swelling data versus the COOH amount. Although there are only three measurement points, due to the three fibre samples, a linear relationship can be assumed.

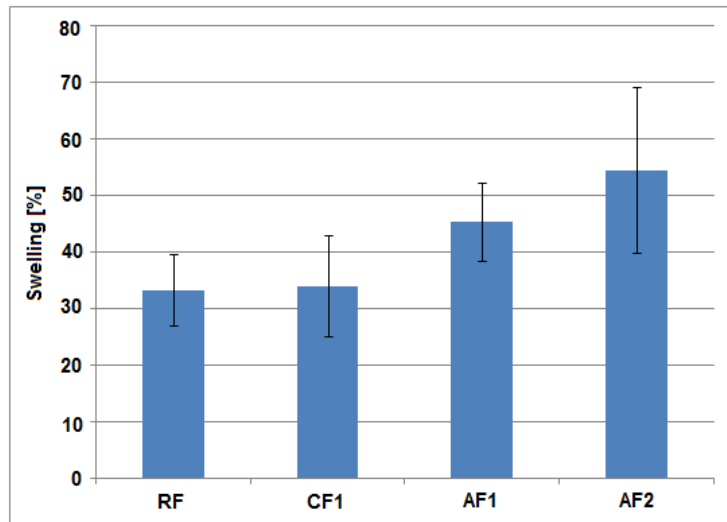


Figure 4.3: Swelling of the investigated fibres. Columns represent the mean value of 10 fibres. Adapted from Weber et al. (2013).

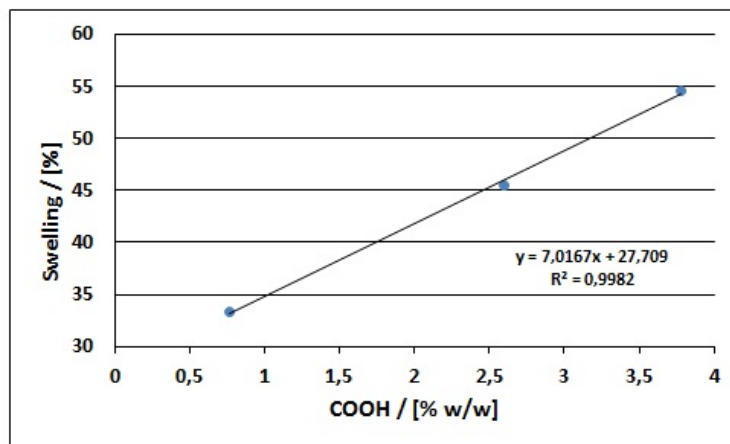


Figure 4.4: Swelling versus COOH content. Even if there are only three measurement points, a linear relationship can be assumed.

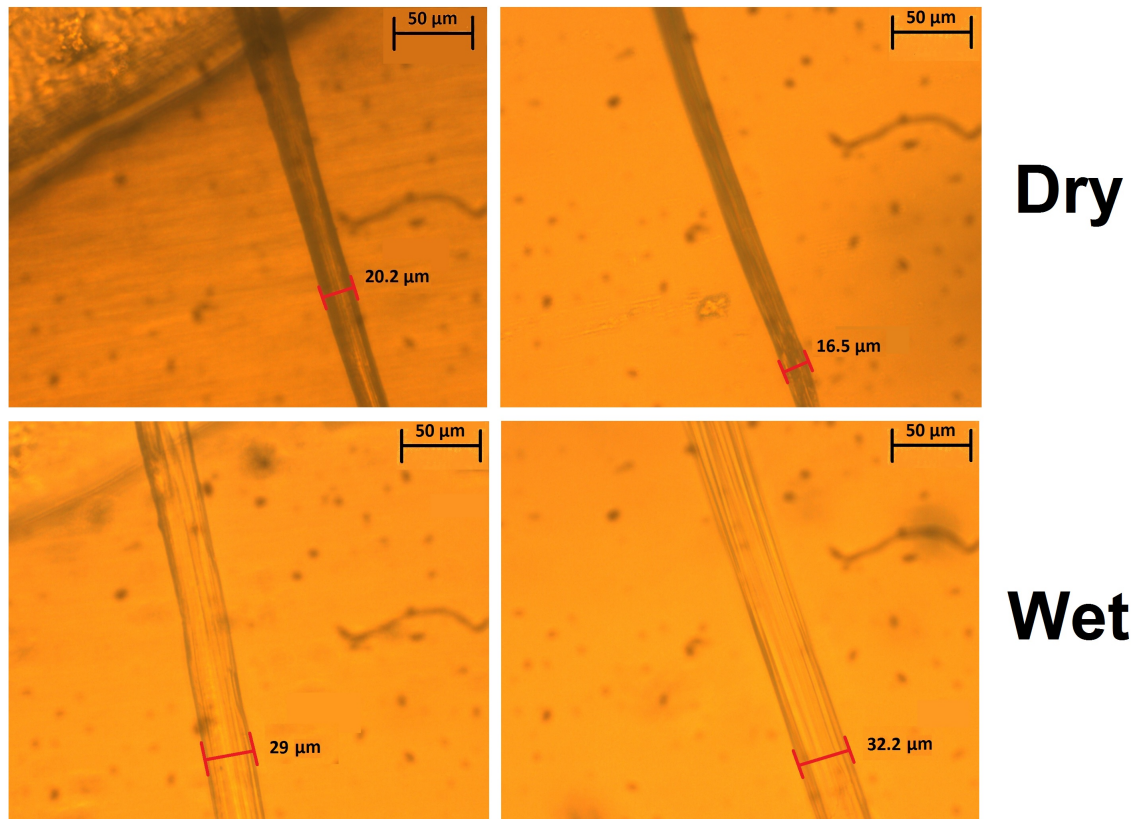


Figure 4.5: Measurement points of the swelling investigations by light microscope. Images on the left hand side show the measurement point near the glue. On the right hand side the free end is seen. The investigated fibre (AF2) is seen in dry and wet state.

To verify these results, the moisture expansion was measured via ESEM. These measurements were done at FELMI Graz, with the help of Herbert Reingruber and Armin Zankel. An ESEM offers a much higher resolution than a light microscope, which enables more precise results. The principles of ESEM and the measuring procedure are explained in chapter 3.2.1. One fibre of each fibre type (RF, AF1, AF2 and CF1) were analysed. Examples of images used for evaluation are given in figure 4.6. On the left side of figure 4.6 a dry AF2 fibre is seen. The measurement conditions are shown at the bottom edge of each picture. At the beginning of the measurement, the specimen stub and therefore the fibre sample had a temperature of 20°C. The measurement chamber was evacuated down to 1.03 Torr. A picture was made of the dry fibre before it was cooled down to 3°C. After that, the pressure was gradually raised by increasing the water vapor pressure. Condensation was seen at a pressure of 6 Torr. This is shown on the right side of figure 4.6 where the swelled fibre and the wet sample stub surface are presented.

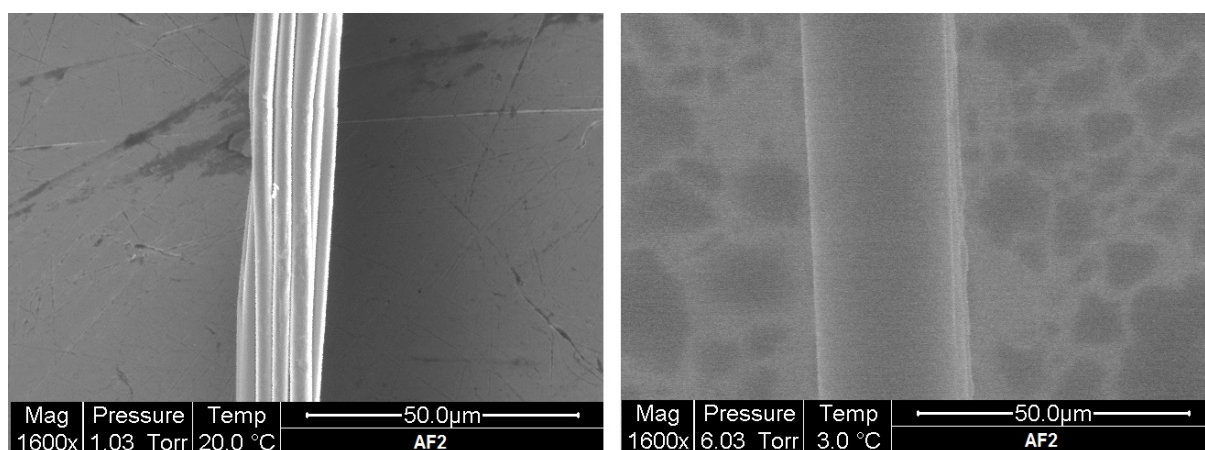


Figure 4.6: ESEM images of a dry (left) and wet (right) AF2. In both cases, the same position on the fibre is seen. Measurement conditions are displayed at the bottom edge. A magnification of 1,600 is used. Images were made at FELMI Graz.

However, there are a number of important issues to consider. Because of radiation damage the investigated area has to be changed after some time. Furthermore, hydrocarbon molecules are polymerized on the fibre surface by the incoming electrons (Egerton et al. 2004). Hydrogen is always present in a vacuum chamber. It arises from the walls of the vessel in which it is dissolved (Eschbach et al. 1963). Since cellulose is a source of carbons, hydrocarbon molecules may be polymerized. Consequently, the fibre surface gets dirty which may influence the swelling behaviour. Finally, a water film can be seen on the fibre (right picture of figure 4.6) which contributes to the measured fibre width. This lead to additional measuring errors.

Figure 4.7 displays the data of all measurements, including the ESEM data (blue columns). Despite the problems caused by the electron beam, the ESEM data fits very well with the first measurements. For that reason and because of the time consuming measurements, only one fibre of each fibre type was investigated by ESEM. The mean values of each fibre type with (red columns) and without the ESEM data (green columns) is shown in figure 4.7.

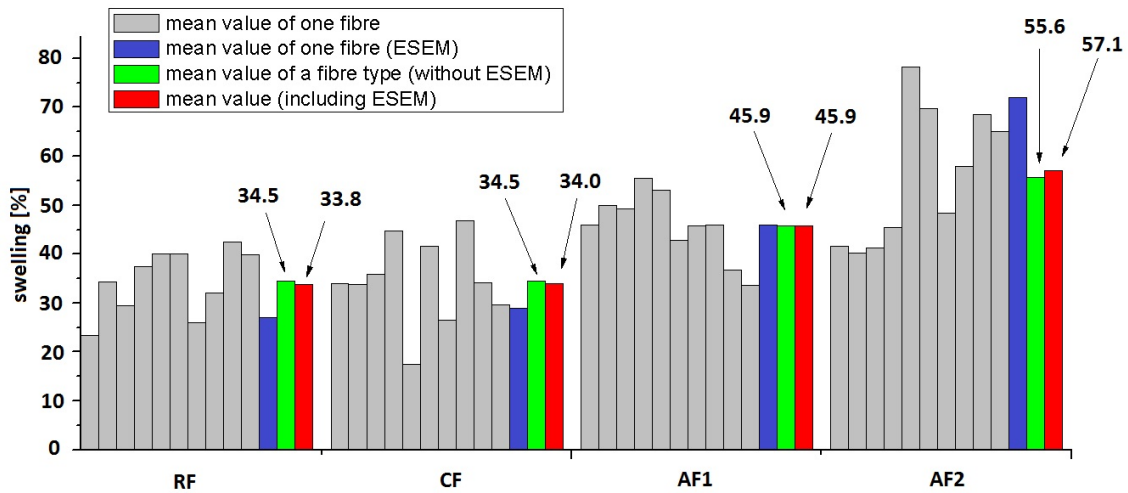


Figure 4.7: Overview of the swelling values of all investigated fibres, including the ESEM data.

4.2 Breaking length

In addition to swelling of single fibres, the breaking length of handsheets was investigated. Ten handsheets of each fibre type (CF1, AF1, AF2) were made. Since handsheets of RF are too bulky, they do not exhibit a measurable tensile strength. After handsheet preparation and conditioning (see chapter 3.3) the grammage was determined. The results are shown in table 4.1. The handsheets were cut into stripes of 15 mm width and 180 mm length. A minimum of 9 stripes were tested for tensile strength. The tensile strength of each stripe is given in table 4.2. Breaking length is then calculated according to equation 3.5. The mean values of grammage and tensile strength were used for the breaking length determination.

The calculated breaking lengths are shown in figure 4.8. Handsheets made of CF1 show a breaking length of 521.4 m. This result is in the same order of magnitude as the result for AF1 which is 693.4 m. The highest value is obtained for AF2 (2,000 m).

Table 4.1: Grammage of the used handsheets for breaking length determination.

Nr.	Grammage [g/m ²]		
	CF1	AF1	AF2
1	79.37	81.14	81.53
2	79.38	80.44	80.08
3	80.32	79.74	81.21
4	80.22	81.04	80.40
5	79.56	79.73	81.26
6	79.99	82.15	78.43
mean value	79.81	80.71	80.49
std. dev.	0.42	0.93	1.15

Table 4.2: Tensile strength of the used handsheets for breaking length determination.

Nr.	Tensile strength [N]		
	CF1	AF1	AF2
1	6.07	7.51	23.69
2	6.59	8.79	21.82
3	7.35	6.88	22.62
4	6.92	9.22	25.04
5	7.51	8.79	25.24
6	5.99	7.07	23.4
7	5.03	7.80	22.63
8	5.60	6.22	24.56
9	4.02	7.84	23.74
10		8.39	22.37
11		9.68	26.25
12		10.52	22.93
13		10.23	23.58
14		7.4	25.41
15		7.69	23.8
16		7.61	21.68
mean value	6.12	8.23	23.67
std. dev.	1.13	1.22	1.33

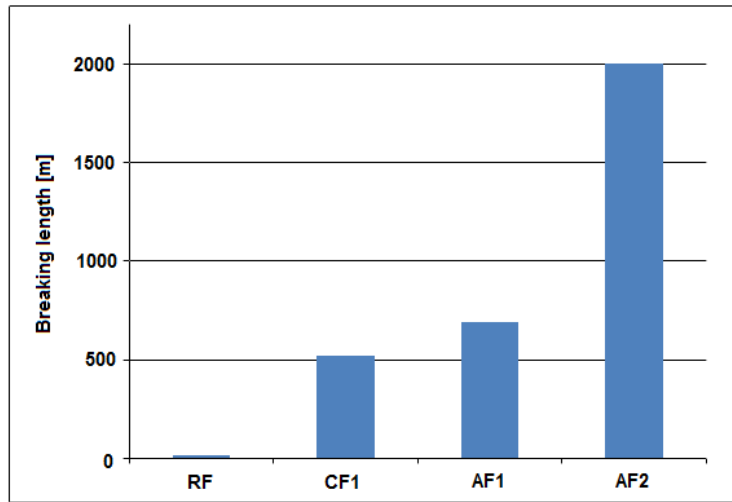


Figure 4.8: Breaking length of hand sheets. No measurable value for handsheets made of RF. Adapted from Weber et al. (2013).

4.2.1 Interpretation of the first results

Improved swelling was seen for anionic fibres. Enhanced fibre swelling leads to larger bonding areas between single fibres during the drying process. Therefore, improved tensile strength of AF1 and AF2 is achieved by introduced charges and larger contact areas between single fibre-fibre joints. These findings are confirmed for kraft pulp fibres by Laine et al. (2002b) and Blomstedt et al. (2007). Laine et al. (2002b) reported a linear relationship between the amount of attached CMC and the water retention value (WRV) which is generally used to determine the swelling capacity of pulps. This would fit with the moisture expansions seen for the used anionic viscose fibres. Laine et al. (2002b) also reported no effect of CMC on sheet consolidation for pulp fibres. In this respect, viscose fibre handsheets differ from pulp fibre handsheets. As it will be shown in chapter 5.2.2 the light scattering coefficient of viscose fibre handsheets is affected by the attachment of CMC. This is due to the differences between viscose and pulp fibres. Viscose fibres are innately rigid and stiff. The addition of CMC leads to enhanced fibre flexibility and therefore to improved fibre consolidation and sheet formation. This matches the results of the used viscose fibres. Due to anionic charges, an increase in swelling and tensile strength was seen. Certainly, a quantification of both effects is not possible by only looking at the anionic fibres.

The influence of charges to the tensile strength is seen by comparing the results of RF and CF1. Both fibre samples have shown the same swelling behaviour. However, CF1 exhibits a much higher tensile strength than RF. It follows from this that the specific bond strength must have been improved by the positive charges.

While both effects, swelling and enhanced Coulombic interaction, leads to larger

breaking lengths for the anionic fibres, only charges contribute to the higher tensile strength of CF1. There is a constant increase of swelling between CF1, AF1 and AF2 of nearly 10%. In contrast to breaking length which does not increase in such a linearly way. A small increase is seen between CF1 and AF1 but a huge boost is seen from AF1 to AF2. Assuming that AF1 and CF1 have the same amount of charges, a breaking length of 521.4 m would be only due to charges. If so, the further increase seen for the anionic fibres is because of enhanced swelling and therefore larger bonding areas. This might possibly indicate that charge is more important for tensile strength than bonding area. According to Laine et al. (2003b) surface charge has a greater contribution to swelling than bulk charge. Hence, investigation of the charge distribution within the used fibre samples seemed to be appropriate.

4.3 Titration

After the investigation of swelling and breaking length, titration was done to evaluate the charge distribution. According to Kelheim Fibres GmbH, the charges should be uniformly distributed within the fibres, due to the production process. To verify this assumption, total and surface charge were determined via titration at Mondi Frantschach GmbH.

The results are given in table 4.3. The reference fibre (RF) exhibit a total charge of 0.17 meq/g. This value increases with the amount of CMC. Figure 4.9 visualizes the data from table 4.3. A linear relation is seen between the total charge measured at Kelheim Fibres GmbH and the data obtained from Mondi Frantschach GmbH (figure 4.9a). Both measurement methods seem to be applicable and comparable.

Table 4.3: Quantified charge of each fibre sample by Titration (total charge and surface charge). CF2 as well as pure CMC were not titrated.

Sample	Total charge [meq/g]	Surface charge [meq/g]
RF	0.170	0.003
AF1	0.578	0.087
AF2	0.839	0.167
CF1	0.186	n.a

Surface charge versus total charge is displayed in figure 4.9b. Nearly no surface charge was seen for RF. The charge seems to be concentrated within the fibre bulk. Increasing the amount of COOH-groups by adding CMC to the fibre suspension leads to increased surface charges, as seen by a factor of ten for AF1. Further increase of COOH-groups lead to even more surface charged sites. The surface charge of AF2 is as high as the total charge of RF. If the polymer used in surface charge determination

does not penetrate into the fibre bulk, these results imply that CMC, and consequently charges, are present in the outermost fibre layer.

Titration has shown that surface charges increase with the amount of additives. The results lead to the assumption that CMC diffuses to some extent onto the surface after spinning. Nevertheless, no information about the charge distribution within the fibres is obtained. Moreover, titration was unapplicable for cationic fibres. To verify the existence of charged species on the fibre surface and for getting a better understanding of the charge distribution, ATR and XPS measurements were done. In addition, the surface of cationic fibres could be investigated by these techniques as well.

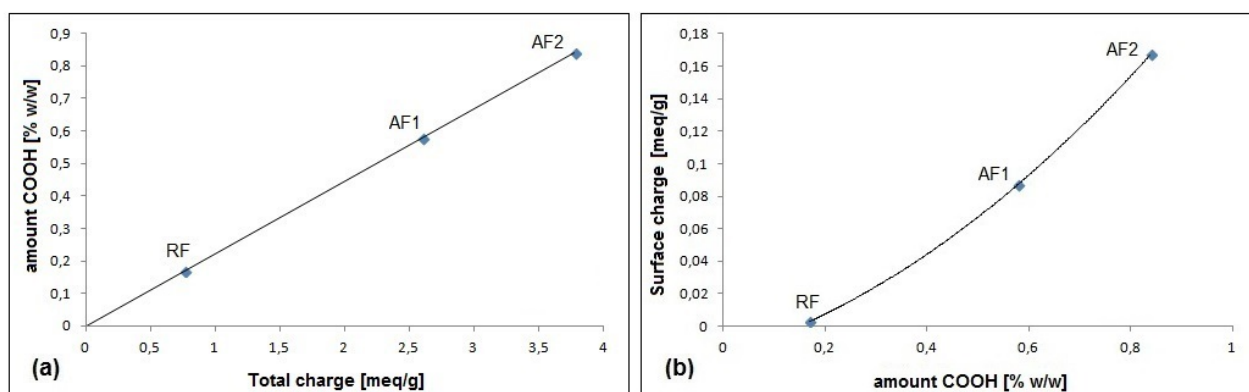


Figure 4.9: Evaluation of the titration data. Lines are just guides for the eyes. Adapted from Weber et al. (2013).

4.4 Attenuated total reflection infrared spectroscopy

A first examination of the surface chemistry of the used fibre samples was done by attenuated total reflection infrared spectroscopy (ATR). Measurements were done according to chapter 3.5.1. Pure CMC as well as CF2 were investigated as well. For this purpose samples of 2x2 cm were cut out of handsheets. In order to obtain an usable sample of pure CMC, CMC was dissolved in deionized water. The solution obtained was dried at 50°C for 24 hours to gain a film which was analysed.

ATR measurements are surface sensitive up to a certain point. The penetration depth of the evanescent wave into the viscose paper can be calculated according to equation 3.11. By adding the parameters into this equation ($n_1 = 2.4175$ (Anthony et al. 2000); $n_2 = 1.51$ (Buchholz et al. 1996; Karabiyik et al. 2009), $\alpha = 45^\circ$, $\lambda = 1580 \text{ cm}^{-1}$) a penetration depth of 1.3 μm is obtained. Therefore, it is possible to measure additives on and near the fibre surface. The amount of the additives can be estimated by integrating the corresponding peak of the ATR spectra. Peaks of the additives were found by means of NIST Chemistry WebBook.

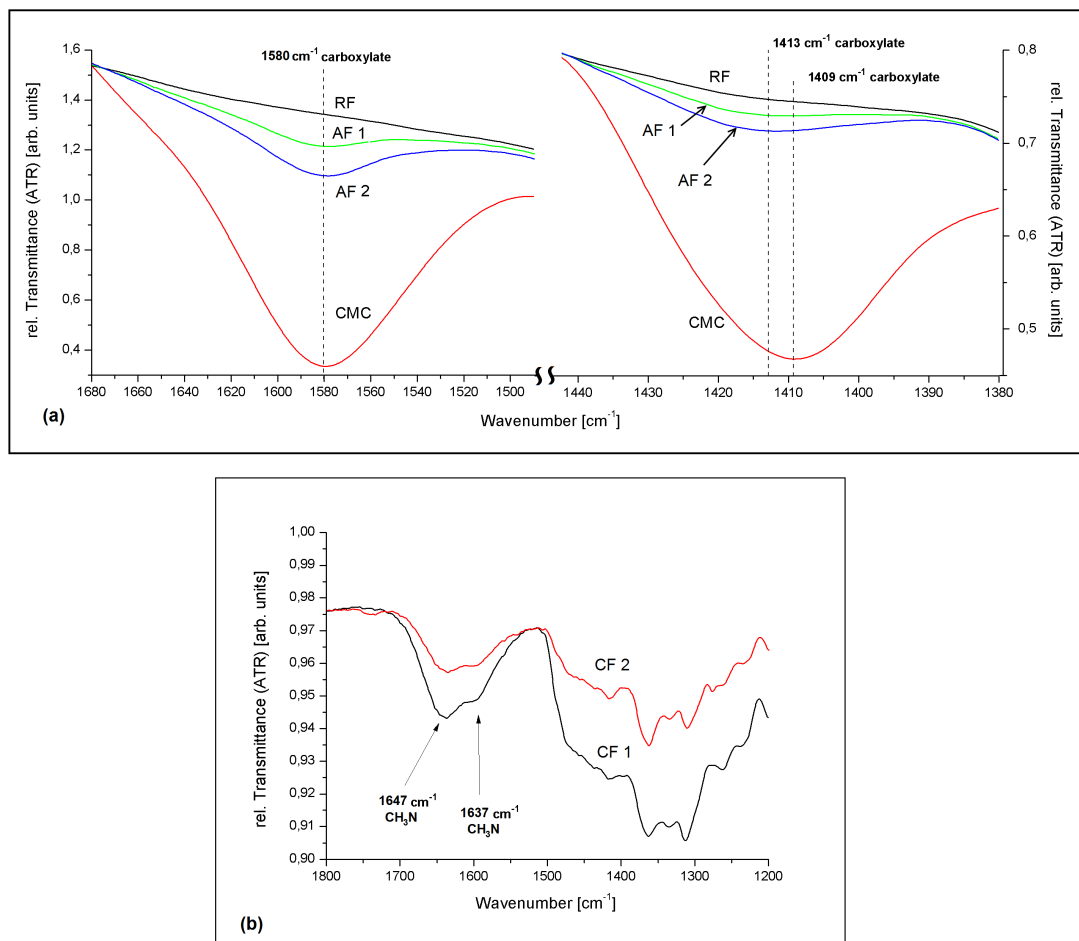


Figure 4.10: ATR spectra of the investigated samples. (a) shows the spectra of the anionic species. (b) shows the spectra of the cationic fibres. RF - reference fibre, AF1 - anionic fibre 1, AF2 - anionic fibre 2, CF1 - cationic fibre 1, CF2 - cationic fibre 2, CMC - pure carboxymethylcellulose. Adapted from Weber et al. (2013).

ATR spectra of pure viscose handsheets are shown in figure 4.10. Figure 4.10a exhibits the peaks of CMC. The background spectrum of the ATR crystal (empty ATR unit) served as background spectrum for these samples. The peaks obtained in this way were normalized to the intensity of the RF spectrum. Peaks representing CMC were found at 1580 and 1413 cm^{-1} (a slight shift for the second peak to 1409 cm^{-1} was seen for pure CMC). According to the amount of CMC, these peaks are growing linearly which is seen in figure 4.11.

The cationic starch is detected by peaks at 1647 cm^{-1} and 1637 cm^{-1} (figure 4.10b). Both peaks originate from the quaternary ammonium group of the starch. In order to obtain these peaks, the RF spectrum had to be used as the reference spectrum. Consequently, these spectra display the differences between RF, CF1 and CF2. In other words, without cationic starch, the reference and the samples would be chemically identical and no peaks were seen. To enable the interpretation of the data, the spectrum of CF1 was normalized with respect to the spectrum of CF2. It can be seen that both peaks are growing with the amount of the additives.

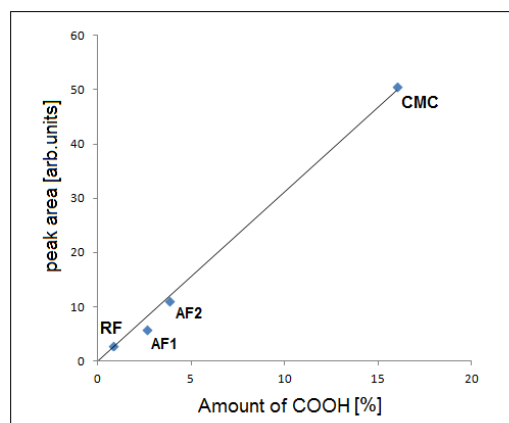


Figure 4.11: Integrated peak area of the peak at 1580 cm^{-1} as a function of COOH amount. Adapted from Weber et al. (2013).

4.5 X-ray photoelectron spectroscopy

In addition to infrared spectroscopy XPS was used to examine the chemical composition of the fibre surfaces. According to Connors and Banerjee (1995), the analysis depth of XPS for paper is in the range of 0.5-10 nm (see chapter 3.6). Hence, it is more surface sensitive than ATR. Using this technique, the amount of additives in the outermost fibre layer can be determined. This information enables one to draw conclusions about the quantity of the surface charges. Similar to infrared spectroscopy, a spectrum is obtained. An example of such a spectrum is seen in figure 3.12 in chapter 3.6.

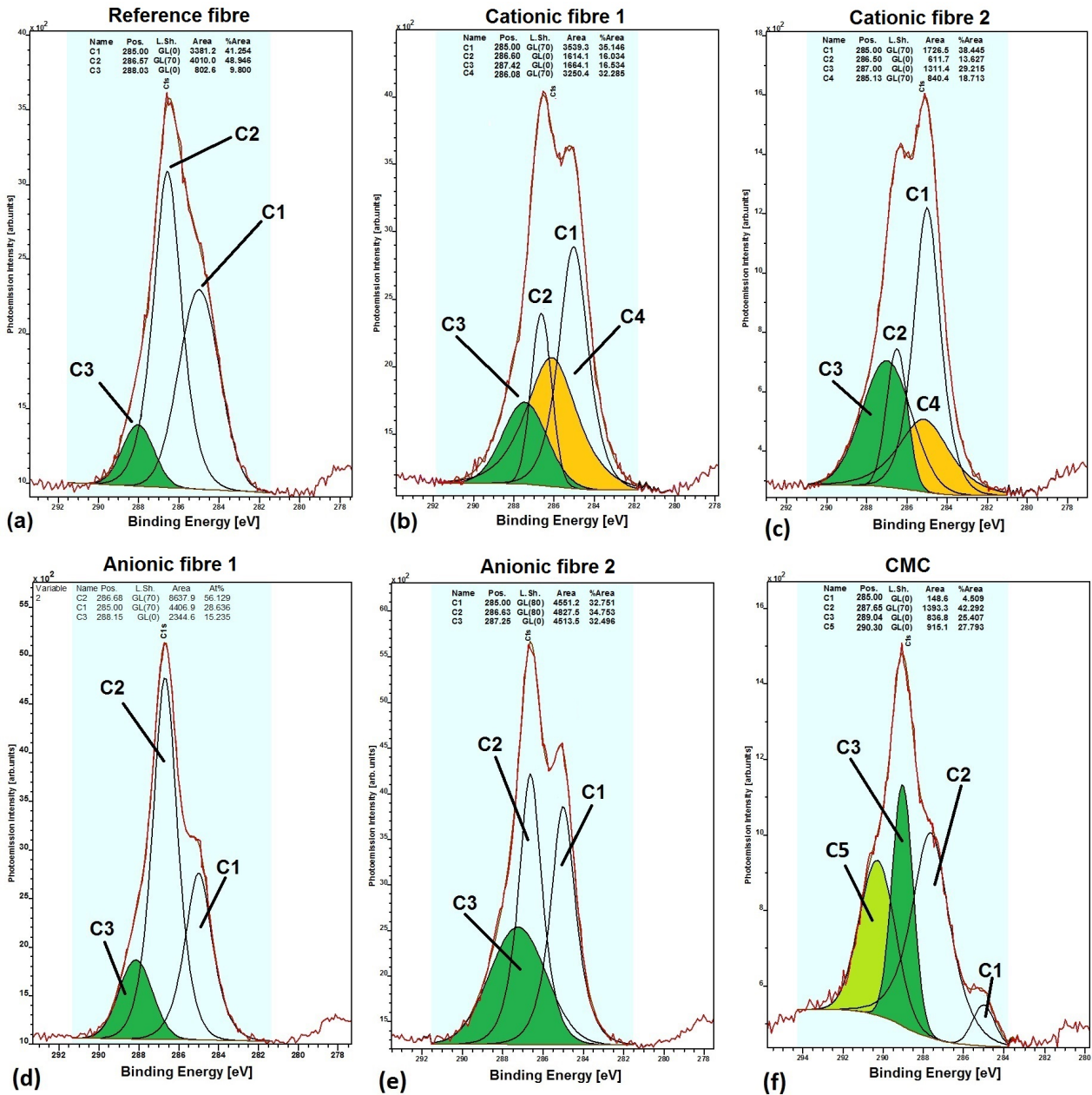


Figure 4.12: Data of the XPS measurements. The C 1s peak of all fibre samples is seen; C1 = C-C, C2 = C-O, C3 = O-C-O/C=O, C4 = C-NR₃; The components, corresponding to the additives are highlighted; figures are adapted from Weber et al. (2013).

The C 1s peak of the anionic fibres is seen in figure 4.12d and 4.12e. Like the reference, these spectra can be fitted by three peaks. The peak positions are the same as well. However, the peak shapes are different to RF and the ACP changes. With increasing amount of additives, C3 (dark green peak area in figure 4.12) is growing due to the additional C=O bonds of CMC.

Finally, the spectrum of pure CMC is shown in figure 4.12f which exhibits substantial differences to the anionic fibres. While C1 becomes the smallest peak, the amount of C-O, O-C-O and C=O bonds become predominant. In addition, a new peak C5 (lime peak area in figure 4.12) is detected at 290.30 eV. According to the literature, this peak corresponds to C=O (Beamson and Briggs 1992) or rather C(=O)OH (Conners and Banerjee 1995). Because of the high COOH content of pure CMC, the C=O part of C3 evolves into a peak (C5). Thus, in the case of pure CMC, C3 represents the O-C-O bonds while C5 corresponds to C=O. However, both peaks originate from COOH-groups.

4.5.1 Interpretation of the results

The most important peaks are C3 and C4, which are corresponding to the additives. The amount of COOH groups is reflected by C3. Figure 4.13 displays a comparison of the XPS and the titration data. „C3, representing the amount of O-C-O and C=O bonds grows with the extend of CMC“ (Weber et al. 2013). Without any additives, the smallest column for both data sets is seen for RF, followed by AF1 where just a slight increase of C3 is seen. Hence, an increase of the COOH amount from 0.77 to 2.60% does not boost C3 similarly. In contrast to AF2. There the C3 peak increases significantly by rising the COOH content up to 3.78%. As expected, the largest C3 peak area is found for pure CMC (COOH amount of 16%). Because both peaks, C3 and C5, represent COOH-groups, C5 was added to C3. According to these results it is assumed that C3 represents the amount of acid-groups.

However, the C3 peak does not increase linearly with the COOH concentration. For the following reason, interpretation of the results has to be done carefully. „The investigated spot diameter on the sample surface is in the range of 4-5mm“ (Weber et al. 2013). The hand sheet samples have shown different flocculation due to different fibre properties. As a result of this, an indefinable distinction in the amount of investigated fibres within this spot may occur. In other words, all XPS measurements were done on a different number of fibres. For this reason, the ACP has to be standardized to the quantity of fibres in the investigated spot. Since this is not feasible, the amount of additives detected by XPS is just a guide value and can not be established quantitatively.

On the other hand, the XPS values of C4 for CF1 and CF2 fit very well with the titration values. The peak area doubles from CF2 (18.71%) to CF1 (32.29%). The same data was obtained by titration measurements. The cationic fibres also show a larger

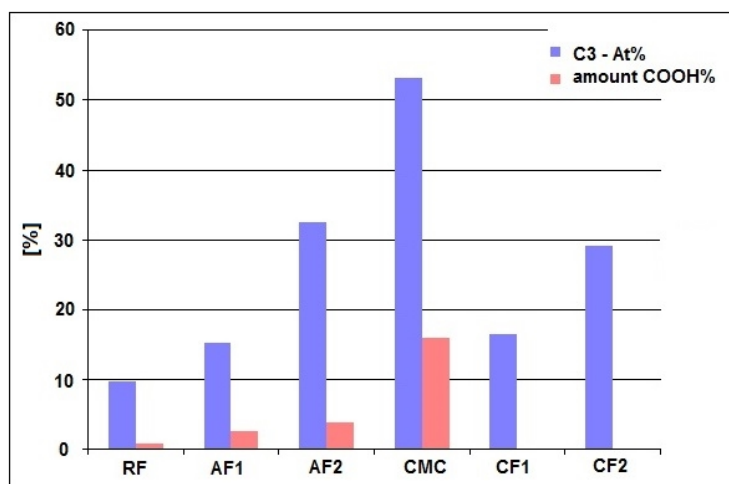


Figure 4.13: Comparison of the C3 peak areas and the amount of COOH groups, detected by titration. For pure CMC, C5 was added to C3. Since both peaks represent the total COOH amount, this seems to be applicable. Figure is adapted from Weber et al. (2013).

C3 peak than RF, resulting from additional O-C-O groups of the starch. Although the cationic fibres contain more O-C-O groups than RF, the C-NR₃ is predominant. This is why in total these fibres are cationic.

4.6 Summary

The influence of charges on fibre swelling and breaking length of round viscose fibres were investigated. Total charge as well as surface charge were determined by Titration and verified via ATR and XPS.

Swelling and breaking length of four fibre samples were investigated. Fibres without any additives were used as reference. To compare the influences of cationic and anionic charges to the fibre properties, a cationic fibre (CF1) and two anionic fibres (AF1, AF2) were analysed. Swelling of single fibres is increased by anionic charges. The moisture expansion rises with the amount of anionic additives. On the other hand, no influence on the swelling behaviour was seen for cationic charges.

After swelling, the breaking length of handsheets was determined, to visualize the influence of charges on the tensile strength. No measurable value was found for RF. Since these fibres only have weak inter-fibre bonds, handsheets of RF are too bulky for tensile strength measurements. Improved breaking length was seen for all other fibre samples. Thereby the best result was seen for AF2. In the case of anionic fibres, two circumstances contribute to the tensile strength: improved Coulombic interaction due to induced charges and enlarged bonding areas due to improved swelling.

Cationic starch only boosts the Coulombic interaction. Without increased swelling, the influence of charge can be seen by comparing RF and CF1. The breaking length of CF1 is nearly the same as for AF1. Therefore Coulomb interaction does play an important role for improving bond strength and subsequently tensile strength of paper sheets.

After analysing the effect of charges to the tensile strength, the charge distribution within the fibres was investigated. For this purpose total charge and surface charge were determined via Titration. The results of this measurements indicated a large amount of surface located charges. To verify the titration results ATR and XPS measurements were done.

Both measurement methods (ATR, XPS) are surface sensitive. An increase of additives were seen on the fibre surface, irrespective of the measurement method. While the corresponding COOH ATR-peak is growing linearly with the amount of the additives no linearity was seen in XPS. It has to be considered, that both methods exhibit different analysis depths. Hence, additives from the bulk may be detected as well by using ATR. On the other hand, XPS also has several drawbacks. The ACP has to be standardized. Additives are seen by XPS but the exact quantity cannot be established since the quantity of fibres in the investigated spot is not known. Finally, no information about the charge distribution across the fibre diameter could be obtained. The measurement methods used are surface sensitive, having an analysis depth of a few nanometer (XPS) or rather micrometer (ATR). Although it is possible that additives from the bulk are measured to some extent by ATR, no charge distribution across the fibre diameter is obtained.

5 Investigation of flat viscose fibres – determination of the relative bonded area within a paper sheet

After the influence of charges on the bond strength, as well as the influence of charge on the swelling behaviour was investigated, the relative bonded area (RBA) of hand sheets made of flat viscose fibres, with and without additives, was determined. For various reasons, there are some difficulties associated with any attempt to analyse the relative bonded area of paper sheets (more details about the problems which may occur are given in chapter 5.2). Using flat viscose fibres (cross section is seen in figure 5.1) simplifies the measurements due to well defined fibre properties and bonded areas. In addition, the influence of charge on the RBA can be analysed by using these fibres. In doing so, two different ways were used: determination of the RBA by light scattering, as well as via calculations using the Page equation. Both methods are compared and the results are discussed.

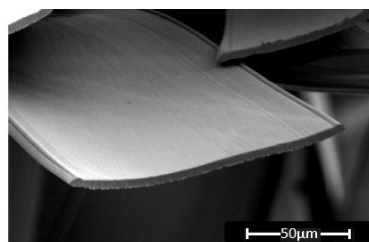


Figure 5.1: Cross section of the investigated fibres. Image adapted from Bernt (a).

5.1 Breaking length

First of all, hand sheets of all fibre samples were made for breaking length determination. The measurement was done in the same way as for the round fibres (see chapter 4.2). After handsheet preparation and conditioning, (see chapter 3.3) the grammage was determined. The results are shown in table 5.1. The tensile strength of each strip is given in table 5.2. Breaking length is then calculated according to equation 3.5. The mean values of grammage and tensile strength were used for the breaking length determination. The calculated breaking lengths are shown in figure 5.2.

Figure 5.2(a) shows the breaking length of all handsheets made of fibres without any additives but having different yarn count (4 dtex (F4), 9 dtex (F9), 12 dtex (F12) and 22 dtex (F22)). As it can be seen, F4 displays the highest value (4,244 m) followed by F9 (2,674 m). The lowest values are seen for F12 (2,127 m) and F22 (903 m). Since F22 are the broadest fibres, one would expect a higher breaking length due to larger fibre-fibre joint areas. Certainly, small fibres are more flexible. Because of this, F4 or F9 fibres conform to each other in a better way, which results in higher tensile strength. Thus, fibre flexibility seems to be another important parameter for tensile strength. Furthermore, a high number of bonds is important in view of bond failure. During tensile strength tests, bonds fail and the remaining fibre-fibre joints have to take the loading. If there are several small bonds, bond failure is not as serious as bond failure of a few large bonds since there are enough other bonds taking the load.

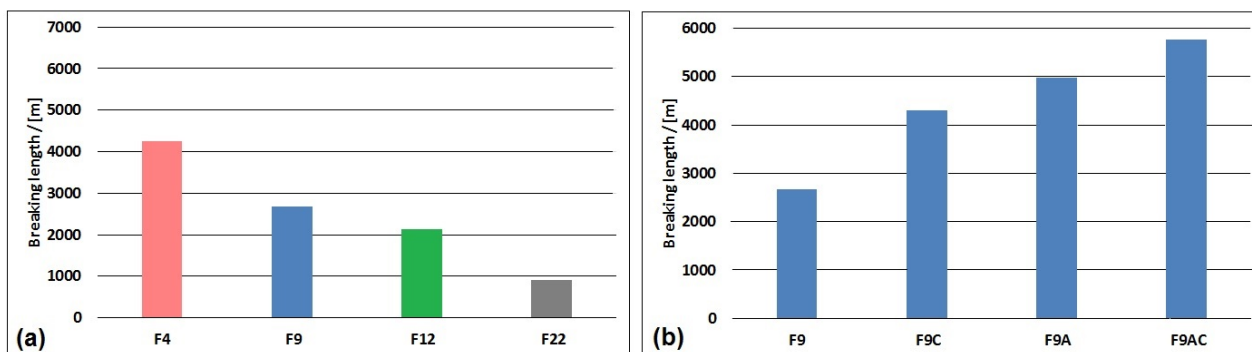


Figure 5.2: Breaking length of hand sheets made of flat fibres. (a) Breaking length of handsheets, made of fibres without any additives; (b) breaking length of handsheets made of different F9 samples (with and without additives). Figure (b) is adapted from Weber et al..

Breaking lengths of charged fibres are seen in figure 5.2(b). As for the round fibres, the smallest breaking length is seen for untreated fibres (F9 - 2,674 m). Breaking length is increased by adding cationic starch (CS) to the viscose dope (F9C - 4,305 m). Even higher tensile strength values are obtained by adding CMC to the fibres (F9A - 4,983 m). Additionally fibres, blended with both additives were investigated (F9AC). These

Table 5.1: Grammage of the used handsheets for breaking length determination.

Nr.	Grammage [g/m ²]						
	F4	F9	F9C	F9A	F9AC	F12	F22
1	74.84	79.68	83.57	80.98	91.06	76.79	78.60
2	76.92	81.75	80.47	80.97	89.94	78.70	77.44
3	75.87	78.91	80.16	80.42	89.80	78.61	77.40
4	76.15	78.68	81.59	83.63	92.03	77.49	78.42
5	75.94	80.60	81.00	80.78	91.41	76.64	78.31
6	75.06		82.73	80.91	91.00		78.13
7	74.89		81.68	82.38	90.77		
8	77.03		81.51	81.29			
9			80.44	78.44			
10			82.11	83.39			
mean value	75.84	79.92	81.53	81.32	90.86	77.65	78.05
std. dev.	0.86	1.27	1.08	0.79	1.51	0.97	0.97

Table 5.2: Tensile strength of the used handsheets for breaking length determination.

Nr.	Tensile strength [N]						
	F4	F9	F9C	F9A	F9AC	F12	F22
1	51.06	34.50	47.77	58.44	79.21	28.05	7.76
2	48.10	29.22	46.67	59.83	74.33	28.96	9.23
3	51.27	33.38	54.75	57.51	81.29	21.10	7.62
4	45.55	32.95	53.15	57.18	72.06	24.57	6.69
5	50.56	33.21	51.49	59.29	81.65	21.45	12.75
6	48.45	34.36	50.60	66.74	73.79	23.21	11.14
7	42.93	28.88	51.34	56.69	75.24	24.82	7.7
8	46.90	30.61	52.28	61.70	76.82	24.79	10.29
9	39.34	28.15	54.60	63.68	72.74	30.85	13.32
10	45.49	25.68	57.33	51.09	79.61	29.42	12.75
11	49.60	33.8	50.70			25.99	14.04
12	49.39	28.42	45.24				11.01
13	46.86	35.45	49.93				
14	45.83						
14	46.21						
14	49.69						
mean value	47.33	31.43	51.11	59.22	76.67	25.75	10.36
std. dev.	3.17	3.08	3.27	4.26	3.56	3.24	2.54

fibres (F9AC) exhibit the highest tensile strength of all (5,760 m). As shown in chapter 4, CMC leads to higher swelling and therefore larger bonding areas while cationic starch only induces charges. Compared to F9A, F9AC has a lower CMC content but a small amount of CS. It seems that adding a small amount of cationic starch to the viscose liquid, has a much larger impact to tensile strength than further increase of the amount of CMC.

Again, the importance of Coulomb interaction for tensile strength is seen. Particularly, a combination of anionic and cationic charges has a major effect on breaking length.

5.1.1 Nanointentation

Wet fibre hardness was investigated to gain a better insight into the influence of surface charge. The measurements were done by Christian Ganser according to 3.7 at Montanuniversität Leoben. The results are seen in figure 5.3 which is adapted from Weber et al.. The data is shown for a better explanation of how additives are improving the fibre properties. As can be seen, fibres are softened by additives, especially by CMC. Therefore, they are more flexible and conform to each other in a much better way. This leads to more fibre-fibre bonds during handsheet formation. Additionally, the area in molecular contact is increased by softening the fibre surface. As a result of this, higher tensile strengths are obtained.

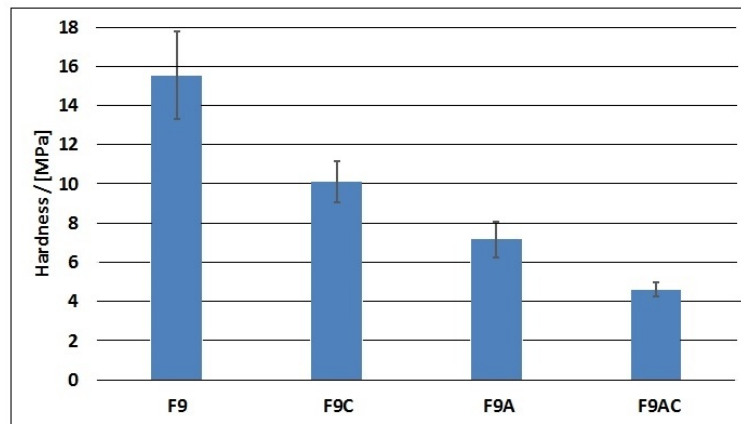


Figure 5.3: Fibre hardness, determined by nanointentation. Measurements were done by Christian Ganser at Montanuniversität Leoben. Figure is adapted from Weber et al..

5.2 Relative bonded area

The relative bonded area (RBA) is known as the fraction of the fibres external surface area that is bonded (Kallmes and Eckert 1964). The determination is not an easy task and several groups have tried to determine the RBA by various methods. One method used in this thesis is the so called *light scattering method* which was introduced by Parsons (1942). Parsons assumed that all the surface which does not scatter, is involved in fibre-fibre bonding. Therefore, the RBA is given by the scattering coefficient of a bonded handsheet (S) and the scattering coefficient of an unbonded handsheet (S_0) according to equation 5.1 (Ingmanson and Thode 1959):

$$RBA = \frac{S_0 - S}{S_0} \quad (5.1)$$

For RBA determination bonded as well as unbonded handsheets are necessary. An unbonded handsheet was prepared according to Haselton (1955): a sheet was formed in water. After that, the water was displaced by swirling the sheet first in acetone (Rotisolv, $\geq 99.9\%$) and then in butanol ($\geq 99.5\%$). Afterwards the scattering coefficient of both samples (bonded and unbonded) were analysed (ISO 2471 and TIP 0804-03) by using a Technidyne - Color Touch 2 Model ISO. Results are given in table 5.4 and 5.5.

However, this technique is not without controversy. Haselton (1955) assumed different scattering values for butanol dried handsheets and water dried but unbonded handsheets, since butanol dried fibres exhibit relatively little shrinkage during drying. Hence, butanol dried fibres appear like water-swollen fibres.

When investigating paper fibres, problems occur due to the uncollapsed part of the lumen which distort the results. This was shown by Kallmes and Eckert (1964) using dark field illumination. They also concluded that the best available technique for RBA determination would be a combination of optical and N_2 -adsorption technique (BET). A totally different approach was given by Batchelor and He (2005). They assumed a linear correlation between scattering coefficient and sheet density if the fibre cross section remains constant. Since paper fibres are always collapsed to some extent after wet pressing, they introduced a fill factor to take this into account. Another approach is given as already mentioned by using BET (Haselton 1955) which was used by several groups in the past (Duker and Lindström 2008; Kallmes and Eckert 1964). An attempt was made to use BET for RBA determination of the given viscose fibre samples but no meaningful data could be achieved.

However, every measurement method has its own drawbacks and incalculable measurement errors due to assumptions and simplifications. In this work, the light scattering method was chosen because it is a fast and comparatively easy method. Contrary to paper fibres, viscose fibres do not have a lumen nor fibrils. Hence, a lot of difficulties for RBA determination are avoided. Because of this, unbonded hand-

sheets were prepared by the solvent drying method according to Haselton (1955).

The Page equation

Another way to determine the RBA is by calculation via the so called Page equation 5.2 (Page 1969). By this equation, the influence of both, single fibre strength and strength of the network itself, are regarded with respect to the paper strength.

$$\frac{1}{T} = \frac{9}{8Z} + \frac{12A\rho g}{bP\lambda RBA} \quad (5.2)$$

The tensile strength (T), is given by the zerospan tensile strength (Z), the cross section (A), fibre density (ρ), shear bond strength (b), fibre perimeter (P), mean fibre length (λ), gravitation constant (g) and relative bonded area (RBA). Thereby, the zerospan tensile strength (Z) can be expressed by the single fibre strength.

Page used his theoretical consideration to calculate the specific bond strength of single fibre-fibre joints (Page 1969). Therefore, he used RBA values according to Ingman and Thode (1959). In this thesis, the equation was used to estimate the RBA. Pulp fibres exhibit a distribution of cross section, strength and coarseness. Using viscose fibres has the advantage that all these parameters are approximately constant. Only tensile strength of hand sheets and specific bond strength of fibre-fibre joints (b) have to be measured. Tensile strength is given by the breaking length (see chapter 5.1). To get the specific bond strength, first the optical bonded area was determined via polarized light microscopy (see chapter 3.10) before the bond strength was measured according to chapter 3.11.

For the derivation of his equation, several assumptions were made by Page (Page 1969). Therefore, the applicability of equation 5.2 will be discussed in chapter 5.3 below.

5.2.1 Nitrogen adsorption measurements

First of all, the determination of relative bonded area by nitrogen adsorption measurements was tried. In a first attempt the applicability of this technique was verified. Round fibres (RF1, AF1, AF2 and CF1) as well as flat fibres (F9, F12, F22) were investigated. Results are given in figure 5.4 and table 5.3. Figure 5.4(a) displays the first problem using this method. All fibres that were used exhibited the same fibre length, cross section and fibre width. Therefore, the specific surface area of the fibre bundles should be the same for all round fibre samples. But this is not the case. According to (Kitla), measurement errors are predominant for areas below $0.5 \text{ m}^2/\text{g}$ which is unfortunately the case for most samples (see table 5.3). Since the data seem to be influenced by large measurement errors, calculation of the relative bonded area does not make sense.

Problems occur using nitrogen adsorption for surface area determination due to the following reasons:

1. Using solvent drying to obtain unbonded fibres may chemical modify the fibre surface. This will change the number of adsorption sites for nitrogen.
2. Cellulosic material cannot be cleaned by heat treatment. BET is usually used in surface science to investigate the surface area of inorganic samples. These samples are cleaned by a heat treatment to desorb any dirt (around 300°C or more (Kitla et al. 2013)). Since this is not possible for cellulose due to pyrolysis, the surface is covered by a mixture of volatile material which could interfere or invalidate the results.

Because of the issues mentioned above, BET is not applicable to investigate the RBA of viscose fibre handsheets.

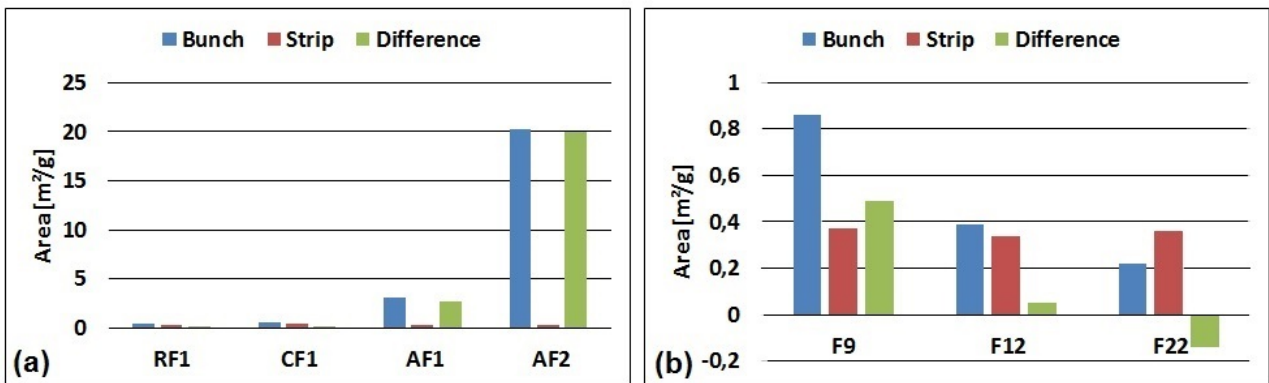


Figure 5.4: Calculated areas by nitrogen adsorption measurements of round (a) and flat fibres (b). Blue column - bundle of unbonded fibres, red column - strip of a handsheet, green column - difference of both areas.

Table 5.3: Detected surface values by using BET.

Sample	BET surface area	
	Bundle [m²/g]	Strip [m²/g]
RF1	0.39	0.26
CF1	0.58	0.45
AF1	3.06	0.35
AF2	20.3	0.31
F9	0.86	0.37
F12	0.39	0.34
F22	0.22	0.36

5.2.2 Light scattering

Since BET is not applicable in this case, light scattering was used for RBA determination. First, the scattering coefficient of bonded handsheets was measured. The results are shown in table 5.4 as well as in figure 5.5. In figure 5.5(a) the data of the untreated fibres is seen, where S decreases with the fibre width. Since the fibres in F4 are much thinner than these in F22, there are more fibres within a handsheet of the same grammage. Hence, there are more interfaces in a sheet made of F4. Because of this, S is higher for F4 than for F22. The opacity decreases as well except for F9 which exhibits the highest value. The results of F9 need further discussion. Since the influence of charges on the RBA was of interest, unbonded handsheets were only made of the different F9 samples. Since unbonded handsheets are too fluffy for the measuring assembly they were put on a glass plate. This glass plate influences the opacity as well as of the scattering coefficient. To get comparable results of bonded and unbonded handsheets of F9, both sheets were measured under the same conditions. In other words, all F9 samples (F9, F9C, F9A, F9AC) were measured lying on a glass plate, in contrast to F4, F12 and F22. This has to be considered while comparing the results with the other samples.

Table 5.4: Optical properties of the bonded handsheets. Data for the fibres F9, F9C, F9A and F9AC are shown in Weber et al. too.

Bonded handsheets			
Sample	S [m^2/kg]	K [m^2/kg]	Opacity [%]
F4	10.23	0.33	55.00
F12	8.89	0.29	53.00
F22	8.26	0.24	50.10
F9	10.91	0.69	63.42
F9C	10.35	0.65	61.72
F9A	8.37	0.52	55.02
F9AC	8.71	0.29	52.02

However, looking at the results of the F9 fibre samples (figure 5.5(b)), a decrease of the scattering coefficient S from F9 to F9A is seen. This is because of improved handsheet quality due to additional charges. On the contrary, F9C exhibits nearly the same S than F9. As it was shown in chapter 4 and confirmed by nanointentation (chapter 5.1.1), carboxymethylcellulose leads to more flexible fibres. Therefore, cationic fibres do not conform to each other as good as anionic fibres which results in more interfaces within the sheet. Because of that, a higher scattering coefficient is seen for F9C.

A comparison of the scattering coefficient of bonded and unbonded handsheets is given in figure 5.6. Figure 5.6(b) displays the data of the unbonded handsheets which is shown in table 5.5 in more detail. Handsheets were prepared according to Haselton

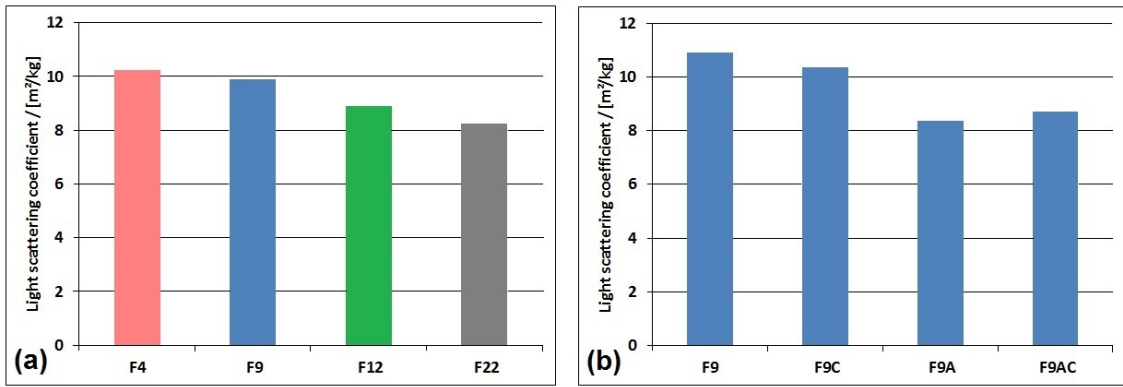


Figure 5.5: Light scattering of the investigated handsheets - bonded handsheets.

(1955) (see chapter 5.2). Since the influence of charges to the paper properties was of major interest, unbonded handsheets were only made of the F9 samples. These data were used for the RBA calculation according to equation 5.1 (see chapter 5.2.5).

Table 5.5: Optical properties of the unbonded handsheets. The given values are mean values of five data points distributed on a handsheet. Data are shown in Weber et al. too.

Unbonded handsheets			
Sample	$S_0 [m^2/kg]$	$K [m^2/kg]$	Opacity [%]
F9	21.88	0.11	69.91
F9C	23.67	0.41	76.87
F9A	23.50	0.61	78.91
F9AC	36.05	0.30	82.97

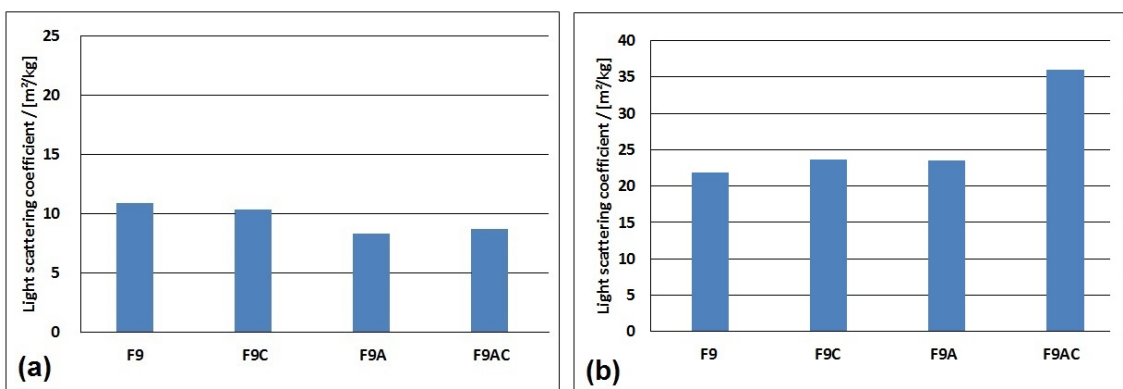


Figure 5.6: Light scattering of the investigated handsheets - bonded (a) and unbonded (b) handsheets. Adapted from Weber et al..

The scattering coefficient varies between $23.50 \text{ m}^2/\text{kg}$ and $36.05 \text{ m}^2/\text{kg}$. An interpretation of these results is difficult. A higher light scattering coefficient should correspond to more interfaces where light is scattered. Therefore, higher values, due to a lack of bonds is seen for unbonded handsheets. As it can be seen, the scattering coefficient is higher for handsheets made of charged fibres. Maybe charged fibres repel each other, which will influence both, S and opacity. Images of all unbonded handsheets made are seen in figure 5.7.

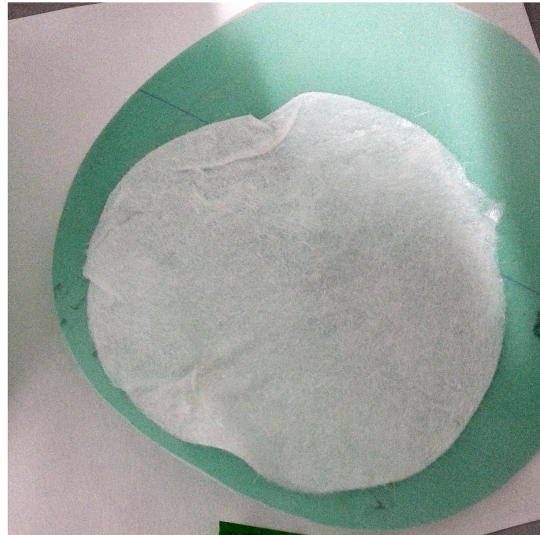
**F9****F9C****F9A****F9AC**

Figure 5.7: Unbonded handsheet of F9, F9C, F9A and F9AC.

5.2.3 Polarized light microscopy

As mentioned in chapter 5.2 RBA was also calculated via the Page equation. Therefore, the specific bond strength (bond strength per area), b in equation 5.2, of the investigated fibres needs to be known. First, the bonded area was determined by polarized light microscopy.

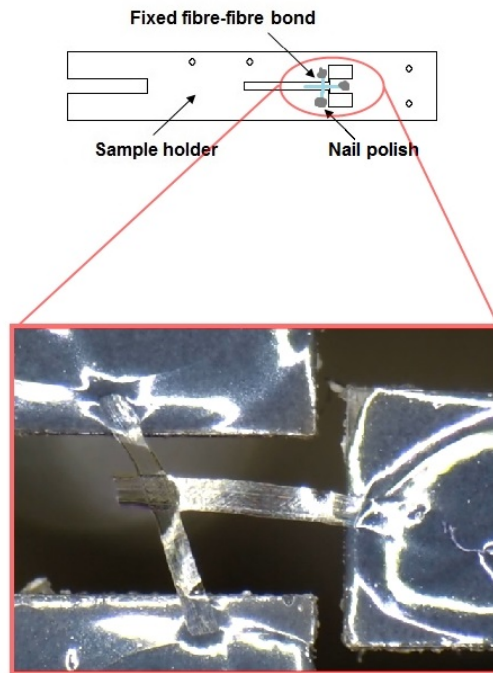


Figure 5.8: Fibre-fibre joint, fixed on the sample holder by nail polish for bonding area and bond strength investigations. An image of the red marked area is shown where the fixed fibre-fibre-joint is seen. Adapted from Weber et al..

Fibre-fibre joints were obtained by putting small drops of a dilute suspension (consistency of about 0.01%) onto a small teflon plate (Kappel et al. 2009). The teflon plate is covered with a second one and both are placed between two paper sheets. Finally, the paper sheet / teflon plate sandwich is dried in a Rapit Köthen sheet dryer for about 45 min. After drying, fibre-fibre joints were searched and selected by using a pair of tweezers. The fibre-fibre joints were fixed with nail polish on the sample holder like shown in figure 5.8. Besides the schematic view of the sample holder, a fixed fibre-fibre joint is pictured in figure 5.8. After mounting, pictures of the joint were taken and evaluated like described in chapter 3.10. Such an image is seen in figure 5.9. As it can be seen, the bonded area appears dark. This area is marked and determined according to chapter 3.10.

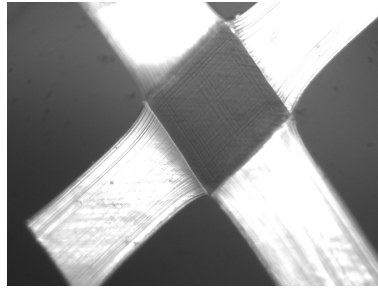


Figure 5.9: Image of a fibre-fibre joint made through the polarized light microscope.

Table 5.6: Optical bonded area of all investigated fibre-fibre joints. Ten joints of each fibre sample were investigated. The mean values are shown.

	Optical bonded area [μm^2]			
	F9	F9C	F9A	F9AC
mean value	25887.09	28268.82	31431.10	43831.60
std. dev.	10099.26	10085.76	8857.26	17667.02

Ten fibres of each fibre type were investigated. Since the fibre-fibre joints are very fragile, on average, only every tenth joint could be tested. The results are given in table 5.6. As it can be seen, the optical bonded area increases from F9 to F9AC. It has to be considered, that the bonding angle is not always the same (reflected by the standard deviation). However, since the bonding strength per unit area is determined, the bonding angle does not matter.

5.2.4 Joint strength measurements

Immediately after polarized light microscopy, the bond strength of the fibre-fibre joints was tested. The measuring procedure is shown in chapter 3.11. An example of a measured force-distance curve is shown in figure 5.10. The bond was broken at a force of 1.4 g (=13,7 mN).

The mean value of all ten investigated fibre-fibre joints of each fibre type are shown in table 5.7. As it can be seen, the highest values are obtained for F9C and F9A. The standard deviation is quite high for all fibre samples. Even for these model fibres, there is a high variation of fibre-fibre bond strengths. Some bonds exhibit very high values whereas others are comparatively weak. This is due to the following reasons. First of all, the area in molecular contact is unknown. The molecular bonded area might be much smaller than the optical bonded area. Hence, a bond may be weaker as suspected in the first place. In addition, the melting of the sample holder bridges has an unknown impact on the bonds.

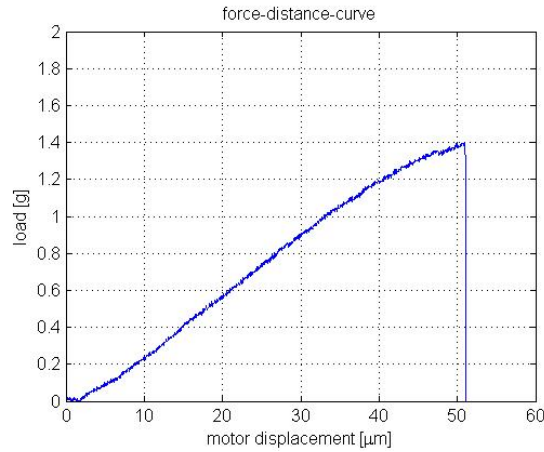


Figure 5.10: Force-distance curve.

However, the bond strengths are a factor 2 to 3 higher than values for unbleached softwood kraft pulp fibres (Fischer et al. 2012). On the other hand, the specific bond strengths are much lower. The specific bond strength (b) is received by simply dividing the strength of each individual fibre-fibre joint by the corresponding area. The results are then averaged and were used for RBA calculation. The mean values of the specific bond strength (b) are shown in table 5.8.

Table 5.7: Bond strength of all investigated fibre-fibre joints. Ten joints of each fibre sample were investigated. The mean values are shown.

	Bond strength [mN]			
	F9	F9C	F9A	F9AC
mean value	12.09	16.23	16.83	15.78
std. dev.	9.08	15.04	10.63	18.43

Table 5.8: Mean value and standard deviation of the specific bond strength. Adapted from Weber et al..

	Specific bond strength [N/mm ²]			
	F9	F9C	F9A	F9AC
mean value	0.51	0.91	0.57	0.38
std. dev.	0.36	1.23	0.34	0.32

Surprisingly the smallest value of b is found for F9AC. Because these fibres give hand-sheets with the highest tensile strength values, this result was not expected. The addition of CMC results in higher fibre swelling (chapter 4.1) and, therefore, larger

bonding areas. The results of the specific bond strength b for F9AC and F9A let assume, that swelling is enhanced. The bond strength is improved as well but not to the same extent as moisture expansion. On the other hand, this assumption does not fit with the results obtained for round fibres. Maybe the influence of melting the sample holder bridges was higher in this test series. The optical bonded area is much higher for F9AC. On the other hand, only a small increase in bond strength is seen. As a result of this, the specific bond strength becomes smaller. Cationic fibres do not exhibit improved swelling. However, the cationic charges lead to stronger fibre-fibre joints. This is because the specific bond strength (b) for F9C shows the highest values. It should be emphasized that measurement errors due to the measurement itself may occur.

Comparing these results with values found for paper fibres exhibits how weak viscose fibre-fibre joints are. An average optical bonded area of $25887 \mu\text{m}^2$ was found for F9. The average bond strength is given by 12.09 mN which gives a specific bond strength of 0.52 N/mm^2 . According to Fischer et al. (2012) a specific bond strength of 5.79 N/mm^2 is found for kraft pulp fibres. Similar results were found by Stratton and Colson (1990) for Loblolly pine. They found a specific bond strength of 2.1 N/mm^2 (early wood) and 6.4 N/mm^2 (late wood). The difference in the specific bond strength between pulp and viscose fibres is most likely due to the absence of mechanical interlocking in viscose fibres. The lack of Coulomb interactions in viscose fibres also contributes to this gap. Additionally, viscose fibres are more rigid than pulp fibres. Hence, they do not resist stress or strain similarly to pulp fibres.

5.2.5 RBA - results

5.2.5.1 RBA - Light scattering

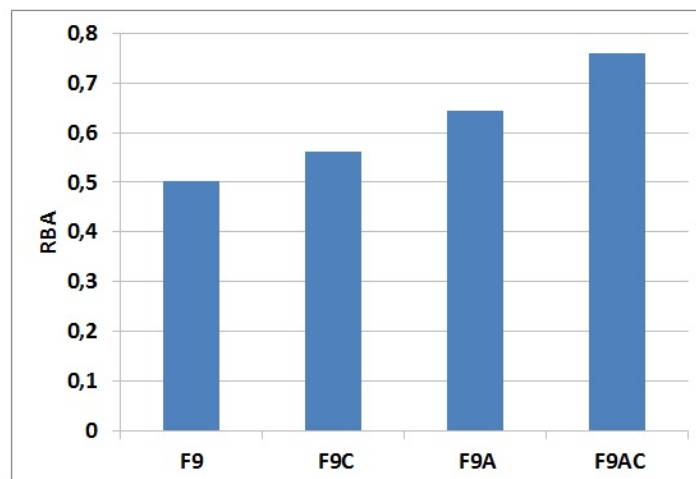


Figure 5.11: Relative bonded area obtained from light scattering measurements.

The RBA was calculated according to equation 5.1. The results are shown in figure 5.11. Using this method, only small differences are seen between F9 and F9C. Since cationic starch does not increase fibre swelling or the bonding area the RBA should be the same for F9 (RBA = 0.50) and F9C (RBA = 0.56). A gap of 0.06 is not significant and may be due to measurement errors. The RBA increases by adding CMC or both additives to the fibres as expected.

5.2.5.2 RBA - Page equation

Before calculating the RBA via the Page equation, equation 5.2 has to be converted to equation 5.3.

$$RBA = \frac{96A\rho gZT}{bP\lambda(8Z - 9T)} \quad (5.3)$$

After tensile strength measurements, polarized light microscopy and joint strength measurement, all parameter of equation 5.3 are known (see table 5.9).

Table 5.9: Parameters, given in units used for RBA calculation via the Page equation.

Fibre parameters known			
A [cm ²]	0.000006		
ρ [g/cm ³]	1.5		
g [cm/s ²]	981		
P [cm]	0.0308		
λ	0.6		
Parameters measured			
	Z [cm]	T [cm]	b [dyn/cm ²]
F9	1962953.71	267400	5044938.74
F9C	1676413.45	430500	5711975.56
F9A	1509180.00	498300	9056390.58
F9AC	1144121.59	576000	3747357.40

Larger differences between F9 and the anionic fibres are seen by using the Page equation (see figure 5.12). Again, F9 (RBA = 0.36) and F9C (RBA = 0.38) have nearly the same RBA. The difference of 0.02 is even smaller than for the RBA determined by light scattering. The RBA of F9A (RBA = 0.95) is almost 1 which would mean that the whole fibre surface of all fibres is bonded. Because of this, the value found for F9AC (RBA = 2.03) does not make sense. Because of these results, further discussion is necessary.

5.2.5.3 RBA - Comparison

Before the results are discussed in more detail, the data from both measurement techniques will be compared. The results are visualized in figure 5.12.

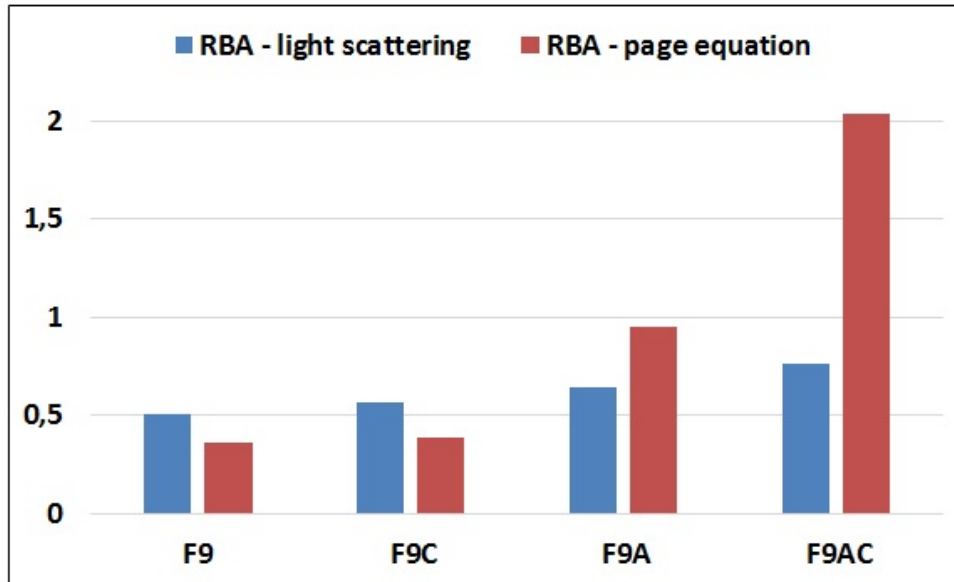


Figure 5.12: Relative bonded area - comparing of the results. Adapted from Weber et al..

Comparing the results shown in figure 5.12, large differences are seen. Using light scattering, larger RBA values for F9 and F9C are obtained. Furthermore, the RBA increases nearly linearly from F9 to F9AC. In contrast to the results obtained by using the Page equation. While F9 and F9C exhibit rather small values, a huge increase is seen for F9A and F9AC. Due to low specific bond strength and high breaking length these values are obtained. However, a RBA of 2.03 does not make sense. Because of this, the Page equation will be discussed in more detail.

Several assumptions were made by Page for the derivation of equation 5.2 (Page 1969).

1. First of all, he assumed, that the load across the line of rupture is taken by progressively fewer fibres because of bond failures at the ends of the fibres. By rising the load, the point of failure is approached. Thereby more bonds fail in the rupture zone. The remaining fibres have to take more of the sheet loading. Finally, the fibres lying in the direction of the load fail as well and the paper ruptures. This circumstances are described by equation 5.4 (Page 1969):

$$T = \frac{n_f Z_e}{n_f + n_p} \quad (5.4)$$

with the number of fibres which fail across the rupture line (n_f), number of fibres which are pulled out intact (n_p), the tensile strength (T) and the finite-span tensile strength (Z_e).

2. Next, it is assumed that the formation of the sheet is good. This means, the number of fibres crossing any line should be equal.
3. Z_e is expressed by the zero-span tensile strength Z (Page 1969):

$$Z_e = Z(1 - \mu^2) \quad (5.5)$$

with the Poisson's ratio μ . According to Page (1969) and Brecht and Wanka (1963) $\mu = 1/3$. Equation 5.4 turns therefore to:

$$T = \frac{8n_f Z}{9(n_f + n_p)} \quad (5.6)$$

4. Another assumption concerns the number of fibres that fail at the instant of rupture and the number of fibres pulled intact. Page presumed that this may be expressed by (Page 1969):

$$\frac{n_p}{n_f} = \frac{\phi}{\beta} \quad (5.7)$$

where ϕ is the mean fibre strength and β the mean force applied along the fibre axis to pull a fibre from the sheet. Thereby, he assumed the fibres to be Hookean fibres to use an expression of ϕ derived from van den Akker et al. (1958):

$$\phi = \frac{8}{3} A \rho g Z \quad (5.8)$$

According to equation 5.8 the fibre strength is given by the average fibre cross section (A), the density of the fibrous material (ρ) and the gravitation acceleration (g). Furthermore, Page assumed all fibre-fibre bonds to act cooperatively along the length of a fibre (Page 1969). Hence, β is given by (Page 1969):

$$\beta = bP \frac{L}{4} RBA \quad (5.9)$$

The mean force to pull a fibre from the sheet (β) is therefore given by the specific bond strength (b), the perimeter of the fibre cross section (P) the fibre length (L - the mean pulled length is given by L/4) and the relative bonded area (RBA).

Ideal conditions were assumed for derivation of the Page equation. But every sheet of paper exhibits some kind of flocculation. Furthermore, paper fibres as well as viscose fibres are not Hookean but viscoelastic fibres. However, Page himself admitted several deficiencies of his theory (Page 1969). The distribution $\frac{\phi}{\beta}$ is in fact unknown.

Moreover, it does not apply to sheets of poor formation or rather high flocculation and it assumes straight fibres without any kinks (Page 1969). External fibrils are neglected as well.

As already mentioned in the beginning, viscose fibres are model fibres. But even these fibres deliver statistically distributed values for specific bond strength. Therefore, the Page equation will never provide exact data or reproduce the complex reality. However, it will give hints if the RBA of a sheet is higher than the RBA of another sheet. On the other hand, unpredictable measurement errors due to bond strength measurement (melting of the sample holder bridges) may lead to wrong values as well. Besides, the optical bonded area may not be equal to area in molecular contact.

Furthermore, the question remains, if specific bond strength is measurable in general. Figure 5.13 illustrates schematically a fibre-fibre joint during bond strength measurement. A force, F , is applied on fibre B to pull it away. In the ideal case (figure 5.13b) both fibres are totally flat. Hence, the whole point of contact is molecular bonded. In this case, the specific bond strength can be measured, if the whole bond is ruptured at once. Since there are always some slightly uneven spots, crack propagation occurs in reality (see figure 5.13c). From fraction mechanics it is well known that the force needed for such crack propagation is smaller than the force which is required to break the whole bond at once. During the measurements, crack propagation was observed almost every time. Therefore, the specific bond strength can not be measured at all. As a consequence, the RBA can not be calculated by using the Page equation. Conversely, if there would be a way to measure the RBA of handsheets, the specific bond strength could be calculated according to the Page equation. However, these results would be afflicted by errors as well, since several assumptions were made by Page.

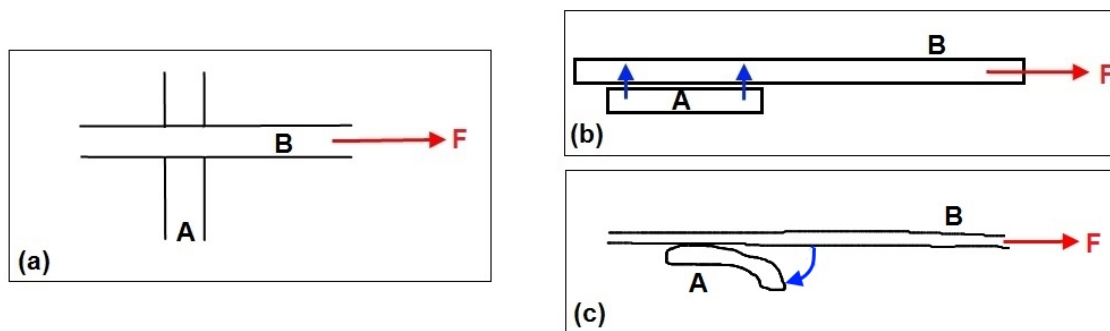


Figure 5.13: Schematic illustration of a bond break. (a) top view, (b) idealised conditions, (c) reality.

Finally, the light scattering method is not without any doubts. First of all this measurement method is based on the Kubelka-Munk theory which is not without controversy in its use for paper. The theory assumes the investigated medium to be a

homogeneous and ideally scattering matter (see chapter 3.9). Since paper does not fulfill this requirements, no absolute value for S , K or opacity is obtained. On the bottom line this technique also gives just an approximation of the RBA.

5.3 Summary

The influence of fibre width on the tensile strength is seen in chapter 5.1. Breaking length decreases with increasing fibre width. Assuming that thin fibres are more flexible, these results are evident. Furthermore, handsheets made of thin fibres exhibit more fibres than handsheets of the same grammage made of broad fibres. Therefore, there are smaller but more fibre-fibre bonds within the sheet. As a consequence, bond failure does not have such a great influence because there are enough remaining bonds left, taking the load.

Again improved tensile strength is seen for physical modified fibres. The results are similar to the data found for round fibres. Cationic starch improves the breaking length due to introduced charges. An even higher tensile strength is achieved by using CMC as additive. A combination of both, CMC and cationic starch seems to deliver the best result.

According to Persson et al. (2013), swelling and surface hardness are linked which was confirmed by the nanointentation measurements. Improved swelling was seen for anionic fibres as well as higher tensile strength for paper sheets made of them (see chapter 4.1 and chapter 4.2). A lower surface hardness of anionic fibres compared to the others is therefore evident. Soft fibres are more flexible and confirm to each other in a better way.

The relative bonded area of handsheets made of fibres with different charges, was tried to be determined by light scattering and calculated according to the Page equation. Both measurements have shown increased RBA for handsheets made of fibres blended with additives. However, no absolute value of RBA can be obtained by these methods. While there is no proof that a change in scattering coefficient is only due to a change in interfaces, the Page equation is based on too many assumptions. Both techniques only deliver approximate values. Therefore, only estimations of which handsheet will exhibit a larger RBA can be made.

6 Summary

6.1 Round fibres - Surface charge investigations

6.1.1 Influence of charge on swelling and breaking length

Four different samples were analysed:

- fibres without any additives (RF1) were used as reference
- a cationic fibre CF1 blended with cationic starch
- two anionic fibres AF1 and AF2 with different amounts of CMC

RF1 and CF1 have shown a moisture expansion of about 34%. Hence, cationic starch does not improve the swelling behaviour. The anionic fibres have shown a swelling of 45.9% (AF1) and 57.1% (AF2).

RF did not deliver a measurable tensile strength. Therefore, no breaking length could be calculated for the reference sample. In contrast to handsheets made of charged fibres. CF1 (521.4 m) exhibits a breaking length almost as large as of AF1 (693.4 m). This is only due to introduced charges, since CF1 did not show enhanced swelling. The highest values for breaking length are seen for the anionic fibres (AF2 - 2,000 m). Introduced charges and enlarged bonding areas due to improved swelling are responsible for this enhancement.

6.1.2 analysing of surface charge

Two additional samples were analysed:

- pure CMC as a second reference
- CF2, another cationic fibre

The amount of anionic surface charges was analysed by titration. To verify the existence of charged species on the fibre surface, attenuated total reflection infrared spectroscopy and X-ray photoelectron spectroscopy were used.

Peaks of COOH-groups were found by ATR at 1580 cm^{-1} and 1413 cm^{-1} . The CH_3N group of the starch was reflected by peaks at 1647 cm^{-1} and 1637 cm^{-1} . A linear ratio between the number of COOH-groups and integrated peak area of 1580 cm^{-1} was found. It seems that the amount of anionic charges grows monotonically with the amount of CMC.

Additives are seen by XPS as well but the exact quantity cannot be established since the quantity of fibres in the investigated spot is not known. The peak area corresponding to the CH_3N doubles from CF2 (18.71%) to CF1 (32.29%). This result fits very well with the data obtained by titration. However, no linear correlation between additives and detected peak was seen for the anionic samples.

The existence of surface charges was verified by all used measurement methods. Nevertheless, the distribution within the fibre bulk remains unclear.

6.2 Flat fibres - Relative bonded area of handsheets

6.2.1 Breaking length

Breaking length of seven different flat viscose fibre samples were determined:

- F4 - flat fibres of 4.31 dTex
- F12 - flat fibres of 11.53 dTex
- F22 - flat fibres of 25.07 dTex
- F9 - flat fibres of 9.56 dTex
- F9C - cationic flat fibres
- F9A - anionic flat fibres
- F9AC - flat fibres blended with both additives

Breaking length of handsheets without any additives exhibits higher values if small fibres are used (F4 - 4,244 m; F22 - 903 m). By rising fibre width, tensile strength decreases. This is due to higher fibre flexibility of smaller fibres which results in a better

sheet formation.

Again, the influence of charges is seen by the breaking length of handsheets made of charged fibres. Also, a decrease of wet fibre hardness due to additives was shown by nanointentation, especially for CMC that leads to a soft fibre surface. Because of this, the fibres are more flexible leading to a better conformation and therefore more fibre-fibre bonds.

6.2.2 Light scattering method

F9 and F9C exhibit nearly the same RBA. An increase of RBA for handsheets made of anionic fibres was seen. This fits very well with the swelling and tensile strength data of round fibres. However, even if this technique is rather fast and simple, it does not deliver absolute values. This is due to the assumptions made by the Kubelka-Munk theory and because of the measurement technique as well. It is unclear whether the change of the scattering coefficient is only due to nonexisting bonds. Furthermore it can not be said if all fibres within an unbonded sheet, made by solvent drying, are really unbonded.

6.2.3 Page equation

Finally, the optical bonded area and the joint strength of fibre-fibre joints were determined to calculate the RBA by using the Page equation. The optical bonded area was analysed by polarized light microscopy and used to calculate the bond strength per unit area. The bond strength of each fibre-fibre joint was determined by using a micro bond tester.

Very small values of specific bond strength, b , were found for F9AC (0.38 N/mm^2) followed by F9 (0.51 N/mm^2) and F9A (0.57 N/mm^2). The highest b values were found for F9C (0.91 N/mm^2). Since, the optical bonded area of F9A and F9AC were very high, but the bond strength was comparably low, this result for b was obtained. This is unexpected, as handsheets of F9A and F9AC exhibit the highest breaking length values. The reason for this may lie in the small-sized statistic of only 10 fibres of each fibre type.

Due to several assumptions made by Page no exact values of the RBA could be obtained by using the Page equation. However, comparing the results of light scattering and received by the Page equation, the same trend is seen. F9 and F9C exhibit nearly the same RBA of about 0.36 or rather 0.38. The RBA increases by adding CMC to the samples. Due to the large breaking length and the low specific bond strength a value of 2.03 was found for F9AC. According to the Page equation, high tensile strength and low specific bond strength result in a large RBA. A lot of circumstances are not considered by this theory as discussed above. Consequently, this empirical equation

can only give approximate values too.

Moreover, the specific bond strength cannot be measured due to crack propagation. Since the force needed to break a fibre-fibre joint by crack propagation is smaller than by instant rupture of the whole bond, the actual bond strength is larger than the measured one.

6.3 Conclusion

It was shown that charges are an applicable way to improve tensile strength of handsheets. While cationic starch only enhances the bond strength, CMC improves moisture expansion of the fibres too. This leads to enlarged bonding areas which gives an additional boost to the tensile strength of handsheets. Charges seems to be located on or near the fibres surface. However, no information about the charge distribution within the fibres was obtained. No absolute value of the relative bonded area could be obtained either. BET seems to be not applicable for viscose fibres. Neither light scattering nor calculations via the Page equation deliver correct results. This is due to the amount of assumptions in the theories behind these techniques and because of unavoidable measurement errors.

7 Outlook

Several measurement methods were used to study the influence of charges on the tensile strength of viscose fibre handsheets. Nevertheless, some questions still remain which require further examinations. As the measured amount of COOH of the reference fibre sample is rather high, additional methods seem to be appropriate. The FDAM method (Bohrn et al. 2006) could be used to verify the data generated by titration. In addition, Young's modulus of the viscose fibres and of the handsheets will be analysed to examine the influence of the additives on this parameter.

In order to provide as accurately as possible, an overall picture of the charge distribution within the fibre bulk, investigations of the fibre cross section by means of IR-microscopy (Wilhelm 1996) and Raman-spectroscopy will be done in the future.

All used methods to determine the relative bonded area of viscose fibre handsheets only delivered approximate values. To gain more reliable values is another objective. Therefore, further developments of the joint strength measurement equipment will be done to gain more precise values using the Page equation. For example, the soldering iron will be replaced by a hot filament. This will reduce the influence on the bond during melting of the sample holder bridges. Using a larger sample size in order to get better statistics is another task. However, since the specific bond strength cannot be determined in a sufficiently way, another method seems to be necessary. At the Institute of Solid State Physics at Graz University of Technology a method was developed which has the potential to measure the area of fibre-fibre bonds in a paper network (Gilli and Schennach 2012). Development of a prototype will give the possibility to determine the RBA by means of ellipsometry.

Bibliography

- Adusumali, R.-B., Müller, U., Weber, H., Roeder, T., Sixta, H., and Gindl, W. (2006). Tensile Testing of Single Regenerated Cellulose Fibres. *Macromolecular Symposia*, 244:83–88.
- Alén, R., editor (2008). *Papermaking Science and Technology - Book 4: Papermaking Chemistry*. Finnish Paper Engineers' Association/Paperi ja Puu Oy.
- Andress, K. (1929). The X-ray diagram of mercerized cellulose. *Zeitschrift für Physikalische Chemie*, B4:190–206.
- Anthony, J., Bideaux, R., Bladh, K., and Nichols, M. (2000). Handbook of Mineralogy. Diamond. *American Mineralogical Society*.
- Batchelor, W. and He, J. (2005). A new method for determining the relative bonded area. *Tappi*, 4, No.6:23–28.
- Beamson, G. and Briggs, D. (1992). *High Resolution XPS of Organic Polymers - The Scienta ESCA300 Database*. John Wiley & Sons Ltd.
- Bergmann, L., Schäfer, C., and Raith, W. (2006). *Lehrbuch der Experimentalphysik; Band 2: Elektromagnetismus*. Walter de Gruyter.
- Bernt, I. private communication, 1.10.2012.
- Bernt, I. private communication, 11.12.2013.
- Bernt, I. private communication, 23.7.2013.
- Bernt, I. (2010a). Fine-tuning of paper characteristics by incorporation of viscose fibres. In *Zellcheming-Hauptversammlung*.
- Bernt, I. (2010b). WO2011012422 (A1) - Use of a regenerated cellulose fibre in a flame-retardant product; European Patent Office.
- Blomstedt, M., Kontturi, E., and Vuorinen, T. (2007). Optimising CMC sorption in order to improve tensile stiffness of hardwood pulp sheets. *Nordic Pulp and Paper Research Journal*, 22, Nr. 3:336–341.

- Bohrn, R., Potthast, A., Schiehser, S., Rosenau, T., Sixta, H., and Kosma, P. (2006). The FDAM Method: Determination of Carboxyl Profiles in Cellulosic Materials by Combining Group-Selective Fluorescence Labeling with GPC. *Biomacromolecules*, 7:1743–1750.
- Brecht, W. and Wanka, R. (1963). Die Querkontraktion von Papieren. *Das Papier*, 4:141–147.
- Buchholz, V., Wegner, G., Stemme, S., and Ödberg, L. (1996). Regeneration, Derivatization and Utilization of Cellulose in Ultrathin Films. *Advanced Materials*, 8, Nr.3:399–402.
- Connors, T. E. and Banerjee, S., editors (1995). *Surface Analysis of Paper*. CRC Press, Inc.
- Demtröder, W. (2013). *Experimentalphysik 2*. Springer.
- Dufek, M. and Hayles, M. *The Quanta FEG 200, 400, 600 User's Operation Manual*.
- Duker, E. and Lindström, T. (2008). On the mechanisms behind the ability of CMC to enhance paper strength. *Nordic Pulp and Paper Research Journal*, 23, No.1:57–64.
- Eckhart, R. Script for the lecture "Primärfaserstoffe", Institute for Paper, Pulp and Fibre Technology, Graz University of Technology, 2012.
- Egerton, R., Li, P., and Malac, M. (2004). Radiation damage in the TEM and SEM. *Micron*, 35:399–409.
- Emmett, P. and DeWitt, T. (1941). Determination of Surface Areas: Pigments, Carbon Blacks, Cement and Miscellaneous Finely Divided or Porous Materials. *Industrial and Engineering Chemistry, Analytical Edition*, 13:28–33.
- Erhard, K., Arndt, T., and Miletzky, F. (2010). Einsparung von Prozessenergie und Steuerung von Papiereigenschaften durch gezielte chemische Fasermodifizierung. *European Journal of Wood and Wood Products*, 68, Nr.3:271–280.
- Ertl, G. and Küppers, J. (1974). *Low Energy Electrons and Surface Chemistry*. Verlag Chemie.
- Eschbach, H., F.Gross, and Schulien, S. (1963). Permeability Measurements with Gaseous Hydrogen for Various Steels. *Vacuum*, 13:543–547.
- Fahrenfort, J. (1961). Attenuated total reflection: A new principle for the production of useful infra-red reflection spectra of organic compounds. *Spectrochimica Acta*, 17:698–709.
- Fengel, D. and Wegener, G. (2003). *Wood; Chemistry, Ultrastructure, Reactions*. Verlag Kessel.

- Fischer, W. private communication, 16.12.2013.
- Fischer, W., Hirn, U., Bauer, W., and Schennach, R. (2012). Testing of individual fibre-fibre joints under biaxial load and simultaneous analysis of deformation. *Nordic Pulp and Paper Research Journal*, 27, No.2:237–244.
- Forest Products Laboratory (2013). *Centennial Edition: Wood Handbook: Wood as an Engineering Material*. CreateSpace Independent Publishing Platform.
- Fras, L., Johansson, L.-S., Stenius, P., Laine, J., Stana-Kleinschek, K., and Ribitsch, V. (2005). Analysis of the oxidation of cellulose fibres by titration and XPS. *Colloids and Surfaces A: Physicochemical and Engineering Aspects*, 260:101–108.
- Freudenberg, U., Zschoche, S., Simon, F., Janke, A., Schmidt, K., Behrens, S., Auweter, H., and Werner, C. (2005). Covalent Immobilization of Cellulose Layers onto Maleic Anhydride Copolymer Thin Films. *Biomacromolecules*, 6:1628–1634.
- Ganser, C., Hirn, U., Rohm, S., Schennach, R., and Teichert, C. (2013). AFM nanoindentation of pulp fibers and thin cellulose films at varying relative humidity. *Holzforschung*, DOI 10.1515/hf-2013-0014.
- Gardner, K. and Blackwell, J. (1974a). The Structure of Native Cellulose. *Biopolymers*, 13:1975–2001.
- Gardner, K. and Blackwell, J. (1974b). The structure of native cellulose. *Biopolymers*, 13, Nr. 10:1975–2001.
- Gilli, E. (2008). IR spectroscopic investigations on the chemical surface properties of cellulose fibers. Master's thesis, Graz University of Technology.
- Gilli, E., Kappel, L., Hirn, U., and Schennach, R. (2009). An Optical Model for Polarization Microscopy Analysis of Pulp Fibre-to-Fibre Bonds. *Composite Interfaces*, 16:901–922.
- Gilli, E. and Schennach, R. (2012). Imaging ellipsometry based method and algorithm for the analysis of fiber-fiber bonds in a paper network. *Applied Optics*, 51, No.2:273–280.
- Gobecht, J. (2009). *Werkstofftechnik - Metalle*. Oldenbourg Wissenschaftsverlag GmbH.
- Goos, F. and Hänchen, H. (1947). Ein neuer und fundamentaler Versuch zur Totalreflexion. *Annalen der Physik*, 436; Issue 6:333–346.
- Griffiths, P. and de Haseth, J. (1986). *Fourier Transform Infrared Spectroscopy*. John Wiley & Sons, Inc. New York/Chichester/Brisbane/Toronto/Singapore.
- Grogger, W. (2008). Rasterelektronenmikroskopie (519.003), TU Graz, lecture notes. page 5.

- Götze, K. (1951). *Chemiefasern nach dem Viskoseverfahren (Reyon und Zellwolle)*. Springer.
- Harrick, N. (1960). Surface chemistry from spectral analysis of totally internally reflected radiation. *The Journal of Physical Chemistry*, 64; No.9:1110–1114.
- Haselton, W. (1955). Gas Adsorption by Wood, Pulp, and Paper II. The Application of Gas Adsorption Techniques to the Study of the Area and Structure of Pulps and the Unbonded and Bonded Area of Paper. *Tappi*, 38, No.12:716–723.
- Herres, W. and Gronholz, J. (1984). Understanding FT-IR Data Processing Part 1: Data Acquisition and Fourier Transformation. *Computer Applications in the Laboratory*, 2, Nr. 4:216–220.
- Hindeleh, A. and Johnson, D. (1974). Crystallinity and crystallite size measurement in cellulose fibres: 2. Viscose rayon. *Polymer*, 15:697–705.
- Horvath, A. and Lindström, T. (2007). Indirect polyelectrolyte titration of cellulosic fibers - Surface and bulk charges of cellulosic fibers. *Nordic Pulp and Paper Research Journal*, 22, No. 1:87–92.
- Horvath, A., Lindström, T., and Laine, J. (2006). On the Indirect Polyelectrolyte Titration of Cellulosic Fibers. Conditions for Charge Stoichiometry and Comparison with ESCA. *Langmuir*, 22:824–830.
- Ingmanson, W. and Thode, E. (1959). Factors Contributing to the Strength of a Sheet of Paper II. Relative Bonded Area. *Tappi*, 42, No.1:83–93.
- Jenkins, L. and Donald, A. (1997). Use of the Environmental Scanning Electron Microscope for the Observation of the Swelling Behaviour of Cellulosic Fibres. *Scanning*, 19:92–97.
- Johansson, L.-S., Campbell, J., Koljonen, K., and Stenius, P. (1999). Evaluation of surface lignin on cellulose fibers with XPS. *Applied Surface Science*, 144-145:92–95.
- Junge, F. (2008). *Einführung in die Grammatik des Neuägyptischen*. Harrossowitz Verlag, Wiesbaden.
- Kaarlo, N., editor (2008). *Papermaking Science and Technology - Book 16: Paper Physics*. Finnish Paper Engineers' Association/Paperi ja Puu Oy.
- Kallmes, O. and Eckert, C. (1964). The Structure of Paper VII. The Application of the Relative Bonded Area Concept to Paper Evaluation. *Tappi*, 47, No.9:540–548.
- Kappel, L., Hirn, U., Bauer, W., and Schennach, R. (2009). A novel method for the determination of bonded area of individual fiber-fiber bonds. *Nordic Pulp and Paper Research Journal*, 24 No.2:199–205.

- Kappel, L., Hirn, U., Gilli, E., Bauer, W., and Schennach, R. (2010a). Revisiting Polarized Light Microscopy for Fiber-Fiber Bond Area Measurement - Part 2: Proving the Applicability. *Nordic Pulp and Paper Research Journal*, 25:71–75.
- Kappel, L., Hirn, U., Gilli, E., Bauer, W., and Schennach, R. (2010b). Revisiting polarized light microscopy for fiber-fiber bond area measurement - Part 1: Theoretical fundamentals. *Nordic Pulp and Paper Research Journal*, 25:65–70.
- Karabiyik, U., Mao, M., Roman, M., Jaworek, T., Wegner, G., and Esker, A. (2009). Optical characterization of cellulose films via multiple incident media ellipsometry. *ACS Symposium Series, Model Cellulosic Surfaces*, 1019:137–155.
- Katz, S., Beatson, R., and Scallan, A. (1984). The determination of strong and weak acidic groups in sulfite pulps. *Svensk papperstidning*, 87 Nr.6:48–52.
- Kitla, A. private communication, 05.06.2012.
- Kitla, A., Safonova, O., and K.Föttinger (2013). Infrared Studies on Bimetallic Copper/Nickel Catalysts Supported on Zirconia and Ceria/Zirconia. *Catalyst Letters*, 143:517–530; DOI: 10.1007/s10562-013-1001-y.
- Kjeldahl, J. (1883). Neue Methode zur Bestimmung des Stickstoffs in organischen Körpern. *Z analy Chem*, 22:366–382.
- Koch, H. (2009). *Experimental and Theoretical Investigation of the Interaction of simple Molecules with Rhodium, Copper and Palladium/Zinc Surfaces*. PhD thesis, Graz University of Technology.
- Kontturi, K., Tammelin, T., Johansson, L.-S., and Stenius, P. (2008). Adsorption of Cationic Starch on Cellulose Studied by QCM-D. *Langmuir*, 24:4743–4749.
- Kubelka, P. (1948). New contributions to the optics of intensely light-scattering materials. *Journal of the Optical Society of America*, 38, Nr.5:448–457.
- Kubelka, P. and Munk, F. (1931). Ein Beitrag zur Optik der Farbanstriche. *Zeitschrift für technische Physik*, 12:593–601.
- Laine, J., Lindström, T., Bremberg, C., and Glad-Nordmark, G. (2003a). Studies on topochemical modification of cellulosic fibres Part 5. Comparison of the effects of surface and bulk chemical modification and beating of pulp and paper properties. *Nordic Pulp and Paper Research Journal*, 18(3):325–332.
- Laine, J., Lindström, T., Bremberg, C., and Glad-Nordmark, G. (2003b). Studies on topochemical modification of cellulosic fibres Part4. Toposelectivity of carboxymethylation and its effects on the swelling of fibres. *Nordic Pulp and Paper Research Journal*, 18, Nr. 3:316–324.

- Laine, J., Lindström, T., Glad-Nordmark, G., and Risinger, G. (2002a). Studies on topochemical modification of cellulosic fibres Part 2. The effect of carboxymethyl cellulose attachment on fibre swelling and paper strength. *Nordic Pulp and Paper Research Journal*, 17, Nr. 1:50–56.
- Laine, J., Lindström, T., Nordmark, G. G., and Risinger, G. (2002b). Studies on topochemical modification of cellulosic fibres Part 2. The effect of carboxymethyl cellulose attachment on fibre swelling and paper strength. *Nordic Pulp and Paper Research Journal*, 17; No.1:50–56.
- Langan, P., Nishiyama, Y., and Chanzy, H. (1999). A revised structure and hydrogen bonding scheme in cellulose II from a neutron fibre diffraction analysis. *Journal of the American Chemical Society*, 121:9940–9946.
- Langan, P., Nishiyama, Y., and Chanzy, H. (2001). X-ray structure of mercerized cellulose II at 1Å resolution. *Biomacromolecules*, 2, No.2:410–416.
- Lindström, T. (1980). Der Einfluß chemischer Faktoren auf Faserquellung und Papierfestigkeit. *Das Papier*, 34(12):561–568.
- Lindström, T., Wågberg, L., and Larsson, T. (September 2005). On the nature of joint strength in paper - a review of dry and wet strength resins used in paper manufacturing. In *Advances in paper science and technology - Transactions of the 13th Fundamental Research Symposium held at Cambridge*; 457-562.
- Matsuo, M., Sawatari, C., Iwai, Y., and Ozaki, F. (1990). Effect of Orientation Distribution and Crystallinity on the Measurement by X-ray Diffraction of the Crystal Lattice Moduli of Cellulose I and II. *Macromolecules*, 23:3266–3275.
- Meyer, K. and Misch, L. (1937). Positions des atomes dans le nouveau modèle spatial de la cellulose. *Helvetica Chimica Acta*, 20:232–244.
- Niemi, H., Paulapuro, H., and Mahlberg, R. (2002). Review: Application of scanning probe microscopy to wood, fibre and paper research. *Paperi ja Puu - Paper and Timber*, 84, No.6:389–406.
- NIST Chemistry WebBook. <http://webbook.nist.gov/chemistry/vib-ser.html>.
- Page, D. (1969). A Theory for the Tensile Strength of Paper. *Tappi*, 52, No.4:674–681.
- Page, D., Tydeman, P., and Hunt, M. (1962). A Study of Fibre-to-Fibre Bonding by Direct Observation, in Formation and Structure of Paper. *11th Fundamental Research Symposium, Oxford*, pages 171–194.
- Parsons, S. (1942). Optical characteristics of paper as a function of fiber classification. *Paper Trade Journal*, 115, No.25:34–42.

- Persson, B., Ganser, C., Schmied, F., Teichert, C., Schennach, R., Gilli, E., and Hirn, U. (2013). Adhesion of cellulose fibers in paper. *Journal of Physics: Condensed mater*, 25:1–11; DOI:10.1088/0953–8984/25/4/045002.
- Reuter, P. (2010). *Probing Inside a Scanning Electron Microscope*. PhD thesis, Graz University of Technology.
- Sakurada, I. and Kaji, K. (1970). Relation between the polymer conformation and the elastic modulus of the crystalline region of polymer. *Journal of Polymer Science Part C: Polymer Symposia*, 31, Nr 1:57–76.
- Sakurada, I., Nukushina, Y., and Ito, T. (1962). Experimental Determination of the Elastic Modulus of Crystalline Regions in Oriented Polymers. *Journal of Polymer Science*, 57:651–660.
- Sarko, A. (1976). Crystalline polymorphs of cellulose: prediction of structure and properties. *Applied polymer symposia*, 28:729–742.
- Scallan, A. (1971). Quantitative picture of the fringed micellar model of cellulose. *Textile Research Journal*, 41; Nr.8:647–653.
- Schennach, R., Hirn, U., Horvath, A., Schmied, F., and Teichert, C. (2011). A model approach to understand the fiber-fiber bond in paper. In *Progress in Paper Physics Seminar*.
- Schmidt, G. (1976). *Die optischen Eigenschaften von Papier*. Verlag Dr. Martin Sändig GmbH, Walluf.
- Schmied, F., Teichert, C., Kappel, L., Hirn, U., Bauer, W., and Schennach, R. (2013). What holds paper together: Nanometre scale exploration of bonding between paper fibres. *Scientific Reports*, 3:2432:DOI: 10.1038/srep0243.
- Siegbahn, K., Nordling, C., Fahlman, A., Nordberg, R., Hamrin, K., Hedman, J., Johansson, G., Bergmark, T., Karlson, S., Lindgren, I., and Lindberg, B. (1967). ESCA [Electron Spectroscopy for Chemical Analysis]. Atomic, molecular, and solid state structure studied by means of electron spectroscopy. *Nova Acta Regiae Societatis Scientiarum Upsaliensis*, 20:1–282.
- Sixta, H. Lecture "Lignocellulosic Biorefinery", Institute for Paper, Pulp and Fibre Technology, Graz University of Technology, 2011.
- Sixta, H., editor (2006a). *Handbook of Pulp, Volume 1*. WILEY-VCH Verlag GmbH & Co. KGaA, Weinheim.
- Sixta, H., editor (2006b). *Handbook of Pulp, Volume 2*. WILEY-VCH Verlag GmbH & Co. KGaA, Weinheim.

- Sixta, H., Harms, H., Dapia, S., Parajo, J., Puls, J., Saake, B., and Fink, H.-P. (2004). Evaluation of new organosolv dissolving pulps. Part I: Preparation, analytical characterization and viscose processability. *Cellulose*, 11:73–83.
- Smith, F. (1980). Alloy rayon.
- Smith, F. (1981). High fluid-holding alloy rayon fiber mass.
- Stratton, R. and Colson, N. (1990). Dependence of fiber/fiber bonding on some papermaking variables. *IPTS Technial paper series*, pages 1–19.
- Terayama, H. (1952). Method of Colloid Titration (A New Titration between Polymer Ions). *Journal of Polymer Science*, 8, No.2:243–253.
- Textechno H. Stein GmbH & Co. KG. <http://www.textechno.com/index.php/en/fibre-testing-products-65/favimat-robot-products-145>.
- Thygesen, A., Oddershede, J., Lilholt, H., Thomson, A., and Ståhl, K. (2005). On the determination of crystallinity and cellulose content in plant fibres. *Cellulose*, 12, Nr.6:563–576.
- Torgnysdotter, A. and Wagberg, L. (2003). Study of the joint strength between regenerated cellulose fibres and its influence on the sheet strength. *Nordic Pulp and Paper Research Journal*, 18, No.4:455–459.
- van den Akker, J. (1949). Scattering and Absorption of Light in Paper and Other Diffusing Media. *Tappi*, 32:498–501.
- van den Akker, J., Lathrop, A., Voelker, M., and Dearth, L. (1958). Importance of Fibre Strength to Sheet Strenth. *Tappi*, 41, Nr. 8:416–425.
- Viswanathan, A. and Shenouda, S. (1971). The helical structure of cellulose I. *Journal of Applied Polymer Science*, 15, Nr. 3:519–535.
- Weber, F. (2010). Reactions of methanol on Pd(111), Pd/Zn- and Pd/ZnO- surfaces. Master's thesis, Graz University of Technology.
- Weber, F., Ganser, C., Schennach, R., Teichert, C., Bernt, I., and Eckhart, R. Application of the Page-equation on viscose fibre - hand sheets. In preparation for publication in *Cellulose*.
- Weber, F., Koller, G., Schennach, R., Bernt, I., and Eckhart, R. (2013). The surface charge of regenerated cellulose fibres. *Cellulose*, 20, Nr. 6:2719–2729; DOI: 10.1007/s10570-013-0047-8.
- Wilhelm, P. (1996). Applications of ft-ir microscopy with materials analyses. *Micron*, 27, No.5:341–344.

- Wågberg, L. and Annergren, G. (1997). Physico-chemical characterisation of paper-making fibres. In Baker, C., editor, *Fundamentals of Papermaking - Transactions of the 11th Fundamental Research Symposium held at Cambridge*; 1-82.
- Young, J. (1972). Bonding on paper made from viscose fibres. *Paper Technology*, pages 25-26.
- Zankel, A. private communication, 11.07.2013.

List of Figures

1.1	Working groups and their object within the CD-Laboratory for Surface Chemical and Physical Fundamentals of Paper Strength	3
2.1	Composition of a tree trunk	7
2.2	Schematic illustration of the cell wall structure of a wood fibre	8
2.3	Spatial configuration of a glucose molecule	9
2.4	The molecular structure of cellulose	9
2.5	Monoclinic unit cell of cellulose I	10
2.6	Molecular structure of the building units of lignin	12
2.7	Workflow of the viscose manufacture	14
2.8	Overview of some viscose fibres with different cross sections	14
2.9	Illustration of the bonding mechanisms in paper	15
2.10	Comparison of a paper fibre and the used viscose fibres (ESEM)	17
3.1	SEM images of the investigated fibres.	18
3.2	Schematic arrangement of swelling determination	21
3.3	Schematic diagram of the signals generated and used in a SEM	21
3.4	Illustration of the Peltier effect	22
3.5	Cold stage assembly	23
3.6	Cold stage assembly without and with specimen stub	24
3.7	Schematic view of a Michelson interferometer	27
3.8	Principle of ATR measurement	28
3.9	The ATR unit and the optical path within	29
3.10	Schematic arrangement of a typical XPS system	30
3.11	Energy level diagram for XPS	31
3.12	X-ray spectrum of cellulose	32
3.13	Principle of atomic force microscopy	33
3.14	Basic considerations for Kubelka-Munk theory	36
3.15	Schematic description of polarized microscopy	40
3.16	Determination of the optical bonded area	40
3.17	Micro bond tester and sample holder for joint strength measurement	41

4.1	Cross section of the investigated fibres	43
4.2	Time dependent swelling of the free end of a RF fibre	44
4.3	Swelling of the investigated fibres.	45
4.4	Swelling versus COOH content	45
4.5	Measurement points of the swelling investigations by light microscope	46
4.6	ESEM images of a dry (left) and wet (right) AF2	47
4.7	Overview of the swelling values of all investigated fibres, including the ESEM data	48
4.8	Breaking length of hand sheets	50
4.9	Evaluation of the titration data	52
4.10	ATR spectra of the investigated samples	53
4.11	Integrated peak area of the peak at 1580 cm^{-1} as a function of COOH amount	54
4.12	Data of the XPS measurements	56
4.13	Comparison of the C3 peak areas and the amount of COOH groups, detected by titration	58
5.1	Cross section of the investigated fibres.	60
5.2	Breaking length of hand sheets made of flat fibres	61
5.3	Fibre hardness, determined by nanointentation	63
5.4	Calculated areas by nitrogen adsorption measurements	66
5.5	Light scattering of the investigated handsheets - bonded handsheets	68
5.6	Light scattering of the investigated handsheets - bonded and unbonded handsheets	68
5.7	Unbonded handsheet of F9, F9C, F9A and F9AC.	69
5.8	Fibre-fibre joint, fixed on the sample holder by nail polish for bonding area and bond strength investigations	70
5.9	Image of a fibre-fibre joint made through the polarized light microscope	71
5.10	Force-distance curve	72
5.11	Relative bonded area obtained from light scattering measurements	73
5.12	Relative bonded area - comparing of the results	75
5.13	Schematic illustration of a bond break	77

List of Tables

3.1	Fibre parameters of the round viscose samples	19
3.2	Fibre parameters of the flat viscose samples	20
4.1	Grammage of the used handsheets for breaking length determination .	49
4.2	Tensile strength of the used handsheets for breaking length determination	49
4.3	Quantified charge of each fibre sample by Titration (total charge and surface charge)	51
4.4	XPS data - Binding energies and atomic concentration percentages . .	55
5.1	Grammage of the used handsheets for breaking length determination .	62
5.2	Tensile strength of the used handsheets for breaking length determination	62
5.3	Detected surface values by using BET	66
5.4	Optical properties of the bonded handsheet	67
5.5	Optical properties of the unbonded handsheets	68
5.6	Optical bonded area of all investigated fibre-fibre joints	71
5.7	Bond strength of all investigated fibre-fibre joints	72
5.8	Mean value and standard deviation of the specific bond strength . . .	72
5.9	Parameters used for RBA calculation via the Page equation.	74